

**UCGE Reports
Number 20364**

Department of Geomatics Engineering

**Planar and Linear Feature-Based Registration of
Terrestrial Laser Scans with Minimum Overlap Using
Photogrammetric Data**

(URL: <http://www.geomatics.ucalgary.ca/graduatetheses>)

by

Sibel Canaz

December, 2012

SCHULICH
School of Engineering



UNIVERSITY OF CALGARY

Planar and Linear Feature-Based Registration of Terrestrial Laser Scans with Minimum
Overlap Using Photogrammetric Data

by

Sibel Canaz

A THESIS

SUBMITTED TO THE FACULTY OF GRADUATE STUDIES
IN PARTIAL FULFILMENT OF THE REQUIREMENTS FOR THE
DEGREE OF MASTER OF SCIENCE

DEPARTMENT OF GEOMATICS ENGINEERING

CALGARY, ALBERTA

December, 2012

© Sibel Canaz 2012

ABSTRACT

Three-dimensional (3D) modeling is crucial for studying, analyzing, reconstructing, and documenting our environment, in general, and man-made structures, in particular. 3D data for a surveyed structure can be directly collected by a Terrestrial Laser Scanner (TLS). However, several TLS scans are necessary to obtain a complete coverage of the surveyed structures. Transformation of the collected scans into a common coordinate system with a registration procedure is necessary in order to acquire a meaningful 3D model of the structure in question. The registration process requires a large overlap area among the TLS scans for reliable results. In this research, this large overlap area requirement between the TLS scans is reduced using a photogrammetric model as additional information for the registration process. Planar and linear features, which can be easily identified in photogrammetric data and TLS scans, were chosen as the registration primitives. Quantitative quality analysis is proposed in this research by calculating the point-to-plane normal distances between the registered surfaces. The experimental results from real datasets show the ability of the proposed technique, where less than 10 cm point-to-plane normal distances between the registered surfaces were observed, which confirmed the reliability of the registration results.

ACKNOWLEDGEMENTS

I would like to express my deepest and sincere gratitude to my supervisor, Dr. Ayman Habib, for his invaluable guidance, advice, and encouragement throughout my study. Dr. Habib patiently responded to all my questions in detail; and a great deal of my knowledge about photogrammetry I owe to him. This thesis would not have been completed without his magnificent support. His great kindness and patience will never be forgotten.

I also wish to thank my thesis committee members, Dr. Naser El-Sheimy, Dr. John Yackel, and Dr. Ruisheng Wang for taking their valuable time to read my thesis, provide many helpful comments, and participate in my defense.

I am grateful as well to the Ministry of Turkish Education for the scholarship which gave me the opportunity to study abroad.

Special thanks are due to Eray Sevgen for his continuous and emotional support during this journey. I am sincerely grateful also to my dear friend, Aysun Kunduracı, for her encouragement and friendship and for editing my thesis writing. I also wish to thank the Hasköylü family, who were my surrogate family during my studies. The enduring friendship, support, and laughs of XiaoJuan, Amr, Sherif, Herve, and all my other friends were greatly appreciated too.

I would also like to thank the past and present members of the Digital Photogrammetry Research Group (DPRG), especially Zahra, Eunju, Hussein, Mohannad, Kutalmis, Ivan, Ana, and all of the other members for supporting and helping me during the hard times of my research. I feel extremely lucky and proud to be a part of the DPRG. I would not have been able to finish my research without them.

Last but not least, I take this opportunity to thank my parents Nazmiye and Abdullah, my sister Aysun, and my brother Murat for their love and emotional support during my life.

DEDICATION

To my little lovely niece Nisa Azra, my source of happiness and inspiration

TABLE OF CONTENTS

ABSTRACT.....	ii
ACKNOWLEDGEMENTS.....	iii
DEDICATION.....	v
TABLE OF CONTENTS.....	vi
LIST OF TABLES.....	viii
LIST OF FIGURES.....	x
LIST OF ABBREVIATIONS.....	xiii
CHAPTER 1.....	1
INTRODUCTION.....	1
1.1 Motivation.....	1
1.2 Research Objectives.....	4
1.3 Thesis Outline.....	4
CHAPTER 2.....	6
BACKGROUND.....	6
2.1 Introduction.....	6
2.2 Close Range Photogrammetry.....	6
2.2.1 Photogrammetric Principles.....	7
2.3 Laser Scanning.....	10
2.3.1 Laser Scanning Principles.....	11
2.3.1.1 Time-of-Flight (TOF) Systems.....	11
2.2.1.2 Phase-Shift Systems.....	12
2.2.1.3 Triangulation-based Systems.....	13
2.4 Photogrammetry vs. Laser Scanning.....	14
2.5 Registration.....	15
2.5.1 Registration Primitives.....	16
2.5.2 Transformation Function.....	19
2.5.3 Similarity Measure.....	20
2.5.4 Matching Strategy.....	20
2.6 Registration Methods.....	22
2.6.1 Iterative Closest Point Registration Method and its Variants.....	22
2.6.2 Feature-based Registration Methods.....	27
2.6.3 Registration Methods Using Photogrammetric Data.....	28
2.7 Summary.....	31
CHAPTER 3.....	33
METHODOLOGY.....	33
3.1 Introduction.....	33
3.2 3D Object Reconstruction from Photogrammetric Data.....	34
3.3 Feature Extraction.....	37
3.3.1 Planar Features Extraction from Photogrammetric Data.....	37
3.3.2 Linear Features Extraction from Photogrammetric Data.....	38
3.3.3 Planar Features Extraction from TLS Scans.....	40
3.3.4 Linear Features Extraction from TLS Scans.....	41

3.4 Similarity Measure.....	42
3.4.1 Modification of the Weight Matrix for Planar Features.....	48
3.4.2 Modification of the Weight Matrix for Linear Features.....	51
3.5. Number and Configuration of Required Features for the Proposed Registration Method.....	53
3.5.1 Number and Configuration of Required Planes for the Proposed Planar Feature-Based Registration Method.....	54
3.5.2 Number and Configuration of Required Lines for the Proposed Linear Feature-Based Registration Method.....	55
3.5.3 Final Step of the Proposed Registration Methods.....	56
3.6 Evaluation of Registration Results.....	57
3.6.1 Qualitative Quality Control.....	57
3.6.2 Quantitative Quality Control.....	57
3.7 Summary.....	60
CHAPTER 4.....	62
EXPERIMENTAL RESULTS.....	62
4.1 Introduction.....	62
4.2 Experiment I.....	62
4.2.1 Data Description.....	63
4.2.2 Planar Feature-Based Registration of Rozsa Center.....	64
4.2.2.1 Bundle Adjustment Results for Planar Features.....	64
4.2.2.2 Results of the Proposed Planar Feature-Based Registration for Rozsa Center.....	66
4.2.2.3 Quality Control of the Planar Feature-Based Registration Results.....	72
4.2.3 Linear Feature-Based Registration of Rozsa Center.....	81
4.2.3.1 Bundle Adjustment Results for Linear Features.....	81
4.2.3.2 Results of the Proposed Linear Feature-Based Registration for Rozsa Center.....	82
4.2.3.3 Quality Control of the Linear Feature-Based Registration Results.....	86
4.2.4 Comparisons of the Results of the Proposed Feature-Based Registration and ICPP Method for Rozsa Center.....	95
4.3 Experiment II.....	96
4.3.1 Data Description.....	96
4.3.2 Bundle Adjustment Results.....	98
4.3.3 Results of the Planar Feature-Based Registration Method.....	100
4.3.4 Quality Control of the Planar Feature-Based Registration Results.....	105
4.3.5 Comparison of the Results of the Planar Feature-Based Registration and ICPP Method for Yamnuska Hall.....	113
CHAPTER 5.....	117
CONCLUSIONS AND RECOMMENDATIONS FOR FUTURE WORK.....	117
5.1 Conclusions.....	117
5.2 Recommendations for Future Work.....	120
REFERENCES.....	122
APPENDIX A.....	126

LIST OF TABLES

Table 2.1. Laser scanning pros and photogrammetry cons.....	14
Table 2.2. Laser scanning cons and photogrammetry pros.....	15
Table 4.1. Percentages of the overlap area among the four TLS scans of Rozsa Center .	67
Table 4.2. The number of planar features in four TLS scans of Rozsa Center.....	71
Table 4.3. The result of the planar feature-based registration procedure for Rozsa Center	72
Table 4.4. The mean, standard deviation and RMSE of the calculated normal distances results of planar feature-based registration method for the planes between the PRD and the TLS scans of Rozsa Center using all of the points of segmented planes from the scans	76
Table 4.5. The mean, standard deviation, and RMSE of the calculated normal distances results of planar feature-based registration method for the planes between the PRD and the TLS scans of Rozsa Center using the points of segmented planes which are inside the polygons whose vertices define the PRD planes	77
Table 4.6. The mean, standard deviation, and RMSE of the calculated normal distances of planar feature-based registration method between different TLS scans planes of Rozsa Center	78
Table 4.7. The number of linear features in the four TLS scans of Rozsa Center.....	85
Table 4.8. The result of the linear feature-based registration procedure for Rozsa Center	85
Table 4.9. The mean, standard deviation, and RMSE of the calculated normal distances results of linear feature-based registration method for planes between PRD and TLS scans of Rozsa Center using all points of segmented planes from the scans	90
Table 4.10. The mean, standard deviation and RMSE of the calculated normal distances results of linear feature-based registration method for the planes between the PRD and the TLS scans of Rozsa Center using only points of segmented planes which are within planar polygon defined by the PRD.....	91
Table 4.11. The mean, standard deviation, and RMSE of the calculated normal distances of linear-feature based registration method for planes between different TLS scans	92
Table 4.12. Comparison of the different registration results of Rozsa Center TLS scans	95
Table 4.13. The percentages of overlap area of the seven TLS scans of Yamnuska Hall.....	98
Table 4.14. The number of planar features in the seven TLS scans of Yamnuska Hall	104
Table 4.15. The results of Yamnuska Hall from the planar feature-based registration procedure.....	105

Table 4.16. The mean, standard deviation, and RMSE of the calculated normal distances results for planes between the PRD and the TLS scans of Yamnuska Hall using all points of the segmented planes.....	109
Table 4.17. The mean, standard deviation, and RMSE of the calculated normal distances for planes between PRD and TLS scans of Yamnuska Hall using only points of segmented planes that are inside the PRD planes borders.....	110
Table 4.18. The mean, standard deviation, and RMSE of the calculated normal distances between different TLS scans of Yamnuska Hall.....	111
Table 4.19. Comparison of the proposed planar feature-based and ICP method results for Yamnuska Hall	113

LIST OF FIGURES

Figure 2.1. Illustration of conjugate light rays for a close range photogrammetric application.....	8
Figure 2.2. The involved parameters for photogrammetric 3D object space reconstruction.....	10
Figure 2.3. Schematic representation of a TOF system.....	12
Figure 2.4. Example of a phase-shift system (source: Petrie and Toth, 2009).....	13
Figure 2.5. Laser triangulation system (source: Bogue, 2010).....	13
Figure 2.6. Point primitives in photogrammetric data (a), original TLS scan points (b)..	17
Figure 2.7. Planar features in photogrammetric data (a) and TLS scan (b).....	18
Figure 2.8. Linear Features in photogrammetric data (a) and TLS scan (b).....	19
Figure 2.9. Original TLS scan1 (a), TLS scan2 (b), TLS scan3 (c), and TLS scan4 (d); four TLS scans together before registration (e) and after registration (f).....	21
Figure 2.10. Tetrahedron using four points (p_1, p_2, p_3, p_4), the centroid of the three points (p_c), the point (p_t) (a); four splitting tetrahedrons defined by the point (p_t) and (p_1, p_2, p_3 , and p_4) (b) (source: Al-Durgham et al., 2011).....	25
Figure 2.11. Example of a hybrid system: Laser scanner and camera rigidly fixed together	30
Figure 3.1. Pixel coordinate system (a) versus image coordinate system (b).....	34
Figure 3.2. Principal distance (c), principal point (pp) and principal point coordinates (x_p and y_p)	36
Figure 3.3. Plane points in different images	37
Figure 3.4. Beginning and ending points and intermediate points of a linear feature in image and object space (Adapted from Habib et al., 2004).....	39
Figure 3.5. Segmented planar features of a TLS scan (a) and a corresponding scene of the scan (b).....	41
Figure 3.6. Extreme points of an infinite line (source: Al-Durgham, 2007)	42
Figure 3.7. Linear features in TLS scan (a) and photogrammetric data (b).....	42
Figure 3.8. Non-conjugate points defining the plane in different coordinate systems	46
Figure 3.9. Non-conjugate points defining the line in different coordinate systems (Adapted from Renaudin et al., 2011)	46
Figure 3.10. Relation between the scans/PRD and the plane coordinate systems.....	49
Figure 3.11. Local UVW coordinate system for a plane (Adapted from Kersting, 2011)	49
Figure 3.12. Relation between the scans/PRD and the line coordinate systems.....	51
Figure 3.13. An example of planes and their contributions for estimating the transformation parameters	55
Figure 3.14. An example of lines and their contributions for estimating the transformation parameters	56
Figure 3.15. Plane borders in the TLS scans versus photogrammetric data.....	60

Figure 4.1. Top view of overlap area among the 16 images covering Rozsa Center	65
Figure 4.2. Top view of camera positions for the 16 images covering Rozsa Center	65
Figure 4.3. Top view of overlap area among the four TLS scans covering Rozsa Center	67
Figure 4.4. Planar features in TLS scan1 (a) and photogrammetric data (b).....	68
Figure 4.5. Planar features in TLS scan2 (a) and photogrammetric data (b).....	69
Figure 4.6. Planar features in TLS scan3 (a) and photogrammetric data (b).....	69
Figure 4.7. Planar features in TLS scan4 (a) and photogrammetric data (b).....	70
Figure 4.8. Examples of planar features with different orientations for Rozsa Center ...	71
Figure 4.9. Top view (a) and 3D view (b) of the four registered TLS scans of Rozsa Center	73
Figure 4.10. Rozsa Center registered TLS scans 2, 3, and 4: top view (a), 3D view (b), and lightning rod (c).....	74
Figure 4.11. Rozsa Center registered TLS scans 1, 2, and 3: top view (a), 3D view, (b), and pipe (c).....	74
Figure 4.12. Plane 40 in TLS scan1 and scan2	78
Figure 4.13. 3D view of the registered four TLS scans of Rozsa Center by planar-feature based registration method (color based on normal distances calculated by using the PRD plane parameters and segmented TLS planes' points that are inside polygons defining the PRD planes).....	80
Figure 4.14. 3D view of the registered four TLS scans of Rozsa Center by planar-feature based registration method (color based on normal distances calculated by using all points of the segmented planes from the TLS scans and PRD planes parameters).....	81
Figure 4.15. Linear features in TLS scan1 (a) and photogrammetric data (b).....	83
Figure 4.16. Linear features in TLS scan2 (a) and photogrammetric data (b).....	83
Figure 4.17. Linear features in TLS scan3 (a) and photogrammetric data (b).....	84
Figure 4.18. Linear features in TLS scan4 (a) and photogrammetric data (b).....	84
Figure 4.19. Rozsa Center registered TLS scan 2, 3, and 4: top view (a), 3D view (b), and lightning rod (c).....	87
Figure 4.20. Rozsa Center registered TLS scan 1, 2, and 3: top view (a), 3D view (b), and pipe (c)	87
Figure 4.21. 3D view of the registered TLS scans of Rozsa Center by linear feature-based registration method (color based on normal distances derived by using only the points of the segmented plane from the TLS scans within the area of PRD planes)	93
Figure 4.22. 3D view of the registered TLS scans of Rozsa Center by linear feature-based registration method (color based on normal distances which were calculated by using all points of the segmented plane from TLS scans)	93

Figure 4.23. An example of the intersection of two planes and the linear features that could be derived from the TLS scans and photogrammetric data: schematic (a) and image (b)	94
Figure 4.24. Top view of Yamnuska Hall with the covered area by the different TLS scans and the position of TLS for each scan	97
Figure 4.25. Top view of the Yamnuska Hall with the covered area by the different images	99
Figure 4.26. Top view of the Yamnuska Hall building with the position of the different images	99
Figure 4.27. Planar features in TLS scan1 (a) and photogrammetric data (b) for the experiment II	100
Figure 4.28. Planar features in TLS scan2 (a) and photogrammetric data (b) for the experiment II	101
Figure 4.29. Planar features in TLS scan3 (a) and photogrammetric data (b) for the experiment II	101
Figure 4.30. Planar features in TLS scan4 (a) and photogrammetric data (b) for the experiment II	102
Figure 4.31. Planar features in TLS scan5 (a) and photogrammetric data (b) for the experiment II	102
Figure 4.32. Planar features in TLS scan6 (a) and photogrammetric data (b) for the experiment II	103
Figure 4.33. Planar features in TLS scan7 (a) and photogrammetric data (b) for the experiment II	103
Figure 4.34. Examples of planar features with different orientation of Yamnuska Hall	104
Figure 4.35. General view of the seven registered TLS scans of Yamnuska Hall: top view (a) and 3D view (b)	106
Figure 4.36. Registered TLS scan3, scan4, and scan5: top view (a), 3D view (b), and close-up of windows (c)	107
Figure 4.37. Registered TLS scan6 and scan7: top view (a), 3D view (b), and close-up of windows (c)	107
Figure 4.38. 3D view of the registered TLS scans of Yamnuska Hall (color based on normal distances calculated using only points of the segmented planes from TLS scans which are inside the polygon of PRD planes points)	112
Figure 4.39. 3D view of the registered TLS scans of Yamnuska Hall (color based on normal distances calculated using all points of the segmented planes from TLS scans)	112
Figure 4.40. The proposed planar feature-based registration method (a) versus ICPP registration results (b) & (c)	114
Figure 4.41. The proposed registration versus the ICPP registration results for TLS scan7 and scan1 (reference frame)	116

LIST OF ABBREVIATIONS

3D	3 (Three) Dimensional
EOPs	Exterior Orientation Parameters
GPS	Global Positioning System
GP-ICP	Geometric Primitive-Iterative Closest Point
GP-ICPR	Geometric Primitive-Iterative Closest Point with RANSAC
INS	Inertial Navigation System
ICP	Iterative Closest Point
ICPP	Iterative Closest Projected Point
IMU	Inertial Measurement Unit
IOPs	Interior Orientation Parameters
LiDAR	Light Detection and Ranging
LSA	Least Square Adjustment
MSAT	Multi Sensor Advanced Triangulation
TIN	Triangular Irregular Network
TLS	Terrestrial Laser Scanner
TLS scan	Terrestrial Laser Scanner scan
TOF	Time of Flight
RMSE	Root Mean Square Error
PRD	Photogrammetrically Reconstructed Data

CHAPTER 1

INTRODUCTION

1.1 Motivation

Three-dimensional (3D) modeling can be defined as representing an object in a digital environment. Nowadays, the interest and demand for 3D modeling of real objects has increased with the continuous improvement in data acquisition systems and the expanding range of potential applications. A 3D model allows the user to analyze real objects for future use; for instance, 3D models of historical buildings can help in the reconstruction of buildings after damage occurs. Moreover, archeological sites/objects can be studied through 3D models; and the medical field also uses 3D models for visualization of organs in details. Other areas that use 3D models of real objects are architecture, forestry, geology, and civil and oil engineering.

How to derive 3D models of real objects/structures is the main question that needs to be answered. First of all, 3D data for the surveyed structure are needed. Currently, 3D data can be obtained through two technologies: photogrammetry and laser scanning. Laser scanning directly provides 3D data, while photogrammetry reconstructs 3D information through a photogrammetric triangulation process using the collected images of the surveyed structure. The advantage of the direct acquisition of 3D data makes laser scanning a popular technique in modeling. However, it is almost impossible to cover a complete structure with a single Terrestrial Laser Scanner (TLS) scan. Therefore, several TLS scans from different positions/orientations are necessary for complete coverage of

the surveyed structure. The collection and processing of TLS scans is a time consuming process; each collected scan has its own coordinate system, and 3D models can only be obtained by alignment of the collected scans in a common coordinate system. This alignment process is known as “registration.” The transformation parameters between the collected scans and the reference coordinate systems (i.e., three translations, three rotations and scale) must be estimated for registration purposes.

The registration paradigm consists of selecting four elements: the appropriate primitives, the transformation function, the similarity measure, and the matching strategy (Al-Ruzouq, 2004). The first paradigm element of registration (making a decision on the primitive) is used for estimating the transformation parameters among the involved scans. The generally used registration primitives for photogrammetric data and TLS scans can be classified into three groups: point, linear, and planar (areal) features. Finding conjugate points in different TLS scans is almost impossible due to the irregular distribution of the TLS scans (point cloud), while identification of the planar and linear features is possible in both photogrammetric data and TLS scans. Furthermore, planar and linear features commonly exist in man-made structures, and the registration primitives of choice in this research therefore are the planar and linear features.

The 3D similarity transformation function is the generally used mathematical model for relating the conjugate primitives in different coordinate systems. After the type of appropriate primitive and transformation function are selected, the next step of the registration procedure is the similarity measure selection. The similarity measure incorporates the matched primitives together with the transformation function for

mathematically describing their correspondence (Renadin et al., 2011). Finally, the matching strategy, which is an overall scheme of the solution for a registration problem, needs to be designed. The matching strategy contains the selection of the registration primitives, the similarity measure, and the transformation function (Al-Ruzouq, 2004).

The most popular and generally used algorithm for registering 3D data is the “Iterative Closest Point” (ICP), which is based on minimizing the point-to-point distance in the overlapping area between different TLS scans (Besl and McKay, 1992). Similarly, another registration method, which was developed by Chen and Medioni (1992), minimizes the point-to-plane distance in the overlapping area of the TLS scans. Iterative Closest Projected Point method (ICPP) (Al-Durgham, 2011), which is a robust registration method and a variant of the ICP method, is considered as both a point-to-point and point-to-plane registration technique. Many registration methods (i.e., the ICP method and its variants) require large overlap areas between the TLS scans in order to obtain a reliable 3D model of the structure of interest. In this research, the large overlap area requirement among the scans is eliminated/reduced using photogrammetric data as additional information of the structure, which can be acquired in a relatively short time.

Real experimental data were collected in order to analyze the ability of the proposed registration methods. “Quality control is a post-mission procedure to ensure/verify the quality of the estimated results” (Habib, 2007). A quantitative quality control method therefore is proposed in this research by calculating the point-to-plane normal distances between the registered surfaces. On the other hand, qualitative quality control was conducted by plotting the registered scans.

1.2 Research Objectives

The main objectives of this research can be listed as follows:

- The primary objective of this research is to avoid the requirement of large overlap areas among the TLS scans using photogrammetric data for the registration of the scans.
- The second objective of this research is to compare and analyze the results of the proposed registration method using the planar and linear features separately.
- Finally, the quantitative quality control technique is proposed by calculating the point-to-plane normal distance among the registered surfaces to analyze the results of the proposed registration method.

1.3 Thesis Outline

The thesis consists of five chapters. Chapter 1 constitutes the introduction. The motivation behind the research is explained and the objectives of the research are also discussed in this chapter.

Chapter 2 describes the basic principles of close range photogrammetry and laser scanning techniques. Moreover, the term “registration” is defined; and the elements of the registration paradigm (i.e., the registration primitives, the similarity measure, the transformation function, and the matching strategy) are explained. Finally, different registration techniques are reviewed in more detail in this chapter.

The proposed registration methods are explained in Chapter 3. First, the extraction of the planar and linear features from the photogrammetric data and TLS scans are described.

Then, 3D point-based similarity transformation, which incorporates the matched primitives, is introduced; and finally, the proposed quantitative quality control technique is explained.

Chapter 4 presents the experimental results of the proposed registration methods for two different building data sets: Rozsa Center and Yamnuska Hall. The quality control of the registration results are conducted and presented.

Chapter 5 concludes the research and provides some recommendations for future work.

CHAPTER 2

BACKGROUND

2.1 Introduction

The basic principles of close range photogrammetry and laser scanning technology will be explained first in this chapter, followed by a comparison of the photogrammetry and laser scanning technologies. The elements of a registration paradigm then will be described; and a review of various studies conducted on registration of TLS scans will conclude the chapter.

2.2 Close Range Photogrammetry

“Photogrammetry is the art and science of deriving accurate metric and descriptive information from analog and digital images” (Habib et al., 2007). Starting in the 1990s, the popularity and development of photogrammetry have increased in tandem with the continuing development of digital cameras and computer vision techniques. Due to the steady decrease in the cost of digital cameras, photogrammetric object space reconstruction has become one of the most popular studies in many fields (e.g., archeology, architecture, biomedical engineering, and civil engineering).

Photogrammetry can mainly be categorized into three groups: space (satellite) photogrammetry, aerial photogrammetry, and close range (terrestrial) photogrammetry. Satellites collect images for space photogrammetric applications and are mainly used for monitoring earth observations (i.e. ice mapping, natural disasters, etc.) Large-format images, which are captured from a high point using a camera that is generally mounted on an aircraft, are used for aerial photogrammetry. Aerial photogrammetry is generally

used for mapping. The technique is considered “close range photogrammetry” when the distance from the camera to the object of interest is less than 100 meters (Cooper and Robson, 2001). Close range photogrammetry has a wide spectrum of applications (e.g., archeology, medicine, heritage conservation, architecture, aerospace industry, automotive, machine industry, natural science, and many others) (Luhmann et al., 2006).

Close range photogrammetry can be performed by simply taking overlapping images from different perspectives around the object of interest. Although, there are some differences in terms of data collection, the same basic principles for reconstructing the object space apply to space, aerial, and close range photogrammetry. The principles of deriving 3D information from 2D images are briefly explained in the following subsection.

2.2.1 Photogrammetric Principles

Object space reconstruction is possible with the intersection of conjugate light rays from overlapping images. Figure 2.1 is an example of conjugate light rays for a close range photogrammetric application. Conjugate light rays must be well defined by the image measurement and the internal characteristics of the camera. Moreover, the position and orientation of the light rays in the object space have to be known for 3D reconstruction of the object of interest.

The internal camera characteristic parameters are commonly known as the “Interior Orientation Parameters” (IOPs) and are obtained through a camera calibration procedure. The orientation and position parameters of the bundle of light rays in the object space,

called the “Exterior Orientation Parameters” (EOPs), are estimated through a georeferencing procedure.

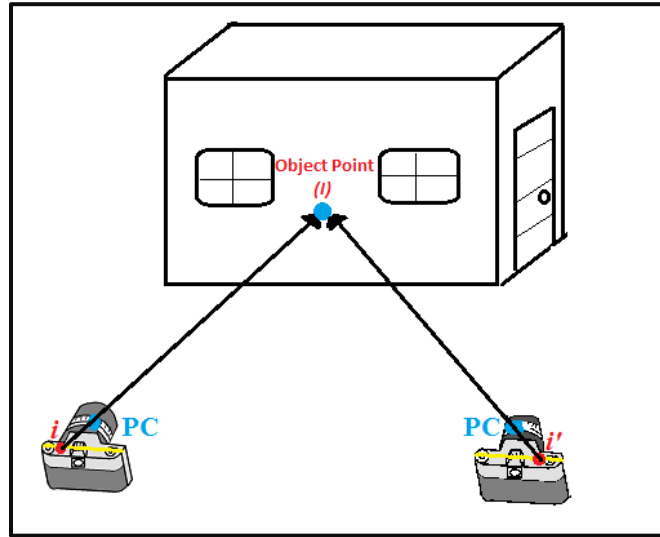


Figure 2.1. Illustration of conjugate light rays for a close range photogrammetric application

In Figure 2.1, (i and i') represents the conjugate points in the image space; (I) is the point in the object space, and (PC) is the perspective center of the camera. The mathematical model, which is used to relate the image and the ground (object space) coordinate systems, is called the “collinearity equations” (Kraus, 1993), (Equations 2.1a and 2.1b).

$$x_i = x_p - c \frac{r_{11}(X_I - X_0) + r_{21}(Y_I - Y_0) + r_{31}(Z_I - Z_0)}{r_{13}(X_I - X_0) + r_{23}(Y_I - Y_0) + r_{33}(Z_I - Z_0)} + \Delta x \quad (2.1a)$$

$$y_i = y_p - c \frac{r_{12}(X_I - X_0) + r_{22}(Y_I - Y_0) + r_{32}(Z_I - Z_0)}{r_{13}(X_I - X_0) + r_{23}(Y_I - Y_0) + r_{33}(Z_I - Z_0)} + \Delta y \quad (2.1b)$$

where:

- x_i and y_i : the image coordinates of point (i);
- x_p, y_p, c , and the coefficients describing Δx and Δy :
- X_i, Y_i, Z_i : the object space coordinates of point (I);
- $R = \begin{bmatrix} r_{11} & r_{12} & r_{13} \\ r_{21} & r_{22} & r_{23} \\ r_{31} & r_{32} & r_{33} \end{bmatrix}$: the rotation matrix relating object and image coordinate system, defined by the angles: ω, φ , and κ ;
- X_0, Y_0, Z_0 : the object space coordinates of the camera perspective center (PC).

The image coordinates of the points are observed by image measurements, while x_p, y_p, c and the distortion parameters (IOPs) are obtained through a camera calibration procedure. The distortion parameters, which are caused by errors in the camera lens (e.g., decentering and radial lens distortions), are added to the collinearity equation to compensate for any deviations from the assumed perspective geometry.

The position of the camera PC in the object space is defined by the translation parameters (X_0, Y_0 , and Z_0); while the orientation of the image coordinate system relative to the object space is represented by the rotation matrix defined by the angles “ ω, φ , and κ .” The unknown parameters in the collinearity equations are the EOPs of each image ($X_0, Y_0, Z_0, \omega, \varphi$, and κ) and the object coordinates of the tie points (X, Y, Z). EOPs can be obtained directly using Global Positioning System (GPS) and Inertial Navigation System (INS) during data capturing or indirectly using control and tie points in the aerial triangulation (bundle adjustment) procedure. Figure 2.2 illustrates the involved parameters for photogrammetric 3D object space reconstruction using collinearity equations.

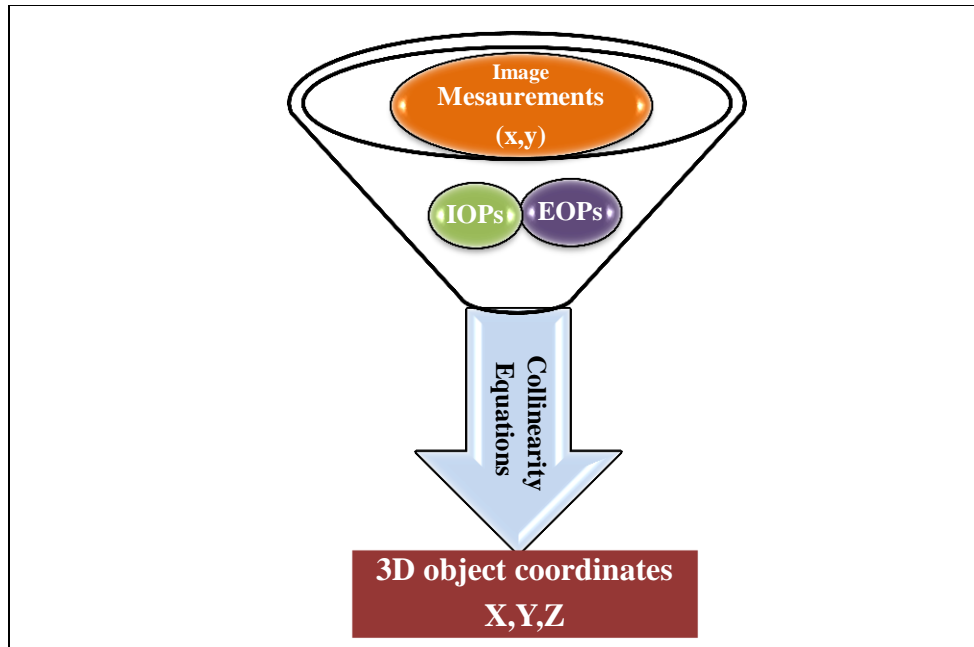


Figure 2.2. The involved parameters for photogrammetric 3D object space reconstruction

2.3 Laser Scanning

A laser scanner is able to directly collect 3D coordinates of surveyed objects. Laser scanning is used in a very wide application area due to the advantage of fast and non-contact 3D data acquisition. Nevertheless, laser scanning is a high-cost technology because the instruments of the scanner are expensive.

Laser scanning can be grouped in two categories: airborne laser scanning and terrestrial laser scanning. Airborne laser scanner is generally mounted on an aircraft and assisted with GPS/INS systems. Airborne laser scanning is generally used for 3D urban mapping, forestry, and military applications. On the other hand, TLS is usually placed on a tripod or on a land vehicle to collect data. Some of the application areas for terrestrial laser scanning are archaeological documentation, topographic surveys, fabrication inspection, manufacturing, and many other engineering surveys.

2.3.1 Laser Scanning Principles

Laser scanning is often referred to as Light Detection and Ranging (LiDAR) in the photogrammetric literature. Point clouds, laser scanning data, scans, laser scans, TLS, and TLS scans are commonly-used terms to express LiDAR data. A laser scanner is an active sensor, and it provides its own energy. In terms of the sensor system, laser scanning can be categorized into three main groups: time-of-flight (TOF), phase-shift, and triangulation-based measurements (Bogue, 2010).

2.3.1.1 Time-of-Flight (TOF) Systems

TOF systems are the most commonly used laser scanners. Basically, a laser pulse is sent from a transmitter and the light particles (photons) are scattered back to the receiver (Figure 2.3). The receiver collects the photons which come back to it. The range is computed by the travel time between signal transmission and reception. Equation 2.2 can be used for the computation of the laser range (Petrie and Toth, 2009).

$$R = \frac{v \cdot t}{2} \tag{2.2}$$

where:

- R : the range;
- v : the speed of the electromagnetic radiation;
- t : the measured time interval.

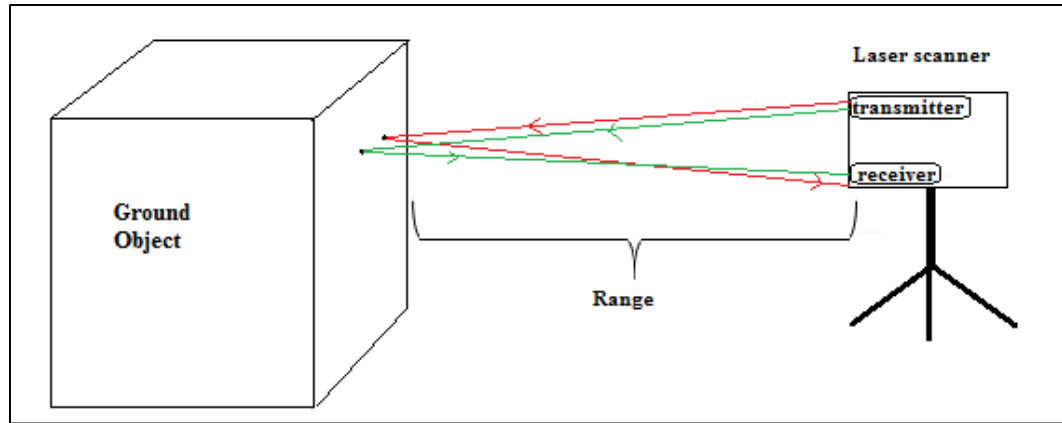


Figure 2.3. Schematic representation of a TOF system

2.2.1.2 Phase-Shift Systems

A phase-shift laser scanner works in a fashion similar to TOF systems. Phase-shift systems send waves and receive them; and the change of the phase is measured (Figure 2.4). The range is computed using the number of wavelengths, the phase-shift angle between the transmitted and received signal (Equation 2.3) (Petrie and Toth, 2009).

$$R = \frac{M\lambda + \Delta\lambda}{2} \quad (2.3)$$

where:

- R : the range;
- M : the integer number of wavelengths;
- λ : the wavelength;
- $\Delta\lambda = \frac{\varphi}{2\pi}$: the fractional part of the wavelength: φ is the phase angle.

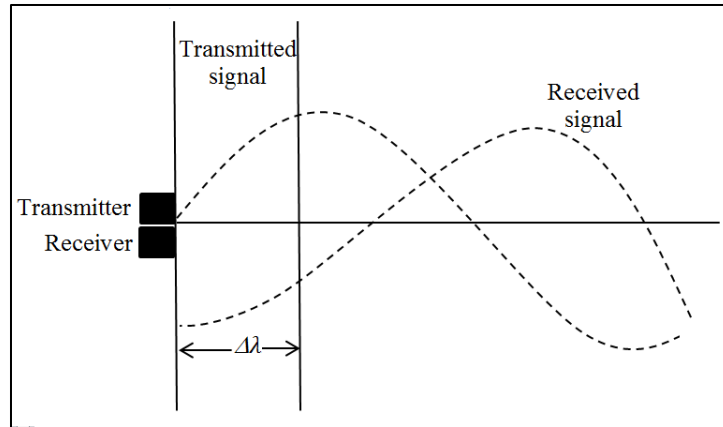


Figure 2.4. Example of a phase-shift system (source: Petrie and Toth, 2009)

2.2.1.3 Triangulation-based Systems

Triangulation-based systems consist of at least two sensors (Figure 2.5). A laser line or point is projected onto an object, and the reflection of the laser is captured with a camera sensor located at a known distance from the laser source. The angle, which results from the reflection, can be interpreted to provide 3D measurements of the object. This method is known as triangulation since the laser dot, the camera, and the laser transmitter are used (Bogue, 2010).

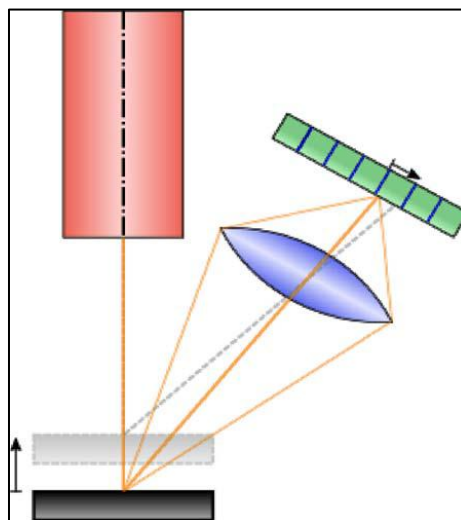


Figure 2.5. Laser triangulation system (source: Bogue, 2010)

2.4 Photogrammetry vs. Laser Scanning

Photogrammetry and laser scanning are the two main technologies for 3D data acquisition. Both technologies have advantages and disadvantages. The advantages of laser scanning technology compared to photogrammetry are listed in Table 2.1 (Habib, 2007).

One of the most important advantages of laser scanning is the direct acquisition of 3D coordinates. On the other hand, obtaining 3D information is a time consuming and sometimes complicated process in photogrammetry. Another main difference between the two systems is that laser scanning can collect data any time of the day because it has an active sensor, which means that it produces its own energy, while photogrammetric instruments (cameras) are passive sensors that are only able collect data during the daytime. Some other advantages of laser scanning are shown in Table 2.1.

Table 2.1. Laser scanning pros and photogrammetry cons

Laser Scanning (Pros)	Photogrammetry (Cons)
Dense information along homogeneous surfaces	Almost no positional information along homogeneous surfaces
Day or night data collection	Day time data collection only
Direct acquisition of 3D coordinates	Complicated and sometimes unreliable matching procedures
The vertical accuracy is better than the planimetric accuracy	The vertical accuracy is worse than the planimetric accuracy

Table 2.2 shows the advantages of photogrammetry compared to laser scanning technology. The main advantage of photogrammetry is its high redundancy, which means that reconstructed surfaces by photogrammetry can be accurately derived because of the inherent redundancy. In addition, photogrammetry is rich in semantic information and

has color information. Another advantage of photogrammetry is that it is cheaper technology than laser scanning, especially for close range applications. Some other advantages of photogrammetry are shown in Table 2.2 (Habib, 2007).

Table 2.2. Laser scanning cons and photogrammetry pros

Laser Scanning (Cons)	Photogrammetry (Pros)
No inherent redundancy	High redundancy
Positional information; difficult to derive semantic information	Rich in semantic information
Almost no positional information along break lines	Dense positional information along object space break lines
The planimetric accuracy is worse than the vertical accuracy	The planimetric accuracy is better than the vertical accuracy
Data collection takes time	Data collection is very fast
Instruments are expensive	Instruments are sometimes inexpensive especially for terrestrial photogrammetry

As can be seen in Tables 2.1 and 2.2, laser scanning and photogrammetry's advantages and disadvantages complement each other. Therefore, researchers have focused on studies which combine the two technologies (e.g., photogrammetry is integrated with scans for more accurate 3D modeling, improving the geometry of the model, and/or color coding of laser points).

2.5 Registration

3D models can be obtained with laser scanning technology. Large areas (i.e., urban modeling, forestry modeling) can be modeled in 3D using airborne laser scanning data (LiDAR data). The large-scale data are collected with a laser scanner mounted on an aircraft. On the other hand, terrestrial laser scanning is generally used for 3D modeling of

structures. Since an airborne laser scanner can collect the 3D data of large areas, one scan might be sufficient to portray the area of interest. However, it is not possible to cover a structure with a single TLS scan in many cases. Therefore, several TLS scans are necessary to obtain complete coverage of the surveyed structures. Each TLS scan has its own coordinate system; and in order to obtain a meaningful 3D model of the structure in question, transformation of the collected scans into a common coordinate system is necessary. The alignment of the collected TLS scan in a common reference frame is known as “registration.”

The registration paradigm has four elements, which are the primitives, the transformation function, the similarity measure, and the matching strategy. The elements of the registration paradigm are discussed in the following sub-sections.

2.5.1 Registration Primitives

After acquiring datasets for 3D modeling, it is necessary to decide which types of primitives will be used to relate the TLS scans’ coordinate systems and to estimate the transformation parameters using conjugate primitives in different scans. The most often used registration primitives for the photogrammetric data and the TLS scans can be classified into three groups: point, linear, and planar (areal) features.

For photogrammetric studies, point primitives are commonly used because points are easily identified in images. Since photogrammetric data are acquired from continuous and regular scanning of the object space (Shin et al., 2007), it is easy to find and select a distinct point in an image (Figure 2.6a). On the other hand, the identification of a specific

point in a TLS scans is difficult and unreliable since the scan's footprints are irregularly-distributed (Habib et al., 2008). Figure 2.6b illustrates that it is not possible to pick a distinct point from a TLS scan, which can be identified in the image. The 3D centers of signalized geometric targets (i.e., circles and spheres) can be used as point primitives for the scans (Lichti and Skaloud, 2010). However, placement of the signalized targets might be difficult and harmful for the surveyed buildings (i.e., historical buildings).

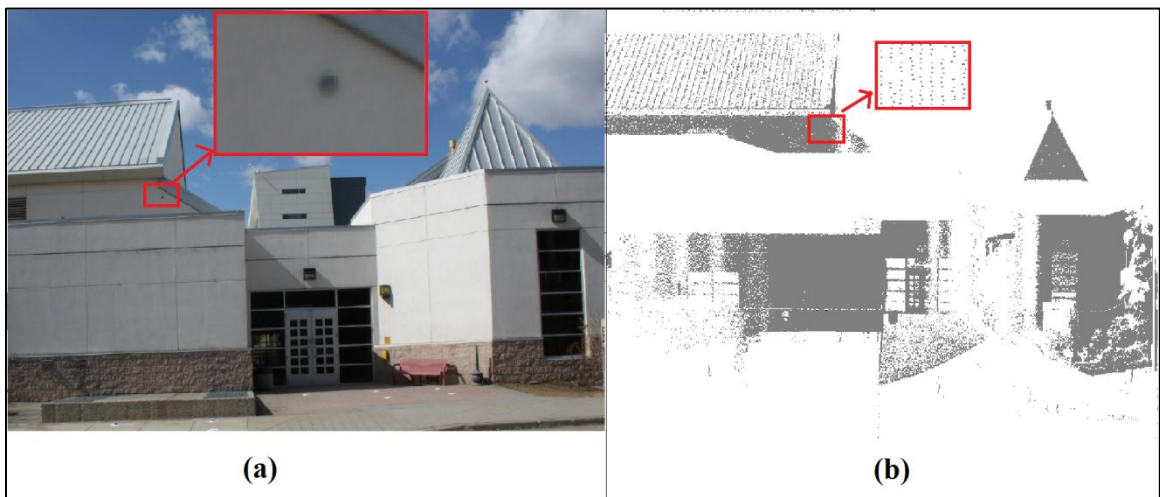


Figure 2.6. Point primitives in photogrammetric data (a), original TLS scan points (b)

Another most often used primitive in photogrammetry and laser scanning technologies is planar features. Planar features can be represented in the photogrammetric and laser scanning data by selecting points along the plane. As can be seen in Figure 2.7a, man-made structures commonly have planar features. The corresponding planar features from imagery (Figure 2.7a) can be easily found in TLS scans after a segmentation process (Figure 2.7b). Therefore, planar features are one of the most often chosen primitives for both data types. Jaw and Chaung (2008) and Dold and Brenner (2006) are example

studies of planar feature-based registration of TLS scans. These studies are explained more fully in the following sections.



Figure 2.7. Planar features in photogrammetric data (a) and TLS scan (b)

Linear features are also suitable for both photogrammetric and laser scanning applications. Figure 2.8 illustrates linear features in photogrammetric data and TLS scan. Linear features was chosen as the registration primitive to estimate the transformation parameters by several authors (e.g., Jaw and Chaung, 2008; Renaudin et al., 2011; and Guan and Zhang, 2011). Linear features in photogrammetric studies are generally represented in object space (3D) with two points (X_1, Y_1, Z_1) & (X_2, Y_2, Z_2) , which are the beginning and ending points of the feature. Similarly, linear features in TLS scans, which are usually extracted from the intersection of two neighboring segmented planar features, are also defined by beginning and ending points. The conjugate linear features are then used to estimate the registration parameters.

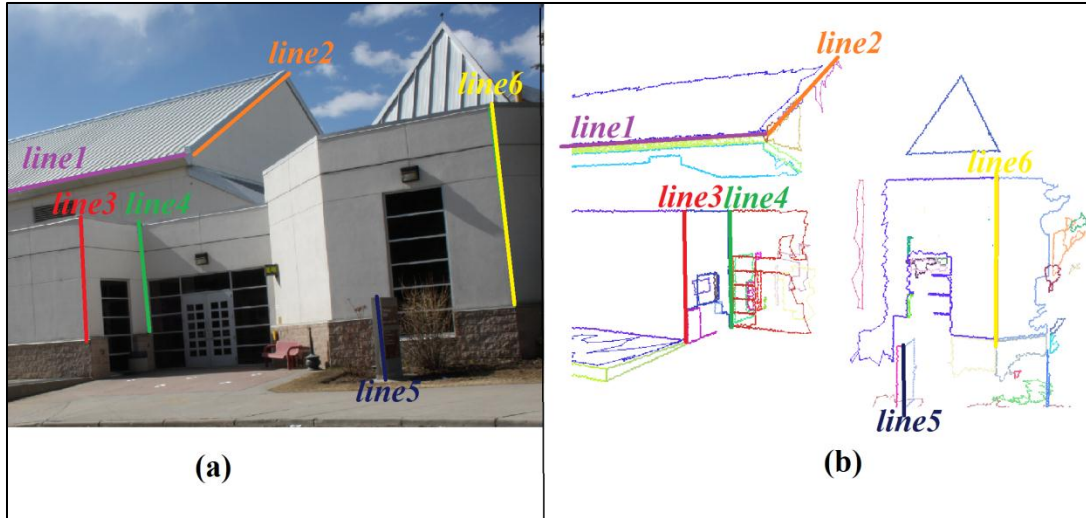


Figure 2.8. Linear Features in photogrammetric data (a) and TLS scan (b)

In contrast to the points, planar and linear features are easy to identify in both TLS scans and photogrammetric data. Moreover, artificial structures commonly have these features. Therefore, planar and linear features were chosen as the primitives for the proposed registration method in this research.

2.5.2 Transformation Function

The second paradigm element of a registration process is establishing a transformation function. The transformation function mathematically describes the relations of the TLS scans and the reference coordinate systems. TLS scans generally have true scale. Only six transformation parameters of the TLS scans (three rotations and three translations) need to be estimated if the reference frame is chosen as one of the scans' coordinate system. Thus, the 3D rigid transformation function is generally used for estimating the six transformation parameters. If the scale parameter needs to be estimated with the other six

parameters, the 3D similarity transformation function can be used to estimate the seven transformation parameters.

2.5.3 Similarity Measure

The third element of the registration paradigm is the similarity measure. After a decision is made on the type of registration primitives and the transformation function, the next step is selection of the similarity measure. The similarity measure defines the constraints, which is necessary to ensure the correspondence of the conjugate primitives (Al-Ruzouq, 2004). The similarity measure formulation depends on the representation scheme of the involved parameters (Renaudin et al., 2011).

2.5.4 Matching Strategy

"Matching can be defined as the establishment of the correspondence between different coordinate systems" (Al-Ruzouq, 2004). The matching strategy can be considered as the framework to solve the matching problem. Therefore, the matching strategy includes the registration primitives, the transformation function, and the similarity measure.

In summary, the registration paradigm consists of four elements, which were discussed in the previous sections. All these steps should be carefully decided and prepared for establishing a registration algorithm. Thus, the collected TLS scans can be registered with the proposed algorithm to produce a meaningful shape for the surveyed structure. Figure 2.9 shows the original four TLS scans of a surveyed building, before and after registration of the scans. As shown in Figures 2.9a, b, c, and d, every TLS scan has its own coordinate system. Before transformation of the TLS scans into a common

coordinate system, all of the TLS scans together do not make any meaningful sense (Figure 2.9e). However, after applying the estimated transformation parameters to the TLS scans, the 3D model of the structure is perceived (Figure 2.9f).

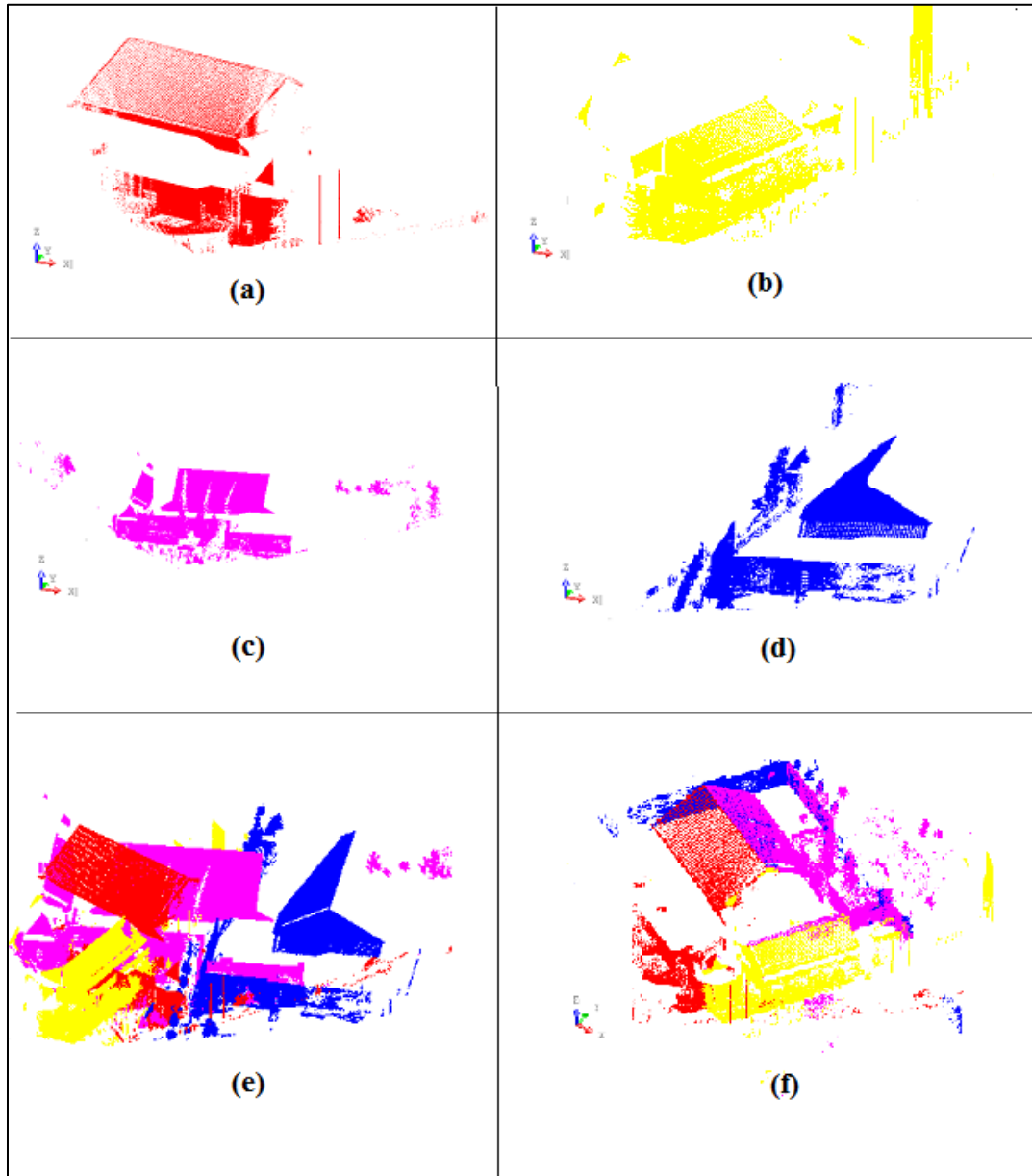


Figure 2.9. Original TLS scan1 (a), TLS scan2 (b), TLS scan3 (c), and TLS scan4 (d); four TLS scans together before registration (e) and after registration (f)

2.6 Registration Methods

Many different registration methods for 3D data have been developed and improved in the last two decades. The main methods can be categorized in three main groups:

- 1- using all available points of the TLS scans (ICP methods and its variants);
- 2- using different registration primitives (feature-based registration); and
- 3- using photogrammetric data to register TLS scans with different primitives.

GPS/INS or the inertial measurement unit (IMU) can be used to geo-reference the scans, which implicitly solves the registration problem. Usage of such systems also might be categorized as another registration group. However, direct geo-referencing is not a commonly used method for ground-based registration studies due to the high cost of the instruments. An example of such a study was established by Talaya et al. (2004) where laser scans were oriented directly in the reference coordinate system by GPS/IMU sensors mounted with a laser scanner on a moving vehicle.

2.6.1 Iterative Closest Point Registration Method and its Variants

The well-known method for the registration of 3D point cloud data is iterative closest point (ICP), which was developed by Besl and McKay (1992). The ICP method uses all of the available points within the data, and it works based on point-to-point correspondence. Basically, the sum of squares of the Euclidean distances between the nearest points of two data sets “ q_i and p_i ” is minimized (Equation 2.4; Lichti and Skaloud, 2010).

$$\sum_{i=1}^n \|R(q_i) + q_0 - p_i\|^2 \quad (2.4)$$

where:

- q_i and p_i : the given two sets points in R^3 ;
- R : the rotation matrix defined by the rotation angles between given two data sets;
- q_0 : the shift between given two data sets (*translation vector*).

It is also very important that before the closest point calculation, the data sets should be pre-aligned using the initial parameters. In other words, before proceeding to the ICP algorithm, one of the data sets should be transformed to the other data set's coordinate system using good initial transformation parameters. The ICP method is performed iteratively. During each iteration, the transformation parameters are computed and applied to one of the data sets to find the change in the mean square error between the two data sets until Equation 2.4 is minimized. A method similar to ICP was also introduced by Chen and Medioni (1992) in the same year as Besl and McKay (1992). Instead of minimizing the point to point distance between two data sets' points, Chen and Meidoni minimized the points to surface distance.

The ICP method has many modifications in the course of the time needed in terms of selecting and matching points, minimizing the error metric, and accelerating the computation time by organizing points using structures such as Kd-tree. Comparisons of some variants of the ICP method were presented by Rusinkiewicz and Levoy (2001). The following studies are examples of variants of the ICP method.

Bae and Lichti (2008) proposed a robust automated registration method for unorganized point clouds. The method is called Geometric Primitive ICP with RANSAC (GP-ICPR).

A modified RANSAC algorithm is used for outlier removal. The GP-ICPR method is a pair-wise registration, which means that the method registers two point clouds, not simultaneously multiple point clouds. The two point clouds are partially overlapping in their study. The GP-ICPR method first estimates the attributes of geometric primitives such as the surface normal vector, the change of curvature, and the variance angle of the estimated normal vector for each point in the two point clouds. Using the attributes of the geometric primitives, the corresponding primitives in the two point clouds are searched to estimate the registration parameters. The Geometric Primitive-ICP (GP-ICP) method, which is a modification of the Chen and Medioni method and a simplified implementation of the GP-ICPR method without the RANSAC procedure, was also proposed and used to compare results with the GP-ICPR method in their research. The authors proved that GP-ICPR improved the precision.

Habib et al., (2010) developed a registration method using point-to-patch correspondence. They created triangular irregular network (TIN) patches in one of the scans and used a point in another overlapping scan. First, the conjugate point-patch pairs detection process was performed using pairwise data, and estimated transformation parameters were used as the initial parameters for simultaneous registration. The sum of the squared normal distances between the conjugate surfaces' elements was iteratively minimized in a least square adjustment (LSA) procedure for estimating the transformation parameters.

The iterative closest projected point (ICPP) method, which is a novel variant of the ICP method, was developed by Al-Durgham et al. (2011). The ICPP method is considered as

both a point-to-surface and a point-to-point-based registration algorithm. The ICP algorithm requires initial alignment of the point clouds with respect to a common coordinate system. Considering a pair-wise registration where S_1 and S_2 are the two point clouds, a point (p_o) in S_1 first is transformed into the S_2 reference frame using initial approximations to establish the projected point p_t . Using the closest three points (p_1 , p_2 , and p_3) to p_t in S_2 , a triangle surface is created. The centroid of the triangle surface (p_c) is then established. Given a search space threshold with a value of N , the centroid (p_c) is extruded to point p_4 (Figure 2.10a). It should be noted that the centroid can be extruded in two directions; in this case, one of the two directions is selected if the following condition is provided: $p_t \in V(p_1, p_2, p_3, p_4)$. Using the projected point (p_t), the tetrahedron in Figure 2.10a can be split into four different tetrahedrons (Figure 2.10b).

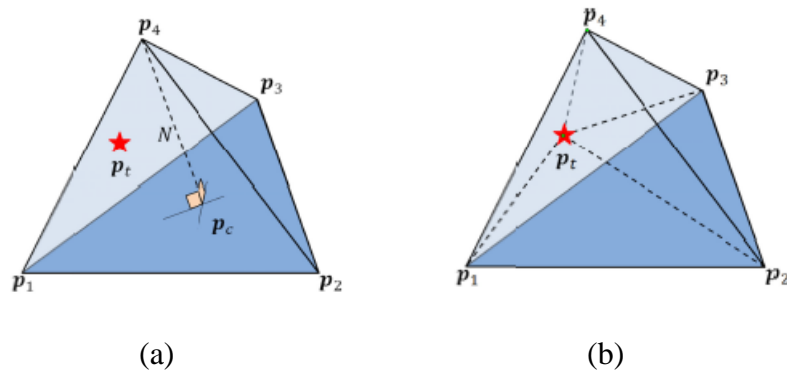


Figure 2.10. Tetrahedron using four points (p_1, p_2, p_3, p_4), the centroid of the three points (p_c), the point (p_t) (a); four splitting tetrahedrons defined by the point (p_t) and (p_1, p_2, p_3 , and p_4) (b) (source: Al-Durgham et al., 2011)

After four tetrahedrons are established using the five points (p_1, p_2, p_3, p_4 , and p_t), the next step is that the point (p_t) is checked as to whether it falls inside the tetrahedron by calculating the determinants of all tetrahedrons ($D1=p_1, p_2, p_3, p_4$; $D2=p_2, p_3, p_4, p_t$; $D3=p_1, p_3, p_4, p_t$; $D4=p_1, p_2, p_4, p_t$; and $D5=p_1, p_2, p_3, p_t$). If all the signs of the determinants

are the same, then the projected point (p_t) is considered as inside the tetrahedron. Finally, the point p_p , which is the projection of the point p_t , is described by Equation 2.5.

$$\begin{bmatrix} x \\ y \\ z \end{bmatrix}_{p_p} = \begin{bmatrix} x \\ y \\ z \end{bmatrix}_{p_t} - \frac{ax_{p_t} + by_{p_t} + cz_{p_t} + d}{a^2 + b^2 + c^2} \begin{bmatrix} a \\ b \\ c \end{bmatrix} \quad (2.5)$$

where;

- a, b, c, d : the plane parameters of the plane derived from p_1, p_2, p_3 ;
- x, y, z : the coordinates of the points p_p and p_t .

The point p_t , and its projection p_p are used as a matching pair between the two data sets. All the possible point-pair matches are then used to estimate the transformation parameters between the two data sets.

In summary, the ICP method has many variants, and they are commonly used for registration of the scans. However, the ICP method requires large overlap areas between data sets and good initial estimation of the transformation parameters; and this is the main disadvantage of the ICP-based methods. Without good initial parameters and large overlapping data sets, the ICP method and its variants might fail to estimate reliable registration parameters. The ICP algorithms use all of the available points in the data sets. Therefore, it is a slow algorithm. During the last decade, instead of using all points, as in the ICP method and its variants, researchers used extracted features as registration primitives. Examples of studies which used different primitives to register the TLS scans are reviewed in the next subsection.

2.6.2 Feature-based Registration Methods

During the last decade, researchers used different geometric primitives (e.g., planes, lines, spheres etc.) to register TLS scans, instead of using all of the available points. For instance, Rabbani et al., (2007) registered scans of an industrial site, which is rich in different geometric features, by extracting and comparing the features of the site. They first detected and extracted different features from the scans, such as cylinders, spheres, planes, etc. Then two different methods were used to register the scans with these extracted features: the direct and indirect methods. One of the scans' coordinate systems was chosen as the world coordinate system for both methods. For the direct method, the sums of squares of the difference between the corresponding extracted features' parameters in different scans were minimized to estimate registration parameters. Then, they used the estimated parameters from the indirect method as the initial approximations for their second method, namely, the direct method. They minimized the sum of squares of the orthogonal distance of the points from their model surfaces to estimate the registration parameters. The direct method produced better registration parameters than the indirect method, while the direct method was slower than the indirect method. Moreover, the direct method required good approximate values so the estimated parameters from the indirect method were used as the initial parameters for the direct method.

Another study in which different primitives were used to register TLS scans was presented by Jaw and Chaung (2008). Point-based, line-based, and planar-based registrations were performed by using the different features individually and also by

combining some of the features. The linear features were established by taking the ending points of the lines for the line-based registration, and the planar features were presented by the normal vector of the planes. Some of the specific corresponding points were used for the point-based registration. After separate usage of the point, linear, and planar features, these features were then combined for registering the scans. According to check point analysis of the results, usage of all of the available features (feature-based registration) produced more reliable registration results than the usage of single features (point-based, line-based, or planar-based registration).

Registration studies using different primitives and photogrammetric data as additional information were focused on and established by many researchers during the last decade. Some examples of registration studies in which photogrammetric data were integrated with TLS scans are reviewed in the next sub-section.

2.6.3 Registration Methods Using Photogrammetric Data

Integration of photogrammetry and laser scanning technologies is possible. Habib et al., (2004) demonstrated the accuracy of integration of LiDAR data and a photogrammetric model. Linear features were preferred as primitives to integrate the LiDAR data and the photogrammetric model, and two experiments were conducted in this study. The first experiment contained planar surfaces. Planar patches were manually identified in the LiDAR data with the help of the images for the first experiment. Taking the intersection of the neighboring planar features, the end points of the linear features were established. The conjugate linear features from the photogrammetric data were extracted using coplanarity constraint in a photogrammetric triangulation procedure for the first

experiment. The second experiment of the study contained cylindrical surfaces. The linear features from the cylindrical surface objects were defined by the centerline of the cylinders' end points from the LiDAR data for the second experiment. The conjugate linear features from the photogrammetric data were extracted by a photogrammetric triangulation procedure. Finally, the transformation parameters between the photogrammetric model and the LiDAR data were estimated with a 3D similarity function by having the conjugate extracted lines' end points from the photogrammetric model and the LiDAR data for the two experiments. The authors proved that the two technologies of photogrammetry and LiDAR could be co-registered accurately.

Since integration of the laser scanning and photogrammetric data is possible as Habib et al. (2004) proved in their study, many researchers have used photogrammetric data as additional information for the surveyed object/structure. For instance, Renaudin et al. (2011) used a photogrammetric model for registering TLS scans with minimum overlap. The linear features were chosen as the registration primitives. Coplanarity constraint was used in the bundle adjustment to extract the linear features from the photogrammetric data, while the linear features from the TLS scan were extracted using a semi-automated process. They identified the planar features and segmented the planes. By taking the intersection of the neighboring segmented planar patches, the linear features were extracted and were represented by their end points. The weight matrix was modified for the end points of the linear features that could not be conjugate in the TLS scans and the photogrammetric model. Finally, the registration parameters were estimated by a point-based 3D similarity function.

Some other researchers used hybrid systems to integrate photogrammetric data and TLS scans for registration purposes. An example of such a system is shown in Figure 2.11. As can be seen in the figure, a camera was mounted on the top of the TLS; and the collected images were used for registering the TLS scans using the estimated mounting parameters between the two systems. These mounting parameters were determined from a prior system calibration process.

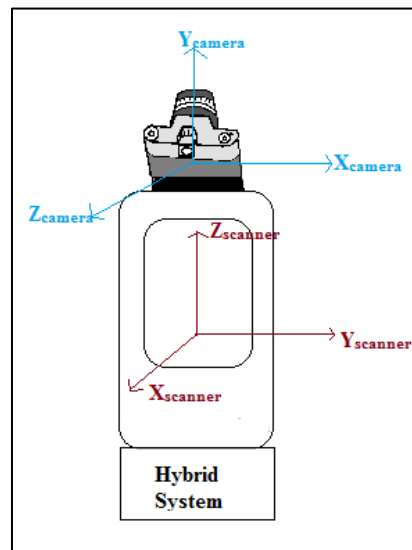


Figure 2.11. Example of a hybrid system: Laser scanner and camera rigidly fixed together

Dold and Brenner (2006) conducted a registration study using a hybrid system. The TLS scans and images were collected by a hybrid system; and the planar features were selected as the registration primitives. Planar patches were extracted automatically from the TLS scans in overlapping areas. First, the registration parameters were estimated using conjugate planar features in the overlapping area. The registered TLS scans' extracted planar patches were then textured automatically by the color information from the collected images using the estimated mounting parameters of the TLS and camera

systems. Moreover, the estimated registration parameters were improved by shifting the planar patches until they fit as much as possible with the texture patches.

Al-Manasir and Fraser (2006) established another example of registration using a hybrid system. Coded targets on the object were used to register TLS scans automatically. After data acquisition with the hybrid system, for each of the collected images, the coded targets were identified, measured, and labeled automatically. Then the targets were automatically estimated in the TLS scans' coordinate system using collinearity equations and the mounting parameters between the TLS and the camera on the hybrid system. After determination of the coded targets in the overlapping TLS scans, the registration parameters were estimated using the point targets within the 3D similarity function.

In summary, it is possible to use a hybrid system for registration purposes. However, it should be noted that a good observation station for collecting a TLS scan might not be a good choice for the photogrammetric data collection (Renaudin et al., 2011).

2.7 Summary

In this chapter, photogrammetry and laser scanning techniques were introduced for acquiring 3D information of objects. Since several TLS scans are necessary to cover the surveyed object, a registration technique must be performed for obtaining a complete 3D model of the surveyed object. Different registration methods are available, some of which were presented in this chapter. The pros and cons of these registration techniques were also discussed.

In this research, a registration method similar to Renaudin et al. (2011) will be presented. The only difference is that, in this research, extraction of the linear features from the TLS scans is fully automated which will be described in more detail in Chapter 3. Moreover, the planar features are also used as registration primitives in this research. A comparison of the usage of planar and linear features for the proposed registration method is presented in Chapter 4.

CHAPTER 3

METHODOLOGY

3.1 Introduction

In this chapter, the proposed registration method is explained in detail. As mentioned in the previous chapters, the main objective of the proposed registration method is to register TLS scans with minimum overlap using a photogrammetric model as additional information. TLS collects the 3D data of objects of interest directly. However, photogrammetric data (images) are in 2D space, and derivation of 3D information from the collected images is necessary in order to integrate them with the TLS scans for registration purposes. Therefore, 3D object space reconstruction from 2D images will be discussed first in this chapter.

Another objective of the proposed registration method is to use different geometric features instead of point, which is a commonly used registration primitive. For the proposed research, planar and linear features are chosen as the registration primitives. These features will be extracted from both the photogrammetric data and the TLS scans. The minimum number and configuration of the planar and linear features requirements to estimate all transformation parameters with the proposed registration method will be explained in this chapter.

Planar features are represented by at least three non-collinear points, while linear features are defined by their beginning and ending points. The points of the corresponding features from the photogrammetric model and the TLS scans are not necessarily

conjugate. Thus, their weight matrices have to be modified for relating the conjugate features. Modifications of such matrices for planar and linear features are described throughout this chapter. The final process of the proposed registration method is to incorporate the extracted features from the photogrammetric model and the TLS scans using 3D similarity transformation. Quality control of the registration will be explained at the end of this chapter.

3.2 3D Object Reconstruction from Photogrammetric Data

The object space reconstruction, which is described in Section 2.1, is possible using conjugate light rays from overlapping images. Therefore, collection of images with good intersecting geometry and large overlapping areas from all around the surveyed objects/structures is an essential step for photogrammetric object space reconstruction.

The object space coordinates of the points (X, Y, Z) are related to the image coordinate observations of the points (x, y) using the collinearity equations (Equation 2.1a and 2.1b). In this research, a digital camera was used for image acquisition, and the points from the digital images, which are in a pixel coordinates system, must be converted into an image coordinate system using Equations 3.1a and 3.1b. (Figure 3.1)

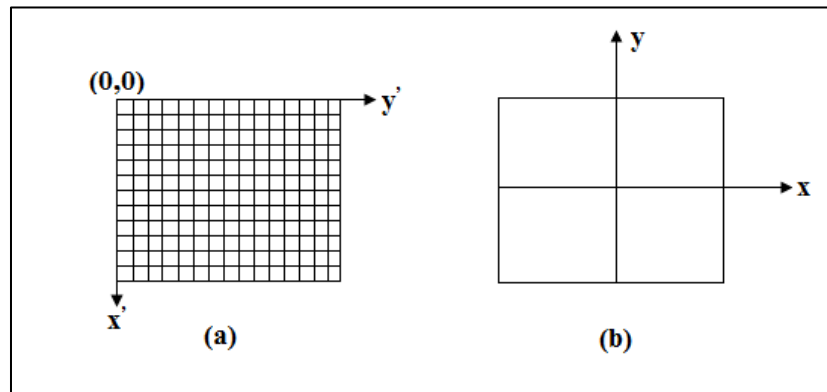


Figure 3.1. Pixel coordinate system (a) versus image coordinate system (b)

$$x = \left(y' - \frac{n_c}{2.0}\right) \times x_{pix_size} \quad (3.1a)^1$$

$$y = \left(\frac{n_r}{2.0} - x'\right) \times y_{pix_size} \quad (3.1b)^1$$

where;

- n_c : the number of columns;
- n_r : the number of rows;
- x_{pix_size} : pixel size along the row direction;
- y_{pix_size} : pixel size along the column direction;
- x and y : the image coordinates;
- x' and y' : the pixel coordinates.

Since the collinearity equations, which are used to relate object and image coordinate system and described in the Section 2.1, assume that the image point, the object point, and the perspective center of the camera are collinear, the camera should be calibrated before data acquisition. As mentioned before, the interior orientation parameters (IOPs), which include the principal point coordinates (x_p , and y_p), the principal distance (c), and the distortions parameters, are estimated through a calibration procedure. Computing the distortion parameters are essential for obtaining straight light rays through the image point, the perspective center, and the object point. The principal point is the projection of the perspective center of the camera onto the image plane. The principal distance is

¹ http://dprg.geomatics.ucalgary.ca/Courses/ENGO667_chapter1

defined as the distance between the principal point and the perspective center of the camera (Figure 3.2).

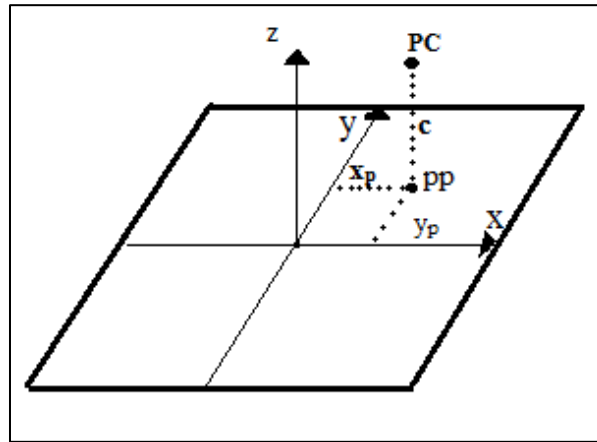


Figure 3.2. Principal distance (c), principal point (pp) and principal point coordinates (x_p and y_p)

Another significant point of photogrammetric object reconstruction is the definition of the datum. Datum can be defined in two ways: 1) using pre-surveyed control points or 2) fixing the object coordinates of certain points and using distance constraints (Detchev, 2010). In this research, the datum is defined arbitrarily by fixing seven coordinates of three well-distributed points within the bundle adjustment procedure. It is essential to define the datum, the image point measurements, and the camera calibration to calculate the unknown parameters with collinearity equations. The unknown parameters, which are the EOPs of the images and the object spaces coordinates of the points, are estimated through a bundle adjustment procedure.

3.3 Feature Extraction

3.3.1 Planar Features Extraction from Photogrammetric Data

A plane is defined as a flat surface. At least three non-collinear points are necessary for defining a plane. Three or four non-collinear points are observed in multiple images and their object space coordinates then are estimated through a bundle adjustment procedure in this research. The reconstructed points from the photogrammetric data define the planes in the 3D model space coordinates. Figure 3.3 is an illustration of the plane points in multiple images.

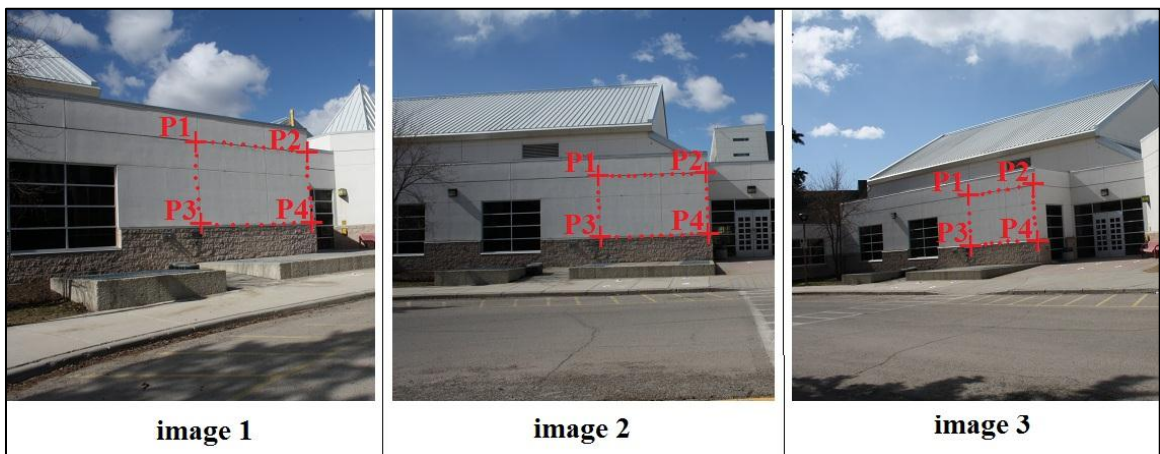


Figure 3.3. Plane points in different images

As illustrated in Figure 3.3, conjugate plane points are available and observed in convergent and overlapping images for object reconstruction. In summary, the 3D points that define planar features are extracted from photogrammetric data through a bundle adjustment procedure.

3.3.2 Linear Features Extraction from Photogrammetric Data

Linear features are extracted from photogrammetric data by adding a coplanarity constraint to the bundle adjustment procedure (Habib et al., 2004; Habib et al., 2007; and Renaudin et al., 2011). The linear features are represented by their beginning and ending points in the object space and a sequence of intermediate points along the represented feature in the image space. The beginning and ending points of the linear features do not need to be identified in several images. These two points can be observed in one image or in two images separately. Various intermediate points along the linear features are essential and can be observed in different overlapping images. The intermediate points need not be conjugate. The observed beginning and ending points in the image coordinates are used in collinearity equations for derivation of these points in the object space. The intermediate points of the line image measurement observations need to be included in the coplanarity constraint within the bundle adjustment procedure. It is worth mentioning again that the observed intermediate points from different images do not need to be conjugate. Equation 3.2 shows the coplanarity constraint used in the bundle adjustment procedure for incorporating the intermediate points of the linear features. Figure 3.4 illustrates the coplanarity constraint. It is also very important to mention that the coplanarity constraint does not introduce any new unknown parameters to the bundle adjustment.

$$(\vec{V}_1 \times \vec{V}_2) \cdot \vec{V}_3 = 0 \quad (3.2)$$

where;

- \vec{V}_1 : the vector connecting the perspective center to the beginning point along the line in object space;
- \vec{V}_2 : the vector connecting the perspective center to the ending point along the line in object space;
- \vec{V}_3 : the vector connecting the perspective center to the intermediate point along the corresponding image line.

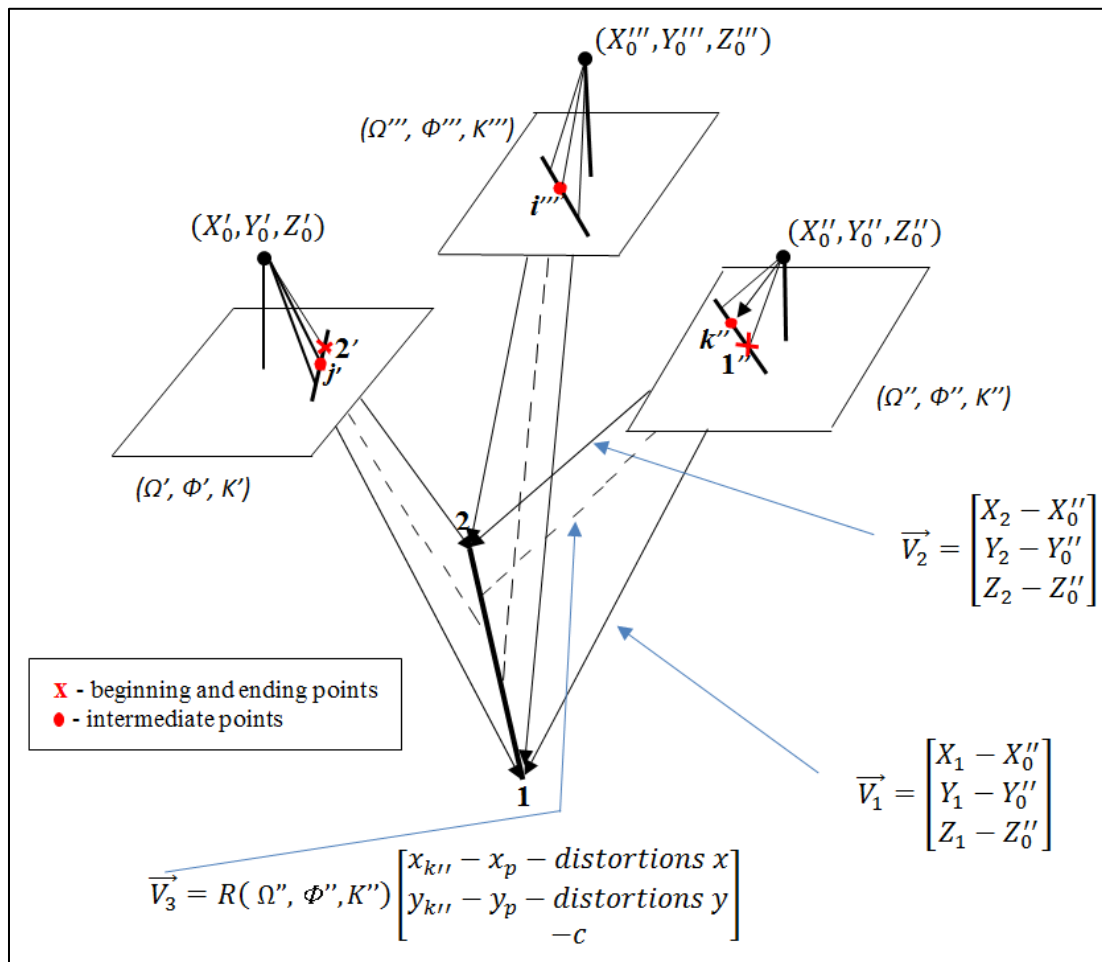


Figure 3.4. Beginning and ending points and intermediate points of a linear feature in image and object space (Adapted from Habib et al., 2004)

3.3.3 Planar Features Extraction from TLS Scans

Points that belong to the same plane can be grouped by a segmentation process in TLS scans. Different planar features can be distinguished by a segmentation process. In this research, a novel segmentation approach, which was presented by Lari et al. (2011), is used. First, the neighborhood of each point is established using an adaptive cylinder in the scans, and then the segmentation attributes are computed based on the defined neighborhood of each point. Finally, clusters of points with similar attributes in the scans are represented by the detected peaks in the array of the estimated attributes (Lari and Habib, 2012).

As previously mentioned, planar features have three or four non-collinear points along the planar surfaces in photogrammetric data. Similarly, three or four non-collinear points from the segmented planes are manually chosen from the TLS scans. The points are not necessarily conjugate to the selected planar points in photogrammetric data. These sets of non-conjugate points along the corresponding planar surfaces are used for the registration process, which will be explained in Section 3.5. Figure 3.5 illustrates the segmented planes in a TLS scan and the photogrammetric data. Different colors represent the segmented planar features in Figure 3.5a.

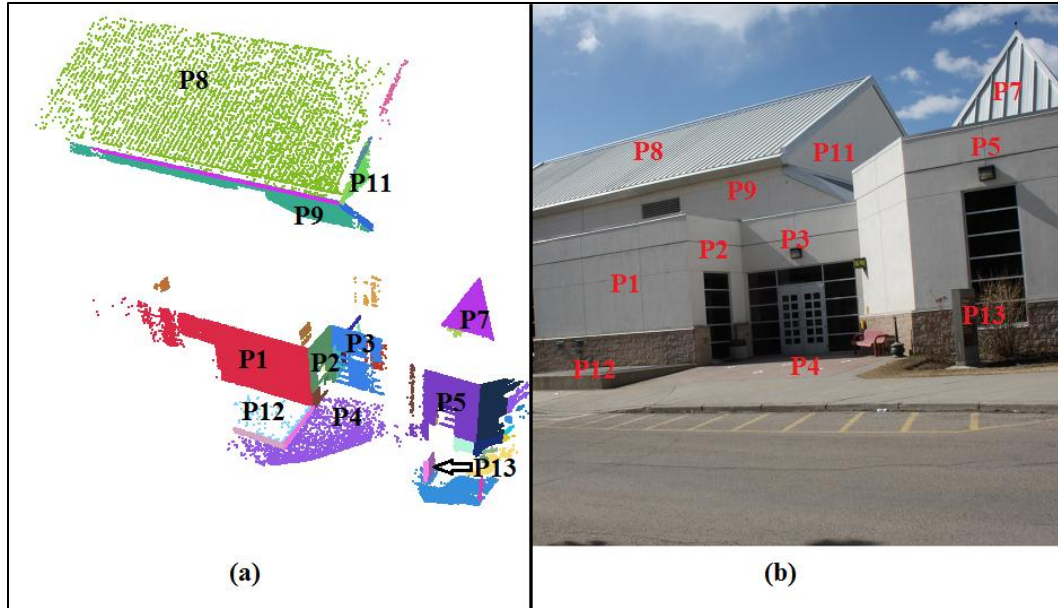


Figure 3.5. Segmented planar features of a TLS scan (a) and a corresponding scene of the scan (b)

3.3.4 Linear Features Extraction from TLS Scans

Linear features are extracted using the segmented planar features from the TLS scans. The intersections of neighboring segmented planes provide infinite lines (Figure 3.6). Linear features are represented by their beginning and ending points in photogrammetric data. Therefore, the beginning and ending points of the infinite lines need to be estimated in the TLS scans. For extracting the beginning and ending points of the infinite line, the extreme points of the line are necessary. To determine the extreme points of the infinite line, points are projected within a certain buffer onto the line segment. Finally the farthest points, which are the beginning and ending points, are selected along the line segment (Al-Durgham, 2007). Figure 3.7 illustrates an example of linear features in a TLS scan and image.

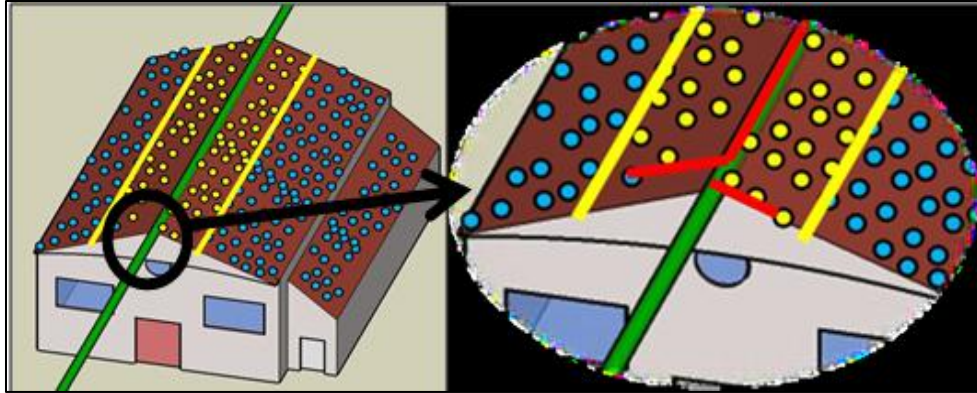


Figure 3.6. Extreme points of an infinite line (source: Al-Durgham, 2007)

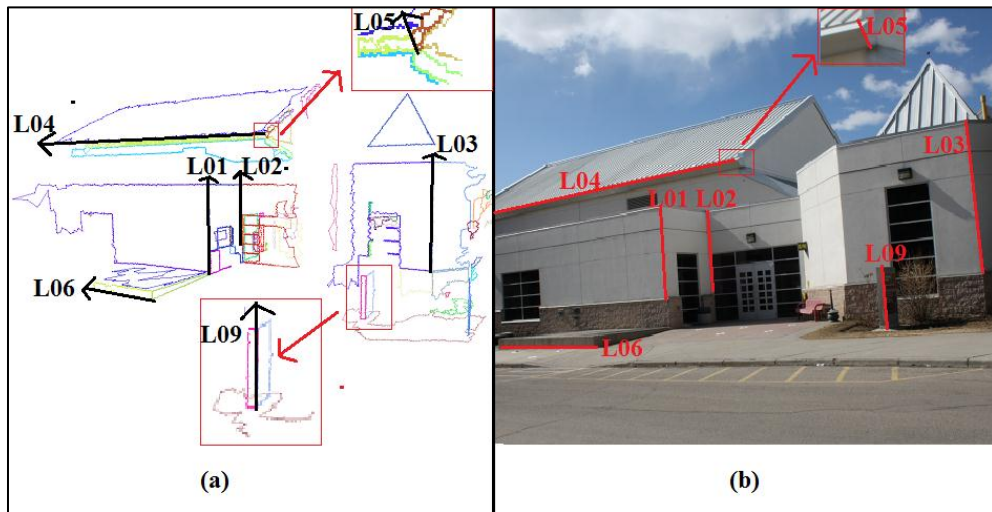


Figure 3.7. Linear features in TLS scan (a) and photogrammetric data (b)

3.4 Similarity Measure

A similarity measure, which is used to incorporate the matched primitives within the transformation function, is described in this section. Since planar and linear features are represented by points, a 3D point-based similarity transformation can be used for relating the observed conjugate features between the photogrammetrically-reconstructed data (PRD)/TLS scans and the global ground coordinate systems (Equation 3.3).

$$\vec{X}_{scan_i/PRD} = \vec{X}_{T_{scan_i/PRD}} + S_{scan_i/PRD} R_{scan_i/PRD} \vec{X}_G \quad (3.3)$$

where;

- The $scan_i$ indicates the i -th TLS scan;

- $\vec{X}_{scan_i/PRD} = \begin{bmatrix} X_{scan_i/PRD} \\ Y_{scan_i/PRD} \\ Z_{scan_i/PRD} \end{bmatrix}$: the observation vector of the points either in the i^{th} -

TLS scan or the photogrammetrically reconstructed data;

- $\vec{X}_{T_{scan_i/PRD}} = \begin{bmatrix} X_{T_{scan_i/PRD}} \\ Y_{T_{scan_i/PRD}} \\ Z_{T_{scan_i/PRD}} \end{bmatrix}$: the translation vector between the either in the i^{th} -

TLS scan or the photogrammetrically reconstructed data and global coordinate system (reference scan);

- $S_{scan_i/PRD}$: the scale factor between the either in the i^{th} -TLS scan or the photogrammetrically reconstructed data and reference coordinate systems;

- $R_{scan_i/PRD} = \begin{bmatrix} r_{11} & r_{12} & r_{13} \\ r_{21} & r_{22} & r_{23} \\ r_{31} & r_{32} & r_{33} \end{bmatrix}$: the rotation matrix relating the either in the i^{th} -

TLS scan or the photogrammetrically reconstructed data and global coordinate systems, defined by the angles: Ω , Φ , and K ;

- $\vec{X}_G = \begin{bmatrix} X_G \\ Y_G \\ Z_G \end{bmatrix}$: the reference coordinate system coordinates.

The total number of unknown parameters between TLS scans, the PRD and the reference (global) coordinate system and the ground coordinates system of the tie points, which are estimated through the 3D similarity function, is equal to following;

$$7 \times n_{scans} + 3 \times n_{tie} + 7.$$

where:

- $7 \times n_{scans}$: “ n_{scans} ” is the number of TLS scans; “7” is the number of the transformation parameters (3 rotations, 3 translations, and the scale);
- $3 \times n_{tie}$: “ n_{tie} ” is the number of tie points; “3” is the unknown ground coordinates (X,Y,Z) for each tie point, which are the points defining the planar and linear features;
- 7 : number of the transformation parameters between the photogrammetric model and the reference scan.

In this research, one of the TLS scans’ coordinate system was chosen as the global coordinate system and the scans have true scale so there was no need to estimate the scale parameter between the TLS scans and the reference scan. Therefore, the total unknown parameters that need to be estimated are:

$$6 \times n_{scans} + 3 \times n_{tie} + 7.$$

The traditional Gauss Markov stochastic model (Equation 3.4) can be used to relate the unknowns and the observations of Equation 3.3.

$$\vec{y} = A\vec{x} + \vec{e} \quad \vec{e} \sim (0, \Sigma) \quad \text{where } \Sigma = \sigma_o^2 P^{-1} \quad (3.4)$$

where:

- \vec{y} : the $n \times 1$ vector of observations ($\vec{X}_{scan_i/PRD}$);

- \vec{x} : the $m \times 1$ vector of unknowns ($X_{T_{scan_i/PRD}}, Y_{T_{scan_i/PRD}}, Z_{T_{scan_i/PRD}}$), (Ω , Φ , and K), ($S_{scan_i/PRD}$), and \vec{X}_G ; three shifts, three rotation angels, the scale, and the ground coordinates of the tie points, respectively;
- A : the $n \times m$ design matrix.
- σ_o^2 : a-priori variance factor;
- P : the weight matrix;
- Σ : the variance-covariance matrix, which is obtained by the product of the a-priori variance factor “ σ_o^2 ” and the inverse of weight matrix “ P ” ;
- \vec{e} :the $n \times 1$ vector of random noise, which is distributed with a zero mean and the variance-covariance matrix “ Σ ” ;

Traditional LSA aims at estimating the unknown parameters. During the LSA procedure, the sum of squares of the weighted residuals is minimized (Equation 3.5, LSA target function). The solution vector can be obtained by Equation 3.6. The predicted residual of the observation vector is represented by Equation 3.7, while the variance-covariance matrix of the solution vector can be obtained by Equation 3.8. Finally, a-posteriori variance factor can be derived by Equation 3.9.

$$\vec{e}^T P \vec{e} = \min |_{\vec{x}} \quad (3.5)$$

$$\vec{\hat{x}} = (A^T P A)^{-1} A^T P \vec{y} = N^{-1} A^T P \vec{y} \quad (3.6)$$

$$\vec{e} = \vec{y} - A \vec{\hat{x}} \quad (3.7)$$

$$\Sigma\{\vec{\hat{x}}\} = \hat{\sigma}_o^2 (A^T P A)^{-1} = \hat{\sigma}_o^2 N^{-1} \quad (3.8)$$

$$\hat{\sigma}_o^2 = (\vec{e}^T P \vec{e}) / (n-m) \quad (3.9)$$

Since the points of the corresponding extracted planar and linear features from the TLS scans and PRD are not necessarily conjugate to each other, the traditional LSA procedure, which is described above, cannot be used for the estimation of transformation parameters. Therefore, traditional LSA procedure needs to be modified (Renaudin et al., 2011; Habib et al, 2011; Kersting, 2012). Illustrations of the non-conjugate points in planar and linear features between TLS scan/PRD and global coordinate systems are represented in Figures 3.8 and 3.9, respectively.

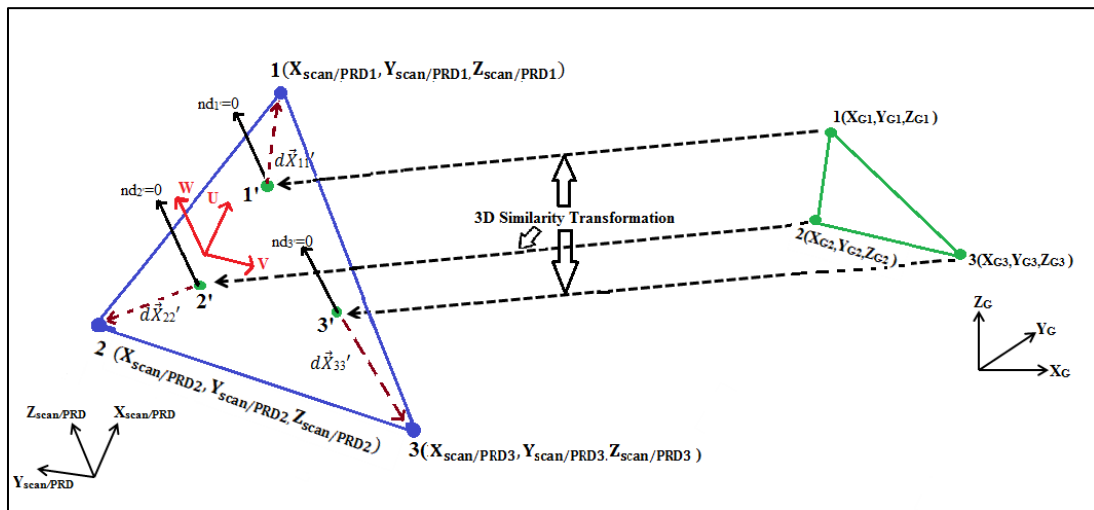


Figure 3.8. Non-conjugate points defining the plane in different coordinate systems

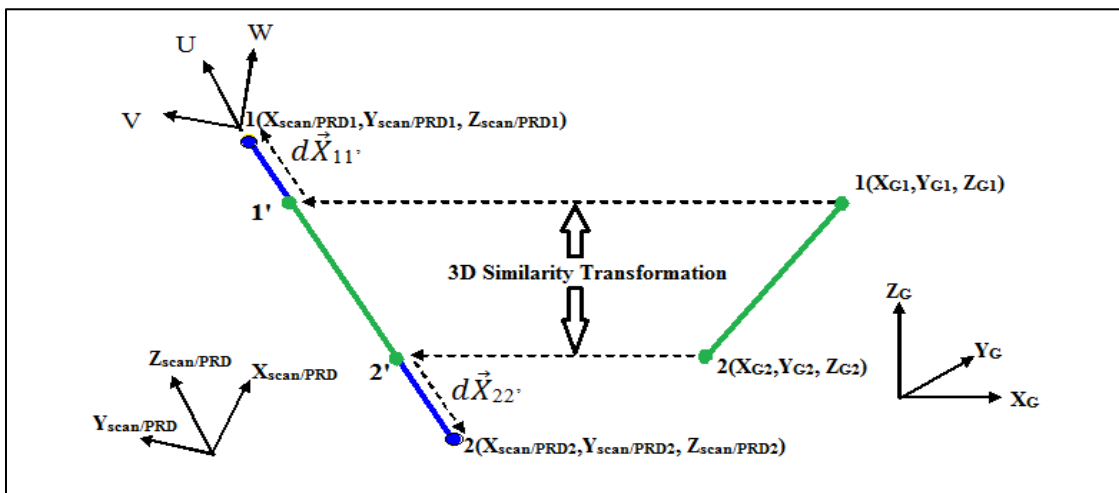


Figure 3.9. Non-conjugate points defining the line in different coordinate systems (Adapted from Renaudin et al., 2011)

In the following equations, modifications of the traditional Gauss Markov stochastic model are represented. The 3D similarity transformation (Equation 3.3) can be modified as in Equation 3.10 for the non-conjugate points of the features in different coordinate systems.

$$\vec{X}_{scan_i/PRD} = \vec{X}_{T_{scan_i/PRD}} + S_{scan_i/PRD} R_{scan_i/PRD} \vec{X}_G + d\vec{X} \quad (3.10)$$

The Gauss Markov stochastic model is modified as in Equation 3.11

$$\vec{y} = A\vec{x} + d\vec{X} + \vec{e} \quad \vec{e} \sim (0, \Sigma) \quad (3.11)$$

As can be seen, the difference between Equations 3.3 and 3.10, and Equations 3.4 and 3.11 is that additional unknown $d\vec{X}$, which is a vector resulting from the non-conjugate points of the corresponding features, is added to Equations 3.10 and 3.11 (see Figures 3.8 and 3.9).

In the following equations, the LSA is modified to eliminate unknown vector $d\vec{X}$ from the estimated parameters. The stochastic properties of the random noise vector can be changed as follows:

$$\Sigma\{\vec{e}\} = \sigma_o^2 P'^+ \quad \text{where;} \quad P' d\vec{X} = 0 \quad P' : \text{the new weight matrix.} \quad (3.12)$$

As can be seen in Equation 3.12, the unknown vector $d\vec{X}$ belongs to the null space of the weight matrix P' , which means that the inverse of the matrix does not exist. The plus sign of the new weight matrix (P'^+) is the indication of the Moore-Penrose pseudo inverse (Koch, 1988). The LSA target function can be modified by using the modified weight matrix as in the following Equation 3.13a. Equation 3.13a can be reduced to the form as in Equation 3.13b because multiplication of the modified weight matrix (P') and the

unknown vector ($d\vec{X}$) is equal to zero (Equation 3.12). Finally, Equation 3.14 is the estimated unknowns (refer to Appendix A for the detailed derivation). Equation 3.15 shows the variance-covariance matrix for the solution vector.

$$\vec{e}^T P \vec{e} = (\vec{y} - A\vec{x} - d\vec{X})^T P' (\vec{y} - A\vec{x} - d\vec{X}) = \min_{|\vec{x}, d\vec{X}} \quad (3.13a)$$

$$\vec{e}^T P \vec{e} = (\vec{y} - A\vec{x})^T P' (\vec{y} - A\vec{x}) = \min_{|\vec{x}} \quad (3.13b)$$

$$\vec{\hat{x}} = (A^T P' A)^{-1} A^T P' \vec{y} = N^{-1} A^T P' \vec{y} \quad \text{where; } N = A^T P' A \quad (3.14)$$

$$\Sigma\{\vec{\hat{x}}\} = \sigma_o^2 N^{-1} \quad (3.15)$$

Finally, a-posteriori variance factor can be derived through the following Equations 3.16-3.18 (refer to Appendix A for the detailed derivation). q is the rank of the modified weight matrix P' and m is the number of unknowns.

$$E(\vec{e}^T P' \vec{e}) = E\{(\vec{y} - A\vec{x} - d\vec{X})^T P' (\vec{y} - A\vec{x} - d\vec{X})\} \quad (3.16)$$

$$E(\vec{e}^T P' \vec{e}) = E\{(\vec{y} - A\vec{x})^T P' (\vec{y} - A\vec{x})\} = (q - m)\sigma_o^2 \quad (3.17)$$

$$\sigma_o^2 = (\vec{y} - A\vec{x})^T P' (\vec{y} - A\vec{x}) / (q - m) \quad (3.18)$$

In summary the modified LSA stochastic model is shown in the following equation;

$$\vec{y} = A\vec{x} + d\vec{X} + \vec{e} \quad \vec{e} \sim (0, \Sigma') \quad \text{where } \Sigma' = \sigma_o^2 P'^+ \quad \text{and } P' d\vec{X} = 0 \quad (3.19)$$

P' is the weight matrix which needs to be derived for the planar and linear features. The following subsections describe the derivation of the weight matrix (P') for the planar and linear features, respectively.

3.4.1 Modification of the Weight Matrix for Planar Features

A local coordinate system of the plane (UVW) is first defined. U and V are the axes along the plane in question; W axis is parallel to plane normal (Figure 3.10).

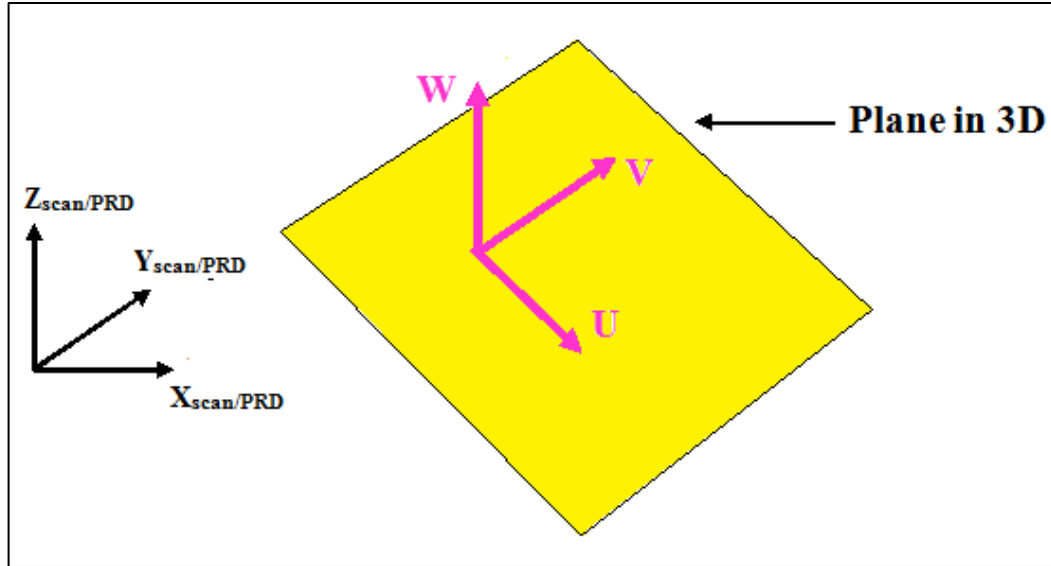


Figure 3.10. Relation between the scans/PRD and the plane coordinate systems

Equation 3.20 shows the relationship between local (UVW) and the scans/PRD coordinate system $(XYZ)_{scan/PRD}$. The M matrix is defined by the components of the unit vectors \vec{u} , v , and \vec{w} along the UVW axes (see Figure 3.11).

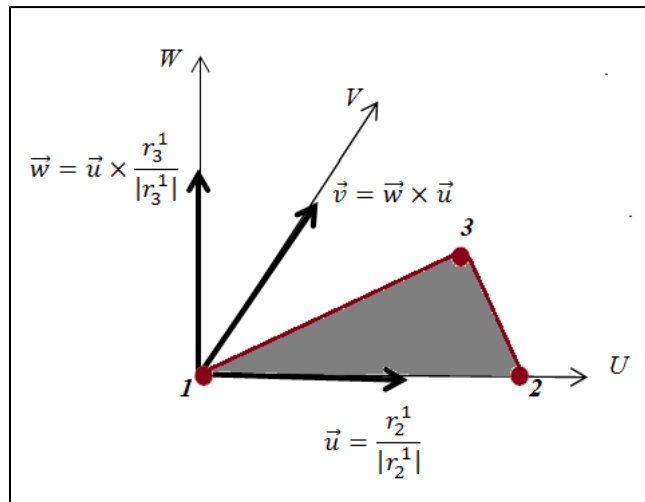


Figure 3.11. Local UVW coordinate system for a plane (Adapted from Kersting, 2011)

$$\begin{bmatrix} U \\ V \\ W \end{bmatrix} = M \begin{bmatrix} X \\ Y \\ Z \end{bmatrix} \quad (3.20)$$

where;

$$- \quad M = \begin{bmatrix} U_x & U_y & U_z \\ V_x & V_y & V_z \\ W_x & W_y & W_z \end{bmatrix} : \text{the matrix between the two coordinate system}$$

The original weight matrix, which is defined by the inverse of the variance-covariance matrix of measured/derived tie points, is represented in Equation 3.21. In Equation 3.22, P_{uvw} , which is the weight matrix in the local coordinate system, is derived by using the law of error propagation. The weight matrix is then modified as in Equation 3.23 by assigning zero values for the weights along the plane. The final step for the modified weight matrix is to establish it in the XYZ system (P'_{XYZ} , Equation 3.24) (Kersting, 2011).

$$P_{XYZ} = \Sigma_{XYZ}^{-1} \quad (3.21)$$

$$P_{UVW} = MP_{XYZ}M^T = \begin{bmatrix} P_U & P_{UV} & P_{UW} \\ P_{VU} & P_V & P_{VW} \\ P_{WU} & P_{WV} & P_W \end{bmatrix} \quad (3.22)$$

$$P'_{UVW} = \begin{bmatrix} 0 & 0 & 0 \\ 0 & 0 & 0 \\ 0 & 0 & P_W \end{bmatrix} \quad (3.23)$$

$$P'_{XYZ} = M^T P'_{UVW} M \quad (3.24)$$

As previously mentioned, the multiplication of the modified weight matrix (P') and the unknown vector ($d\vec{X}$) is equal to zero and is shown in Equation (3.25). In this equation, dX , dY , and dZ are the components of the unknown vector ($d\vec{X}$) with respect to the (w.r.t) XYZ system. On the other hand, dU , dV , and dW represent the components of the

unknown vector ($d\vec{X}$) w.r.t the UVW system. dW is assigned to zero since the non-conjugate points lie on the same plane (Kersting, 2011).

$$P'_{XYZ} d\vec{X} = M^T P'_{UVW} M \begin{bmatrix} dX \\ dY \\ dZ \end{bmatrix} = M^T P'_{UVW} \begin{bmatrix} dU \\ dV \\ dW \end{bmatrix} = M^T \begin{bmatrix} 0 & 0 & 0 \\ 0 & 0 & 0 \\ 0 & 0 & P_W \end{bmatrix} \begin{bmatrix} dU \\ dV \\ 0 \end{bmatrix} = 0 \quad (3.25)$$

3.4.2 Modification of the Weight Matrix for Linear Features

As was done for the planar features, the local coordinate system (UVW) is defined for the linear features. The U axis is defined along the line in question. Figure 3.12 illustrates the line and scan/PRD coordinate systems.

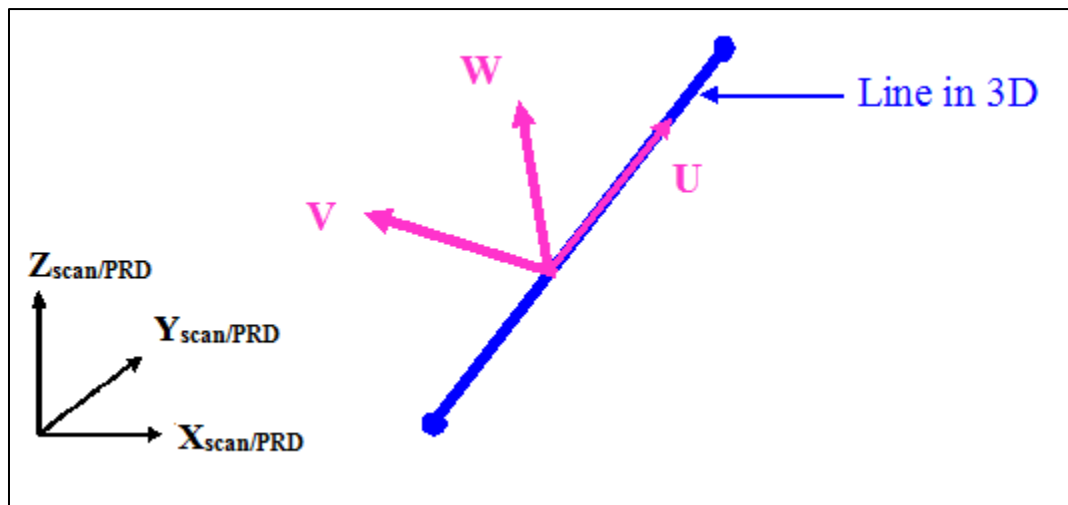


Figure 3.12. Relation between the scans/PRD and the line coordinate systems

Equation 3.26 shows how the scans/PRD coordinate system $(XYZ)_{scan/PRD}$ and the local coordinate system (UVW) are related. The M matrix is defined by using the end points of the linear features. Equation 3.27 represents the original weight matrix, which is defined by the inverse of the variance-covariance matrix of measured/derived tie points. P_{uvw} can be derived by using the law of error propagation (Equation 3.28). The weight matrix can

be modified as in Equation 3.29 by assigning a zero value for the weights along the line. Finally, the modified weight matrix P'_{XYZ} , which is in the XYZ coordinate system can be derived using Equation 3.30 (Renaudin et al., 2011).

$$\begin{bmatrix} U \\ V \\ W \end{bmatrix} = M \begin{bmatrix} X \\ Y \\ Z \end{bmatrix} \quad (3.26)$$

where;

$$- \quad M = \begin{bmatrix} U_x & U_y & U_z \\ V_x & V_y & V_z \\ W_x & W_y & W_z \end{bmatrix} : \text{the matrix between two coordinate system.}$$

- where, U is the axis along the line in question.

$$P_{XYZ} = \Sigma_{XYZ}^{-1} \quad (3.27)$$

$$P_{UVW} = MP_{XYZ}M^T = \begin{bmatrix} P_U & P_{UV} & P_{UW} \\ P_{VU} & P_V & P_{VW} \\ P_{WU} & P_{WV} & P_W \end{bmatrix} \quad (3.28)$$

$$P'_{UVW} = \begin{bmatrix} 0 & 0 & 0 \\ 0 & P_V & P_{VW} \\ 0 & P_{WV} & P_W \end{bmatrix} \quad (3.29)$$

$$P'_{XYZ} = M^T P'_{UVW} M \quad (3.30)$$

In the following equation (3.31), it is shown that $P' d\vec{X} = 0$ for the linear features. In this equation, dV and dW are assigned as zero since the non-conjugate points lie on the same line (Figure 3.9).

$$P'_{XYZ} d\vec{X} = M^T P'_{UVW} M \begin{bmatrix} dX \\ dY \\ dZ \end{bmatrix} = M^T P'_{UVW} \begin{bmatrix} dU \\ dV \\ dW \end{bmatrix} = M^T \begin{bmatrix} 0 & 0 & 0 \\ 0 & P_V & P_{VW} \\ 0 & P_{WV} & P_W \end{bmatrix} \begin{bmatrix} dU \\ 0 \\ 0 \end{bmatrix} = 0 \quad (3.31)$$

3.5. Number and Configuration of Required Features for the Proposed Registration

Method

Artificial structures are rich in planar and linear features. More features lead to more reliable results for the proposed registration method. If there are not enough features, the method may fail. In this section, the minimum required number and the orientation of features to estimate the registration parameters are introduced for the planar and linear feature-based registration techniques.

As previously described, the surveyed structure's TLS scans, whose coordinate systems are different from each other, have to be transformed into a common (reference) coordinate system for deriving a 3D model. One of the TLS scans of the surveyed structure was selected as the reference coordinate system in this research. Since a TLS scan provides true scale, only three translations and three rotations parameters need to be estimated between the coordinate systems of the scans and the reference scan. On the other hand, the photogrammetric model (or the photogrammetrically reconstructed data (PRD)) and the TLS scans have different scales. Therefore, the scale parameter between the reference frame and the photogrammetric model has to be estimated together with the three rotations and three translations parameters. In total, six transformation parameters between the TLS scans/PRD and the reference frame have to be estimated, while an additional scale parameter is necessary between the photogrammetric model (or PRD) and the reference (TLS scan) frame for registering scans with minimum overlap using a photogrammetric model.

3.5.1 Number and Configuration of Required Planes for the Proposed Planar Feature-Based Registration Method

The orientations of the planes are very crucial for estimating all of the registration parameters. One shift and two rotation parameters can be determined by having one plane. Therefore, to cover three rotations and three orientation parameters between a TLS scan and the reference scan, at least three planes are needed; and these planes should be in different orientations. Furthermore, for the scale parameter between the photogrammetric model and the reference scan, at least one additional plane to the other three planes is needed. Figure 3.13 illustrates an example of the estimated parameters by the different planes.

In summary, at least three planes with different orientations are necessary to solve for three shift and three rotations parameters, while one more plane is needed to solve the scale parameters if it is essential between two coordinate systems. In total, seven transformation parameters can be solved by having at least four planes which do not intersect in a single point. If the four planes intersect in one point, the scale parameter cannot be estimated.

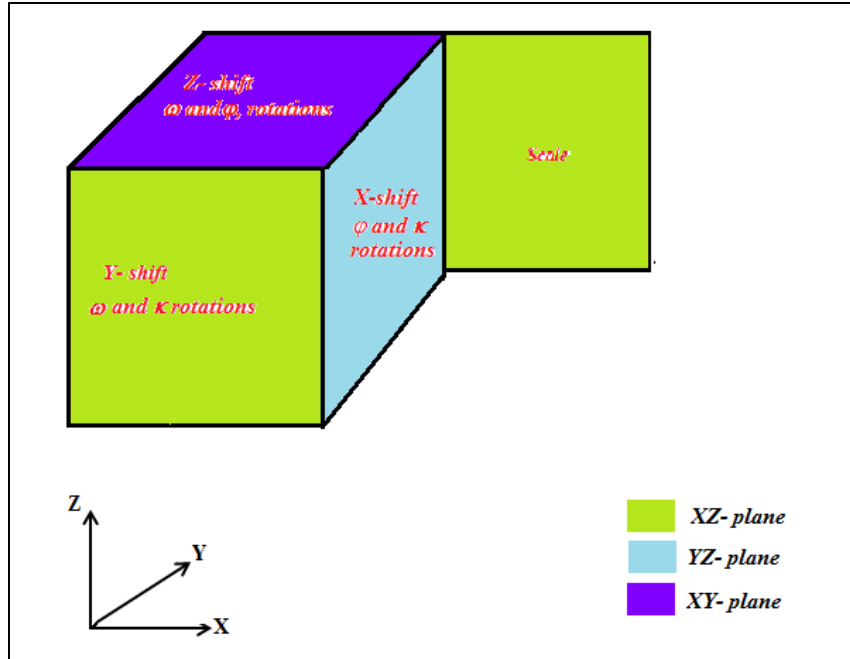


Figure 3.13. An example of planes and their contributions for estimating the transformation parameters

3.5.2 Number and Configuration of Required Lines for the Proposed Linear Feature-Based Registration Method

Two rotation angles and two shifts can be estimated from one linear feature between two coordinate systems. Two linear features, which do not intersect, are also enough to solve for the scale. Therefore, in total, two non-coplanar linear features are necessary to solve for the seven transformation parameters between two different coordinate systems. Figure 3.14 illustrates an example of the minimum number and the orientation of the linear features and the parameters that are estimated by the different linear features.

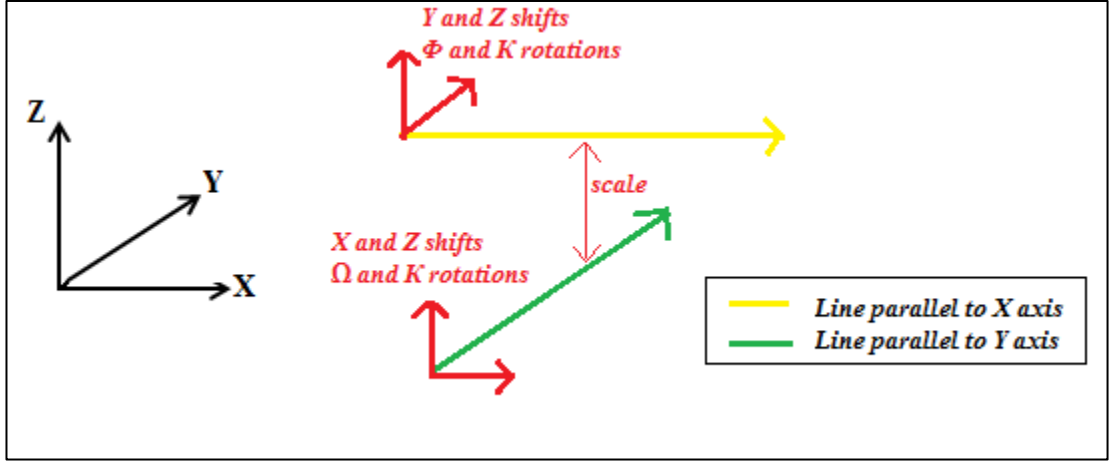


Figure 3.14. An example of lines and their contributions for estimating the transformation parameters

3.5.3 Final Step of the Proposed Registration Method

The unknown parameters $(\vec{X}_T, S, R)_{scan/PRD}$ and \vec{X}_G of ties points are estimated through the LSA procedure. As previously mentioned, one of the TLS scans was chosen as the reference frame. Therefore, during the LSA procedure, the scans and the PRD are rotated, shifted and scaled until they fit the reference scan as well as possible.

The estimated transformation parameters are applied to all the TLS scans for transforming them into the reference coordinate system using Equation 3.32.

$$\vec{X}_G = -\frac{1}{S_{scan_i}} R'_{scan_i} (\vec{X}_{T_{scan_i}} - \vec{X}_{scan_i}) \quad (3.32)$$

where:

- \vec{X}_G : point coordinates in the reference coordinate system;

- $S'_{scan_i} = \frac{1}{S_{scan_i}}$: the scale between the TLS scans and the reference coordinate system. Since one of the TLS scans was chosen as the reference coordinate system and the scans provide true scale, the scale between the scans and the reference coordinate system is equal to 1 in this research;
- $R'_{scan_i} = R_{scan_i}^T$: the rotation matrix between the TLS scans and the reference coordinate system;
- $\vec{X}_{T_{scan_i}}$: the shift between the TLS scans and the reference coordinate system.

3.6 Evaluation of Registration Results

In this section, qualitative and quantitative quality control measures are described.

3.6.1 Qualitative Quality Control

Qualitative quality control is conducted by transforming all of the TLS scans to the reference coordinate system using the estimated registration parameters and plotting them together (Equation 3.32). By examining the registered TLS scans more closely, the quality of the proposed registration method is evaluated. More specifically, if there are any overlapping areas between the TLS scans, they are analyzed in more detail. Since the overlap area is limited in this research, quantitative quality controls of the estimated parameters are necessary. In the next sub-section, the quantitative quality control will be described.

3.6.2 Quantitative Quality Control

Quantitative quality control is performed in two ways. First, the estimated registration results are compared with the ICPP registration method's results. The ICPP method was

described in detail in Chapter 2. It is worth mentioning that additional TLS scans are used for the ICPP method since the ICPP method requires large overlap areas among the scans. Second, the point-to-plane normal distances are calculated between the registered PRD and the TLS scans as well as between some of the scans if possible. The normal distances are calculated as follows.

- 1- The PRD and the TLS scans are transformed into the reference coordinate system using the estimated parameters from the proposed method.
- 2- A segmentation process is applied to the TLS scans, which are in the reference coordinate system.
- 3- The conjugate planes in the TLS scans and the PRD are determined. The parameters (a, b, c, d) of the PRD planes are calculated with four PRD points along the plane (X, Y, Z) using Equation 3.33

$$aX+bY+cZ+d=0 \tag{3.33}$$

- 4- The calculated plane parameters are used together with the points of the conjugate segmented planes from the TLS scans to establish the point-to-plane normal distances between the PRD and the TLS scans.
- 5- The root mean square error (RMSE), the mean, and the standard deviation of the calculated point-to-plane normal distances for each plane are calculated using Equation 3.34, 3.35, and 3.36, respectively.

$$RMSE = \sqrt{\frac{\Sigma(nd)^2}{n}} \quad (3.34)$$

$$mean = \overline{nd} = \frac{\Sigma nd}{n} \quad (3.35)$$

$$Standard\ Deviation = \sigma = \sqrt{\frac{\Sigma(nd - \overline{nd})^2}{n}} \quad (3.36)$$

where;

- nd ; the calculated normal distance between the points within the TLS scans and the PRD planes;
- n ; number of points within a segmented TLS scan.

It should be noted that the segmented planes from the TLS scans and the polygon of the PRD planes generally do not have the same area size. The PRD planes are smaller than the segmented planes from the TLS scans. Therefore, the point-to-plane normal distance in Steps 4 and 5 are performed for the following two scenarios.

- a) All of the points of the segmented planes from the TLS scans are used for normal distance calculation (Figure 3.15 red borders). Some of these points are not inside the vertices of the PRD plane as defined by the yellow polygon.
- b) Also, only the points, which are inside the polygon defining PRD planes, are used for the normal distance calculation (Figure 3.15 yellow borders).

The two scenarios were performed to see whether the results of the point-to-plane normal distances change when the sizes of the conjugate planes area from the PRD and TLS scans are different.

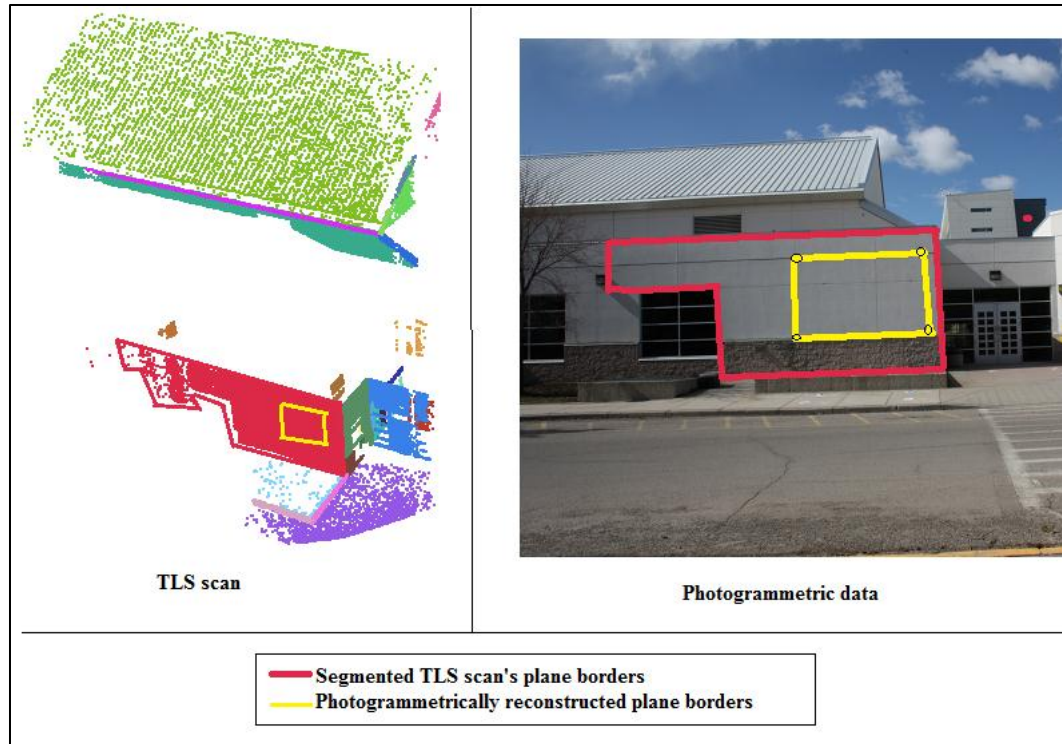


Figure 3.15. Plane borders in the TLS scans versus photogrammetric data

3.7 Summary

In summary, the following four steps were applied to register TLS scans with the proposed method.

- 1- The planar and linear features were extracted from the TLS scans and the photogrammetric data. The linear features are represented by their beginning and ending points, while three or four non-collinear points along the planes are used for planar features representation.
- 2- Since the features are represented by points, a point-based 3D similarity function was used to estimate the transformation parameters through the modified LSA. However, the points of the corresponding planar and linear features might not be conjugate; therefore, their weight matrices and the traditional LSA were modified.

- 3- The TLS scans were transformed into the reference coordinate system using the estimated transformation parameters for establishing the 3D model of the structure.
- 4- Qualitative and quantitative quality controls were performed to evaluate the estimated registration results of the proposed method.

In conclusion, a registration method was proposed to register the TLS scans with minimum overlap using photogrammetric data. Moreover, a quantitative quality control method was proposed for evaluating the registration results by calculating the point-to-plane normal distances between the registered surfaces.

CHAPTER 4

EXPERIMENTAL RESULTS

4.1 Introduction

In this chapter, the experimental results of the proposed registration method for two different data sets are presented, and the results are evaluated qualitatively and quantitatively as well. The planar and linear feature-based registrations were separately performed for the first experiment, while only planar feature-based registration was conducted for the second experiment.

4.2 Experiment I

Rozsa Center, a meeting and conference center at the University of Calgary, was chosen for the first experiment. TLS scans of the building were registered by using photogrammetric data. Many registration methods require large overlap areas between TLS scans; but in this research, the aim is to eliminate/reduce the large overlap area requirement by using photogrammetric data. Additional 3D information about the building was reconstructed from the photogrammetric data in order to use them as a 3D model of the building and to register the scans with minimum overlap.

The planar and linear features were chosen as the registration primitives because man-made structures commonly have these features. The planar and linear features of the building were reconstructed first from the photogrammetric data using a bundle adjustment procedure, and then the conjugate features were extracted from the TLS scans using a segmentation procedure. A 3D similarity transformation algorithm was performed

to estimate the relationship between the coordinate systems of the photogrammetrically-reconstructed data (PRD), the TLS scans, and the reference frame, which was one of the coordinate systems of the TLS scans in this experiment.

The planar and then the linear feature-based registration results of the Rozsa Center's TLS scans were performed and are presented in the following subsections. The proposed planar and linear feature-based registration results are compared to find out whether one of the feature primitives produces better results than the other for registering TLS scans with the proposed registration method. Moreover, comparisons between the results of the proposed feature-based registration and the ICP method (Al-Durgham et al., 2011) were conducted for quality control purposes.

4.2.1 Data Description

Four minimally overlapping TLS scans were collected around the Rozsa Center using a Trimble Terrestrial Laser Scanner (GS200) with a maximum range of 200m and a resolution up to 32 milliradians (or 3mm at 100m). As mentioned before, the ICP method requires a large overlap area among the TLS scans to register them. Therefore, additional two TLS scans and an airborne scan, which have large overlap areas with the other minimum overlapping four scans, were added for the ICP registration approach. Sixteen images of Rozsa Center were collected for photogrammetric object reconstruction by using a Canon EOS Rebel XS camera. The pixel size of the camera is 0.00571 mm. The camera has an array dimension of 3888×2592 pixels and a nominal focal length of 18 mm.

4.2.2 Planar Feature-Based Registration of Rozsa Center

In this section, the results of the bundle adjustment procedure are presented first, and then the results of the proposed planar feature-based registration method for the Rozsa Center building are presented and evaluated.

4.2.2.1 Bundle Adjustment Results for Planar Features

To acquire 3D information of Rozsa Center from the photogrammetric data, the bundle adjustment procedure was applied. Reliable camera parameters are necessary to derive 3D information from the photogrammetric data accurately. Therefore, calibration of the camera, one of the most important steps in object space reconstruction from the images, was carefully carried out before the data collection.

Another significant requirement for accurate object space reconstruction is that the collected images should have a large overlap area and good intersection geometry between adjacent images. Figure 4.1 illustrates the overlap area of the 16 images covering Rozsa Center from a top view, and Figure 4.2 represents the position of the camera for each image. The black line represents the top view of Rozsa Center, while the other colors indicate the coverage of the different images as per the legend on the right side of Figures 4.1 and 4.2. As can be seen in Figures 4.1 and 4.2, the overlap areas of the images are very large, and the intersection geometry of the images is good.

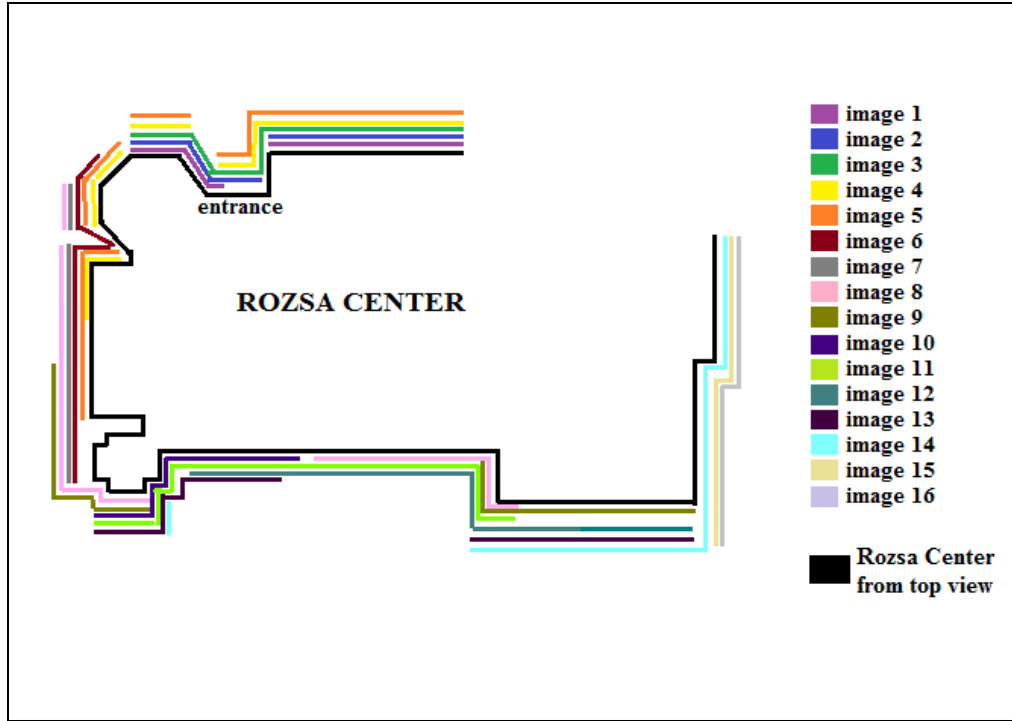


Figure 4.1. Top view of overlap area among the 16 images covering Rozsa Center

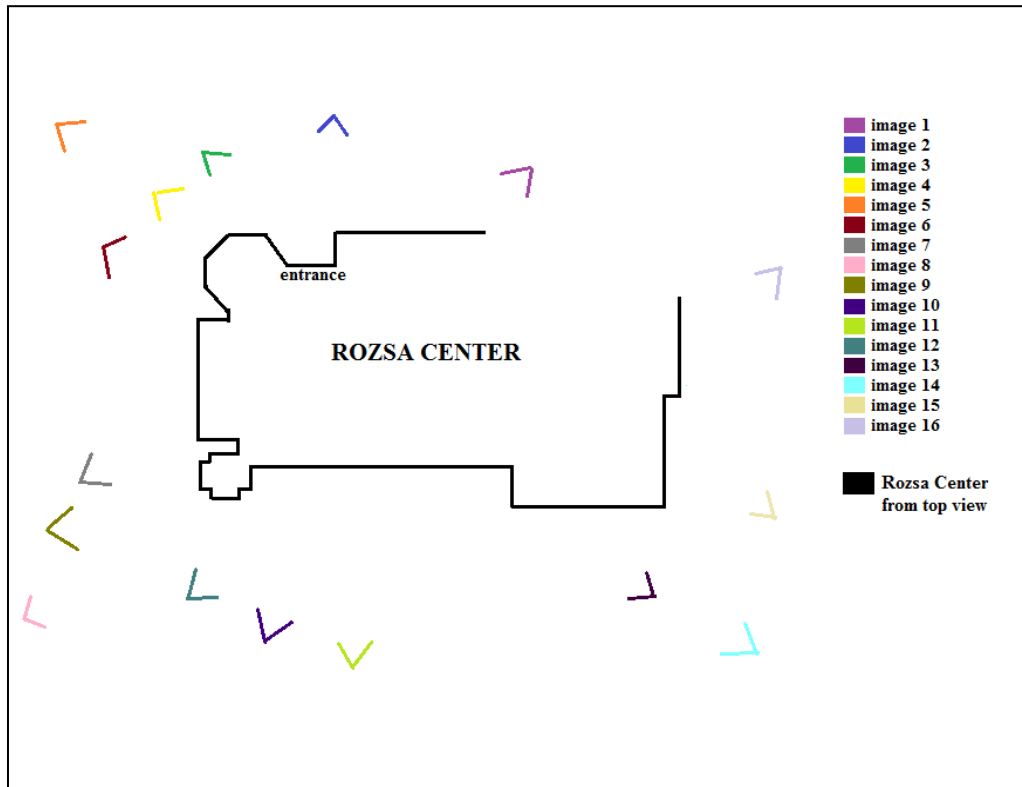


Figure 4.2. Top view of camera positions for the 16 images covering Rozsa Center

After the photogrammetric data collection, the final step was to tie all these images using well distributed points in order to acquire reliable 3D information about the building. A total of 199 different tie point IDs were assigned, and 649 image coordinate measurements of the tie points were made for the bundle adjustment procedure. 30 planar features were measured for Rozsa Center. Approximations of the ground coordinates of the tie points and the orientations of the camera position for the 16 images were prepared carefully. The datum between the image and the ground coordinate system was chosen arbitrarily.

MSAT (Multi Sensor Advanced Triangulation) software was used for bundle adjustment procedure. Bundle adjustment terminated after four iterations. The square root of the a-posteriori variance factor, which is used to check the quality of the bundle adjustment results, was observed as 0.00501, which was below the pixel size of the camera (0.00571 mm). To evaluate the bundle adjustment results, the average standard deviation of the reconstructed tie points was calculated and observed as 0.109 meters, which is also an indication of the reliability of the results.

4.2.2.2 Results of the Proposed Planar Feature-Based Registration for Rozsa Center

Four TLS scans with minimum overlap were used for the Rozsa Center experiment. A top view of the areas covered by the TLS scans from the top view of Rozsa Center and the locations of the four TLS scans are shown in Figure 4.3. Different color represents TLS scans as per the legend on the right side of Figure 4.3. The black line shows the top view of Rozsa Center. The “V” symbols in Figure 4.3 show the locations of the TLS scans.

The percentages of the overlap area between adjacent TLS scans were roughly evaluated by taking the ratio between the number of points in the overlap area and the total number of points in the TLS scans, and are shown in Table 4.1. The number of points in the overlap area was calculated by computing the distance between the points of the registered adjacent TLS scans using the ICP method results. If the distance between two points in different TLS scans was less than 10 cm, the point was assumed and counted as being in the overlapping area.

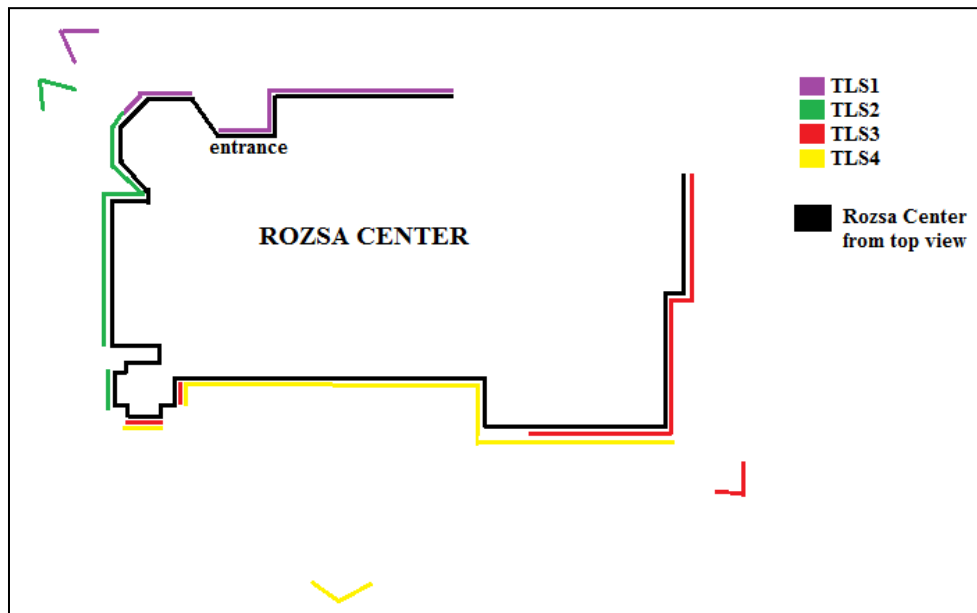


Figure 4.3. Top view of overlap area among the four TLS scans covering Rozsa Center

Table 4.1. Percentages of the overlap area among the four TLS scans of Rozsa Center

	TLS scan1	TLS scan2	TLS scan3	TLS scan4
TLS scan1		%1	%0	%0
TLS scan2	%1		%0	%0
TLS scan3	%0	%0		%19
TLS scan4	%0	%0	%19	

In order to register the four TLS scans, the planar features were chosen as the registration primitives to use them in a 3D similarity function. Three or four points from the PRD were manually selected to define a plane for each planar feature. To find the corresponding planar features in the TLS scans, a segmentation of the laser scans approach was performed (Lari et al., 2011). Three or four points were also picked as far as possible from each other from segmented planes in the TLS scans.

Figures 4.4, 4.5, 4.6, and 4.7 illustrate the planar features, which were used for the registration process in this experiment, between the photogrammetric data and TLS scan1, scan2, scan3, and scan4, respectively.

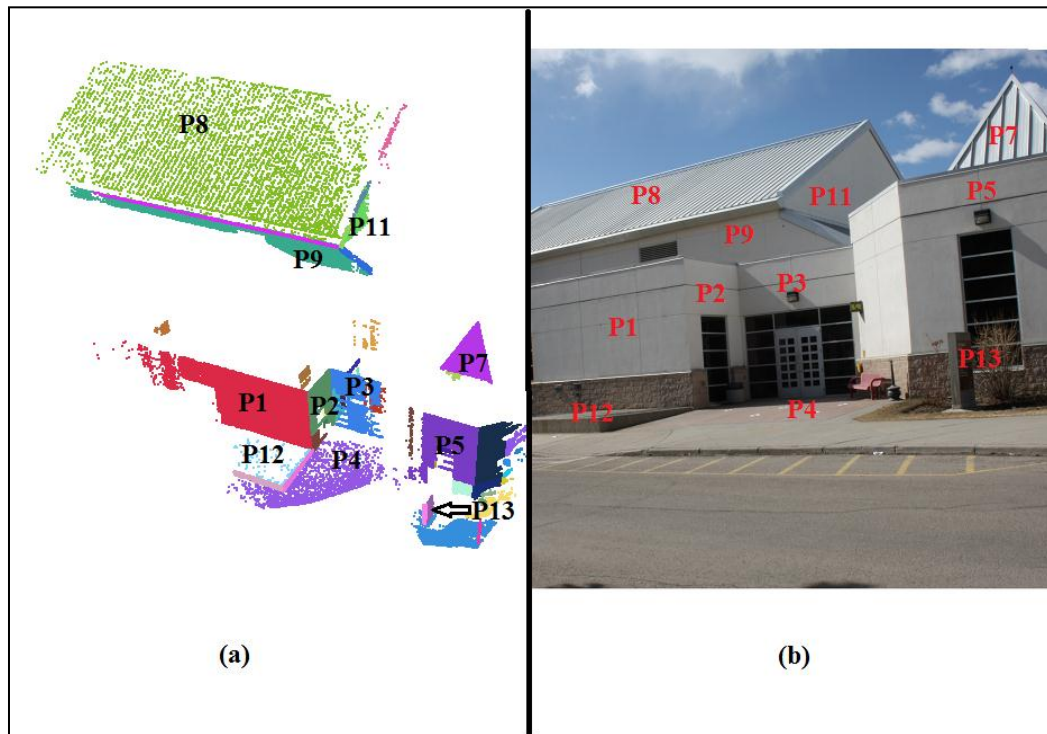


Figure 4.4. Planar features in TLS scan1 (a) and photogrammetric data (b)

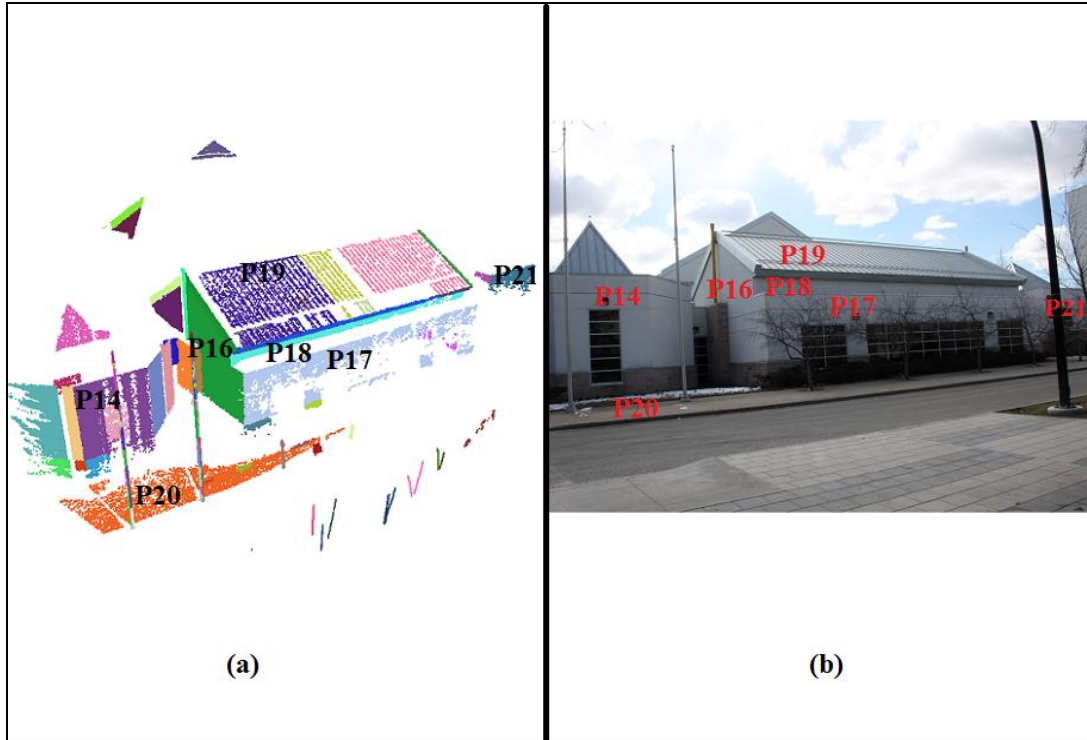


Figure 4.5. Planar features in TLS scan2 (a) and photogrammetric data (b)

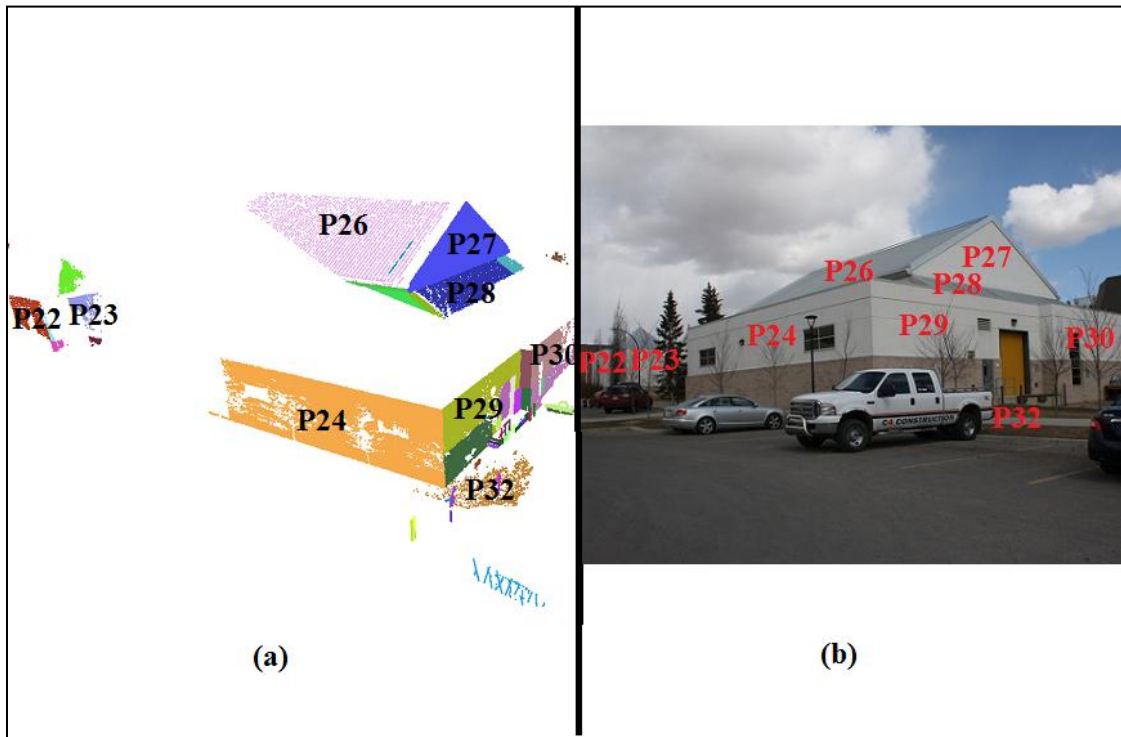


Figure 4.6. Planar features in TLS scan3 (a) and photogrammetric data (b)

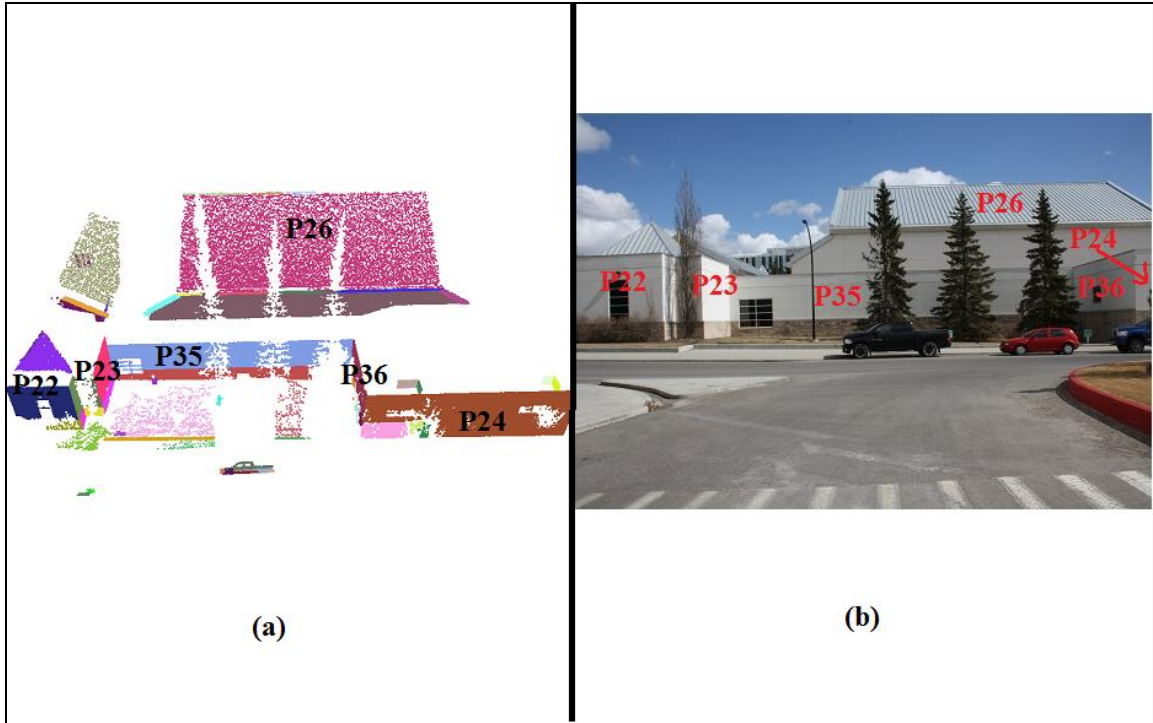


Figure 4.7. Planar features in TLS scan4 (a) and photogrammetric data (b)

The number of planar features in each TLS scan that was used in this experiment are summarized in Table 4.2. The planes were separated in groups with respect to their orientation. Examples of the planes with different orientations for Rozsa Center can be seen in Figure 4.8. For instance, the YZ-plane refers to the plane that is parallel to the Y and Z axes and is perpendicular to X axis.

Three planar features with different orientation, such as the pyramid shape, are needed for estimating the translation and rotation parameters, while one additional plane, which is parallel to one of the three planes, is required for estimating the scale parameter between different coordinate systems. More explanation of the minimum number of planar features required and the configuration to determine the transformation parameters

was provided in Chapter 3. As can be seen in Table 4.2, more than the minimum number of required planar features was available to register the TLS scans of Rozsa Center.

Table 4.2. The number of planar features in four TLS scans of Rozsa Center

	YZ-plane	XZ-plane	XY-plane	Slope Plane	Total
TLS scan1	3	4	2	2	11
TLS scan2	4	1	1	1	7
TLS scan3	4	2	1	2	9
TLS scan4	2	3	-	1	6

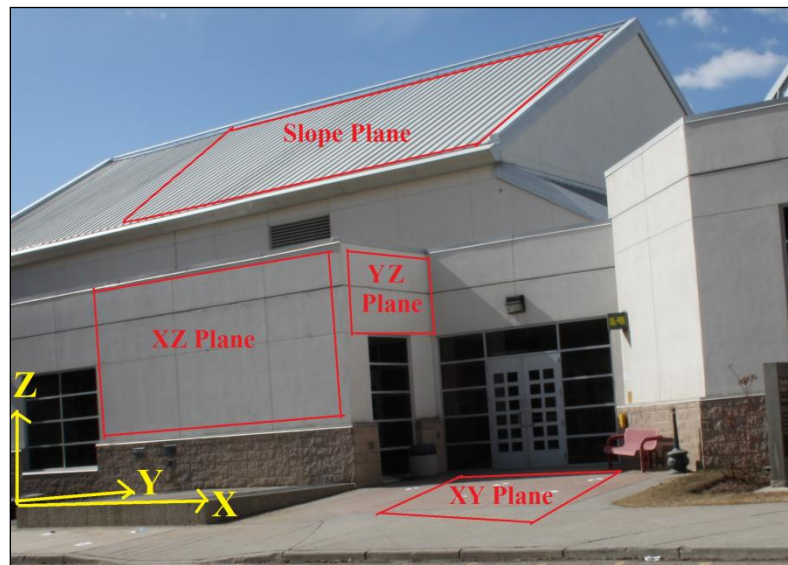


Figure 4.8. Examples of planar features with different orientations for Rozsa Center

The 3D point-based similarity function using the planar features' points was performed to estimate the registration parameters, which consisted of three translations (XT , YT , ZT), three rotation parameters (Ω , Φ , K), and the *scale*. Since the planar feature points from the PRD and the TLS scans might not be conjugate along corresponding planes, the weight matrices were modified for these planes. As previously mentioned, the TLS scans provide true scale. Therefore, the scale between the reference scan and the other scans'

coordinate systems was fixed during the LSA procedure. However, the scale between the PRD and the reference frame was estimated.

The estimated registration parameters are listed in Table 4.3. The values in parentheses are the standard deviations of the estimated registration parameters. It also should be noted that TLS scan1 was chosen as the reference coordinate system in this experiment. The standard deviations of the estimated parameters were below 10 cm for the translation parameters and below 0.23 degrees for the rotation angles, which would be less than a 1 cm error on the registration if the TLS location is around 10 m away from the building. The standard deviation values of the registration parameters indicate that reliable results were estimated.

Table 4.3. The result of the planar feature-based registration procedure for Rozsa Center

	XT (m)	YT (m)	ZT (m)	Scale	Ω (°)	Φ (°)	κ (°)
TLS scan1	0	0	0	1	0	0	0
TLS scan2	-23.186 (±0.0287)	-14.801 (±0.0219)	-0.687 (±0.0805)	1	0.234 (±0.1133)	-0.429 (±0.2092)	8.373 (±0.0484)
TLS scan3	69.677 (±0.0221)	92.511 (±0.0293)	1.335 (±0.0431)	1	0.243 (±0.0624)	0.313 (±0.0781)	121.373 (±0.0441)
TLS scan4	-41.693 (±0.0298)	91.370 (±0.0234)	-0.251 (±0.0916)	1	-0.291 (±0.1273)	0.165 (±0.0769)	-145.531 (±0.0447)
PRD	5.372 (±0.0184)	1.610 (±0.0163)	37.383 (±0.0143)	0.998 (±0.000)	30.584 (±0.2271)	-74.546 (±0.0419)	91.168 (±0.2261)

4.2.2.3 Quality Control of the Planar Feature-Based Registration Results

The quality control of the registration results was evaluated and is first presented qualitatively and then quantitatively in the following subsections.

a) Qualitative Quality Control

The registration results were evaluated for qualitative quality control, which involves transforming the TLS scans to the reference coordinate system by using the estimated registration parameters and plotting them together. Figure 4.9 illustrates the general view of the registered four TLS scans, which is colored based on height.

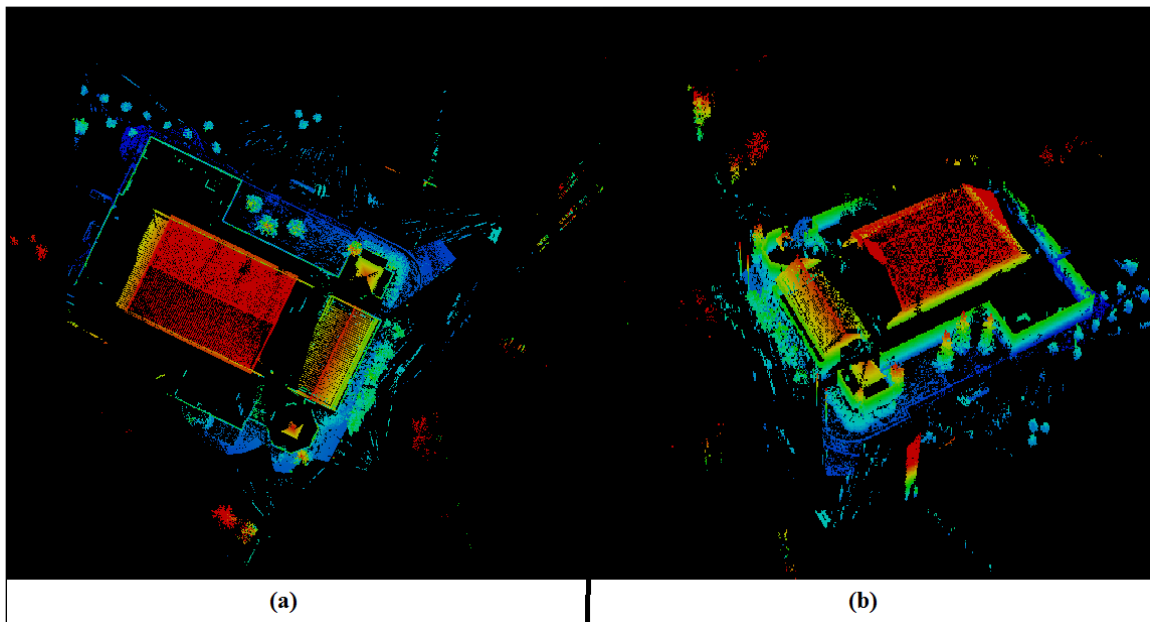


Figure 4.9. Top view (a) and 3D view (b) of the four registered TLS scans of Rozsa Center

To analyze the results in a more detailed way, closer examination of the registered TLS scans was needed. Since the overlap areas between the scans were very small, only few overlapping parts of the four registered scans were evaluated more closely. The available common features in the overlap areas, such as the lightning rod and pipes in the registered TLS scans, are illustrated in Figures 4.10 and 4.11. As illustrated in the figures, the TLS scans are registered very well.

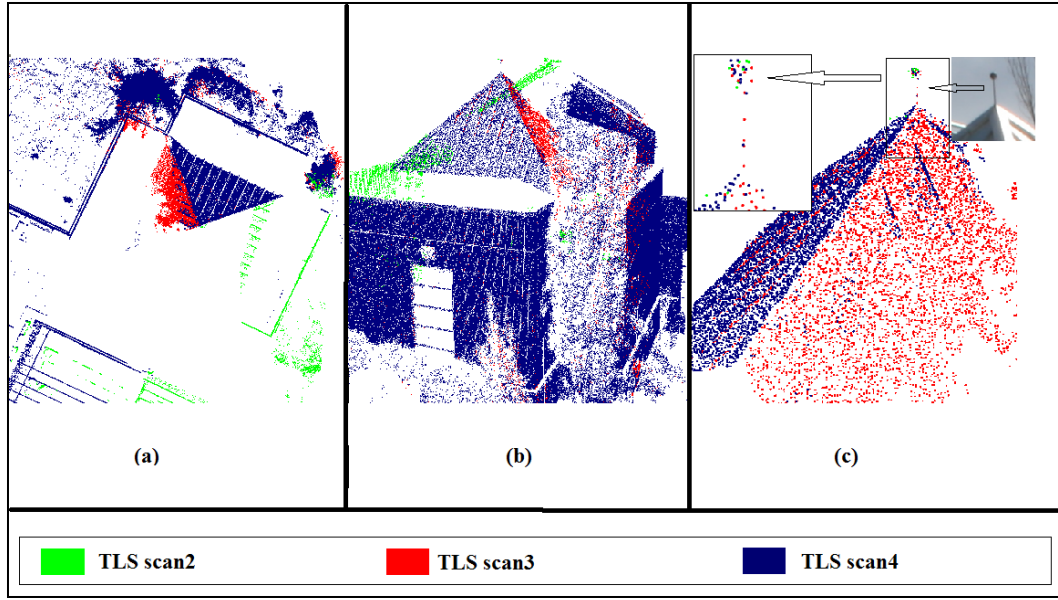


Figure 4.10. Rozsa Center registered TLS scans 2, 3, and 4: top view (a), 3D view (b), and lightning rod (c)

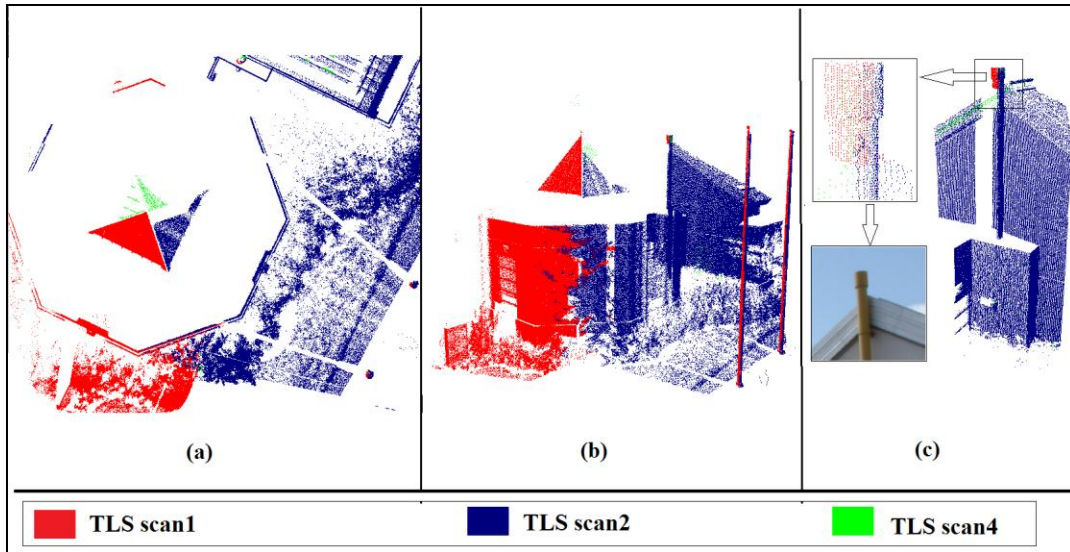


Figure 4.11. Rozsa Center registered TLS scans 1, 2, and 3: top view (a), 3D view, (b), and pipe (c)

b) Quantitative Quality Control

The quantitative analysis of the registration results was analyzed by calculating the point-to-plane normal distances for the planes between the PRD and the TLS scans and also between TLS scans which had any available planes in overlap areas. Using the estimated

registration results, the PRD and all of the TLS scans were transformed in a common coordinate system. The plane parameters were determined from the PRD planes for each plane which had correspondence in the TLS scans. The calculated plane parameters were used with X , Y , Z of the points in the corresponding TLS scan's plane to calculate the point-to-plane normal distances between the PRD and the TLS scans. The mean, standard deviation, and RMSE of the point-to-plane normal distances for the XY , XZ , and YZ -planes between the TLS scans and the PRD are presented in Table 4.4. The normal distances of the XY planes indicate the quality for Z translation, the Ω and Φ rotation angles. The normal distance of the XZ -planes indicate the quality for the Y translation, the Ω and K rotation angles. The normal distance of the YZ -planes indicates the quality for the X translation, the Φ and K rotation angles parameters.

The plane's area, which is defined by the four points from the PRD, is generally smaller than the area of the corresponding segmented plane in the TLS scans. The normal distances in Table 4.4 were calculated by using segmented planes points from the TLS scans and many of these points are not inside the polygons defining the PRD planes. Therefore, the normal distances for the planes between the TLS scans and the PRD were then calculated only using the segmented plane points that are inside the polygons whose vertices define the PRD planes. The results are listed in Table 4.5. Planes together with the given IDs in Tables 4.4 and 4.5 can be seen in Figures 4.4, 4.5, 4.6, and 4.7. The comparative analysis of the results in Tables 4.4 and 4.5 will be discussed in the following pages.

Table 4.4. The mean, standard deviation and RMSE of the calculated normal distances results of planar feature-based registration method for the planes between the PRD and the TLS scans of Rozsa Center using all of the points of segmented planes from the scans

TLS scan1 vs. PRD	Plane ID	Plane 1	Plane 2	Plane 3	Plane 4	Plane 5	Plane 8	Plane 9	Plane 12	Plane 13
	Plane Orientation	XZ-plane	YZ-plane	XZ-plane	XY-plane	XZ-plane	Slope plane	XZ-plane	XY- plane	YZ-plane
	\overline{nd} (m)	-0.017	0.018	0.010	-0.058	0.023	0.009	-0.059	0.059	-0.022
	σ (m)	0.048	0.035	0.034	0.067	0.015	0.034	0.035	0.004	0.006
	RMSE (m)	0.051	0.039	0.036	0.089	0.028	0.035	0.069	0.060	0.023
TLS scan2 vs. PRD	Plane ID	Plane 14	Plane 16	Plane 17	Plane 20	Plane 21				
	Plane Orientation	YZ-plane	XZ-plane	YZ-plane	XY-plane	YZ-plane				
	\overline{nd} (m)	0.064	-0.069	0.015	-0.099	0.015				
	σ (m)	0.093	0.076	0.025	0.064	0.021				
	RMSE (m)	0.113	0.103	0.029	0.111	0.026				
TLS scan3 vs. PRD	Plane ID	Plane 22	Plane 23	Plane 24	Plane 26	Plane 27	Plane 28	Plane 29	Plane 30	
	Plane Orientation	XZ-plane	YZ-plane	XZ-plane	Slope plane	YZ-plane	Slope plane	YZ-plane	YZ-plane	
	\overline{nd} (m)	0.018	0.007	0.045	-0.016	-0.043	-0.008	0.015	-0.047	
	σ (m)	0.007	0.006	0.053	0.013	0.054	0.018	0.013	0.057	
	RMSE (m)	0.020	0.010	0.070	0.021	0.069	0.020	0.020	0.074	
TLS scan4 vs. PRD	Plane ID	Plane 22	Plane 23	Plane 24	Plane 26	Plane 35	Plane 36			
	Plane Orientation	XZ-plane	YZ-plane	XZ-plane	Slope plane	XZ-plane	YZ-plane			
	\overline{nd} (m)	0.011	0.018	0	-0.012	-0.102	-0.005			
	σ (m)	0.009	0.006	0.019	0.016	0.127	0.033			
	RMSE (m)	0.014	0.019	0.019	0.021	0.163	0.033			

Table 4.5. The mean, standard deviation, and RMSE of the calculated normal distances results of planar feature-based registration method for the planes between the PRD and the TLS scans of Rozsa Center using the points of segmented planes which are inside the polygons whose vertices define the PRD planes

TLS scan1 vs. PRD	Plane ID	Plane 1	Plane 2	Plane 3	Plane 4	Plane 5	Plane 8	Plane 9	Plane 12	Plane 13
	Plane Orientation	XZ-plane	YZ-plane	XZ-plane	XY-plane	XZ-plane	Slope plane	XZ-plane	XY-plane	YZ-plane
	\overline{nd} (m)	0.012	0.004	0.005	0.032	0.023	0.009	-0.037	0.059	-0.024
	σ (m)	0.012	0.007	0.008	0.016	0.008	0.034	0.019	0.004	0.004
	RMSE (m)	0.017	0.009	0.010	0.036	0.025	0.035	0.042	0.059	0.025
TLS scan2 vs. PRD	Plane ID	Plane 14	Plane 16	Plane 17	Plane 20	Plane 21				
	Plane Orientation	YZ-plane	XZ-plane	YZ-plane	XY-plane	YZ-plane				
	\overline{nd} (m)	0.051	-0.09	0.019	-0.033	0.016				
	σ (m)	0.070	0.043	0.013	0.036	0.020				
	RMSE (m)	0.087	0.108	0.023	0.049	0.026				
TLS scan3 vs. PRD	Plane ID	Plane 22	Plane 23	Plane 24	Plane 26	Plane 27	Plane 28	Plane 29	Plane 30	
	Plane Orientation	XZ-plane	YZ-plane	XZ-plane	Slope plane	YZ-plane	Slope plane	YZ-plane	YZ-plane	
	\overline{nd} (m)	0.021	0.007	0.003	-0.016	-0.037	-0.008	0.017	-0.008	
	σ (m)	0.004	0.006	0.010	0.013	0.047	0.018	0.007	0.004	
	RMSE (m)	0.021	0.010	0.011	0.021	0.060	0.020	0.018	0.009	
TLS scan4 vs. PRD	Plane ID	Plane 22	Plane 23	Plane 24	Plane 26	Plane 35	Plane 36			
	Plane Orientation	XZ-plane	YZ-plane	XZ-plane	Slope plane	XZ-plane	YZ-plane			
	\overline{nd} (m)	0.012	0.018	-0.001	-0.013	-0.018	-0.015			
	σ (m)	0.007	0.006	0.011	0.015	0.025	0.004			
	RMSE (m)	0.014	0.019	0.011	0.020	0.031	0.016			

Since the TLS scans did not have large overlap area, only a few planes' normal distances were calculated between the scans. The plane parameters, which were derived from the segmentation process, were used from one TLS scan, and the points were used from another TLS scan for the same plane to calculate the point-to-plane normal distances between two overlapping scans. The normal distances between different TLS scans are provided in Table 4.6. Planes together with the given IDs in Table 4.6 can be seen in Figures 4.4, 4.5, 4.6, and 4.7. Plane 40 in Tables 4.6 was not used to calculate the registration parameters because the plane was not visible in the images with good intersection geometry. The illustration of plane 40 can be seen in Figure 4.12.

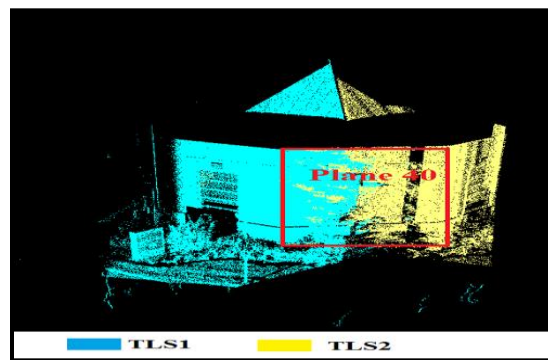


Figure 4.12. Plane 40 in TLS scan1 and scan2

Table 4.6. The mean, standard deviation, and RMSE of the calculated normal distances of planar feature-based registration method between different TLS scans planes of Rozsa Center

TLS scan1 vs. TLS scan2	Plane ID	Plane 40			
	Plane Orientation	Vertical-plane			
	\bar{nd} (m)	0.037			
	σ (m)	0.036			
	RMSE (m)	0.052			
TLS scan3 vs. TLS scan4	Plane ID	Plane 22	Plane 23	Plane 24	Plane 26
	Plane Orientation	XZ-plane	YZ-plane	XZ-plane	Slope plane
	\bar{nd} (m)	-0.007	0	-0.014	0
	σ (m)	0.007	0.006	0.027	0.016
	RMSE (m)	0.010	0.006	0.031	0.016

The analysis of the normal distance results for each plane indicates that the proposed registration method is capable of good alignment between the TLS scans and the photogrammetric data. The mean, standard deviation, and RMSE of the calculated point-to-plane normal distances of each plane were all below 10 cm, which substantiates the quality of the registration results (Tables 4.4, 4.5, and 4.6). However, the results of the calculated normal distances using the points of the segmented planes, which are in the region of the same plane area from the PRD (Table 4.5), are generally smaller than the calculated normal distances using all of the points of the segmented planes from the TLS scans that are generally larger in size than the plane area in the PRD (Table 4.4). Therefore, the calculated normal distances in Table 4.5 are slightly smaller than the distances in Table 4.4.

Finally, the visual illustration of the calculated point-to-plane normal distances was done by plotting the registered TLS scans by color based on the normal distance (Figure 4.13). The plotted normal distances in Figure 4.13 were calculated using the PRD plane parameters and the points of the conjugate segmented planes from the TLS scans, which are in the polygons whose vertices define the PRD planes.

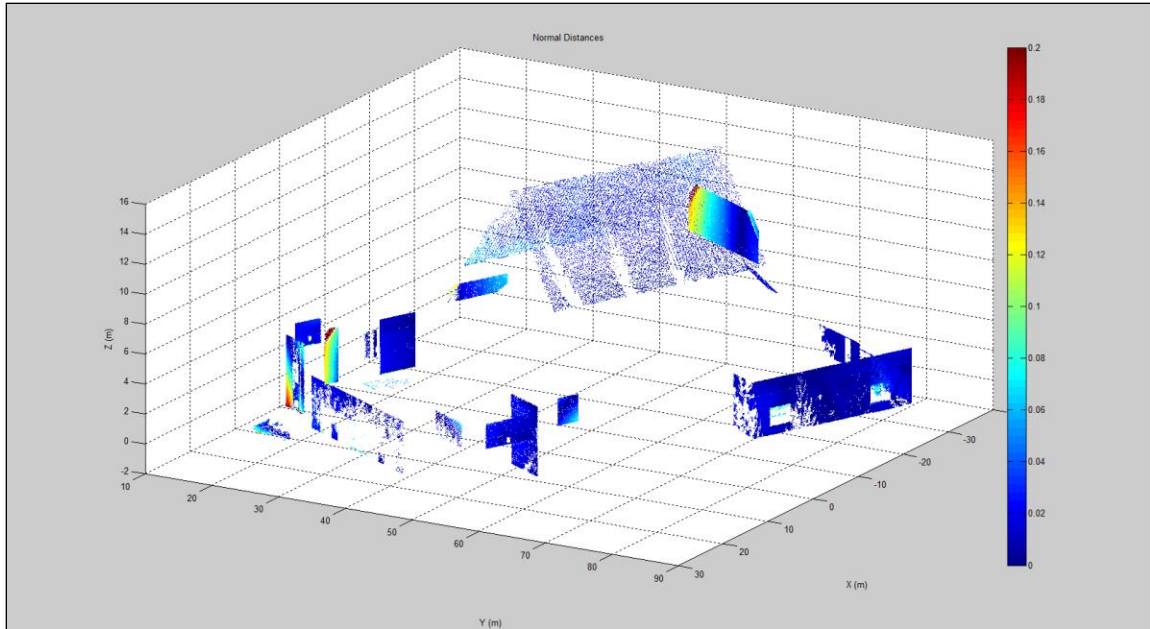


Figure 4.13. 3D view of the registered four TLS scans of Rozsa Center by planar-feature based registration method (color based on normal distances calculated by using the PRD plane parameters and segmented TLS planes' points that are inside polygons defining the PRD planes)

Figure 4.14 also shows the registered four TLS scans of Rozsa Center in color based on the normal distances, which were calculated using the PRD plane parameters and the TLS scans' segmented plane points whose areas are larger than the corresponding PRD planes. The normal distance differences seen in Tables 4.4 and 4.5 easily can be seen in Figures 4.13 and 4.14. The differences occurred because of under segmentation of the planes in the TLS scans. In other words, sometimes more than one neighboring and similar planes in the scans are segmented as one plane and all of the points of these planes are used for normal distance calculation between the scans and the PRD, while the PRD planes only represent unique planes.

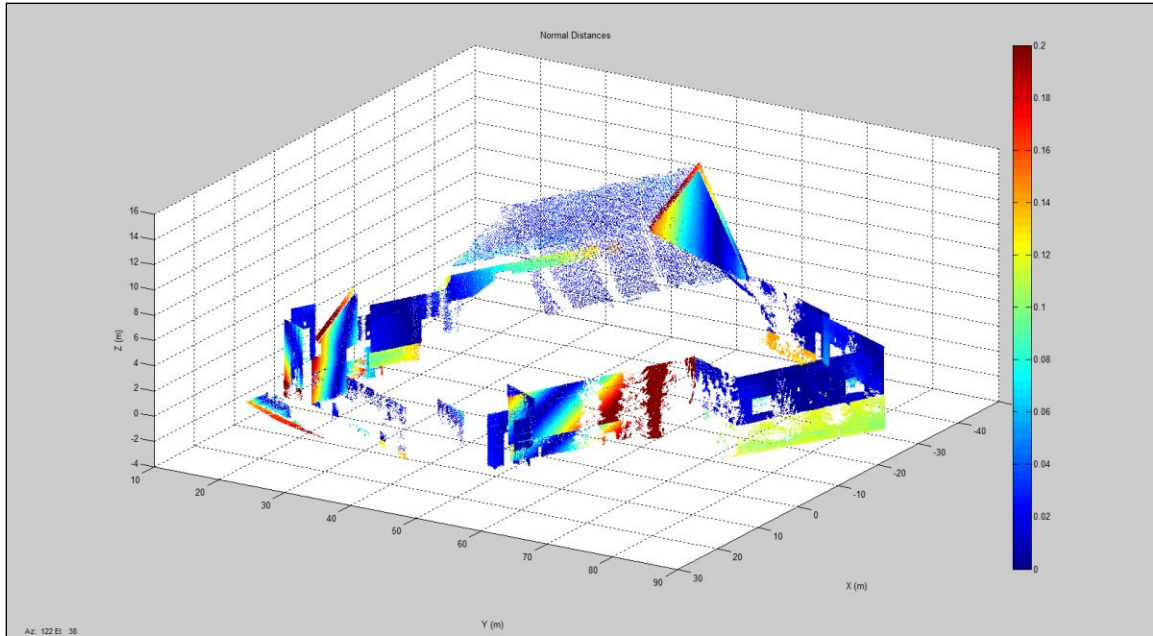


Figure 4.14. 3D view of the registered four TLS scans of Rozsa Center by planar-feature based registration method (color based on normal distances calculated by using all points of the segmented planes from the TLS scans and PRD planes parameters)

4.2.3 Linear Feature-Based Registration of Rozsa Center

As already mentioned, man-made structures commonly have planar and linear features. Therefore, after the planar features were used for the proposed registration method, the linear features were used as the registration primitives for the same experiment data to investigate the quality of the registration results with a different type of feature. The bundle adjustment results are analyzed first, and then the registration results, in the following sub-sections.

4.2.3.1 Bundle Adjustment Results for Linear Features

To derive linear features from the photogrammetric data, the beginning and ending points of the linear features were measured in one or more images in addition to several

intermediate points for these features. The coplanarity-based method (Habib et al. 2004) described in Chapter 3 was used in the bundle adjustment procedure to derive the linear features in object space. In total, 20 linear features were measured for Rozsa Center. The number of iterations was 8 and the square root of the a-posteriori variance factor was 0.0048, which is less than the pixel size of the images, for the bundle adjustment results with linear features. The average standard deviation of the reconstructed tie points was calculated as 0.09 meters, which indicated that the results are reliable.

4.2.3.2 Results of the Proposed Linear Feature-Based Registration for Rozsa Center

The same four TLS scans of Rozsa Center, which were employed for the planar feature-based registration, were used for the linear feature-based registration. The beginning and ending points were necessary to define a linear feature. To find the corresponding linear features in the TLS scans, a segmentation of the laser scans approach (Lari et al. 2011) first was used to segment the planar features from the TLS scans, and the linear features were derived from the intersection of the neighboring segmented planes automatically. Figures 4.15, 4.16, 4.17, and 4.18 illustrate the linear features, which were used for registering the TLS scans in the photogrammetric data and TLS scan1, scan2, scan3, and scan4, respectively.

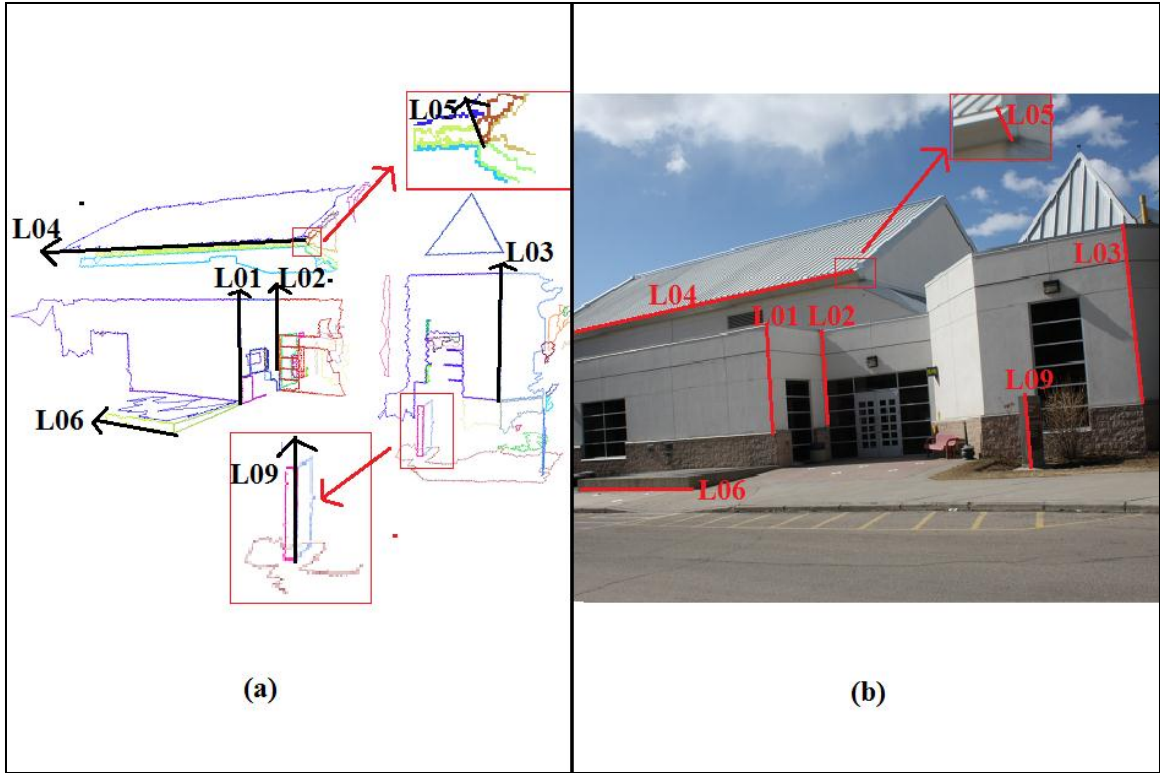


Figure 4.15. Linear features in TLS scan1 (a) and photogrammetric data (b)

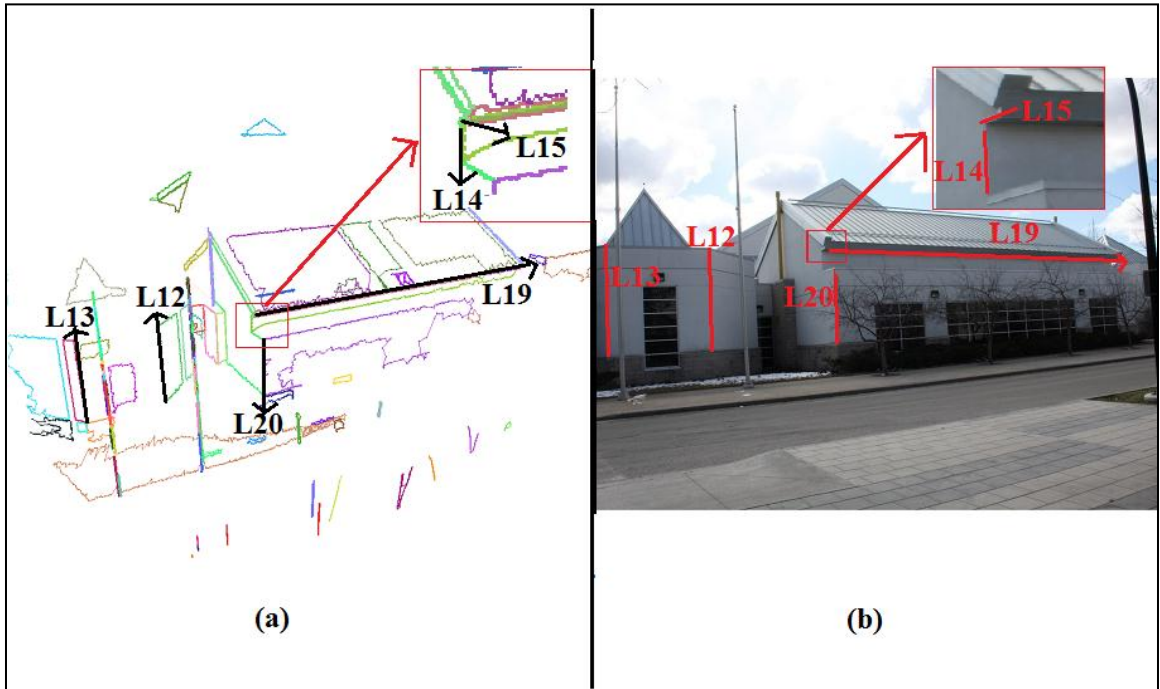


Figure 4.16. Linear features in TLS scan2 (a) and photogrammetric data (b)

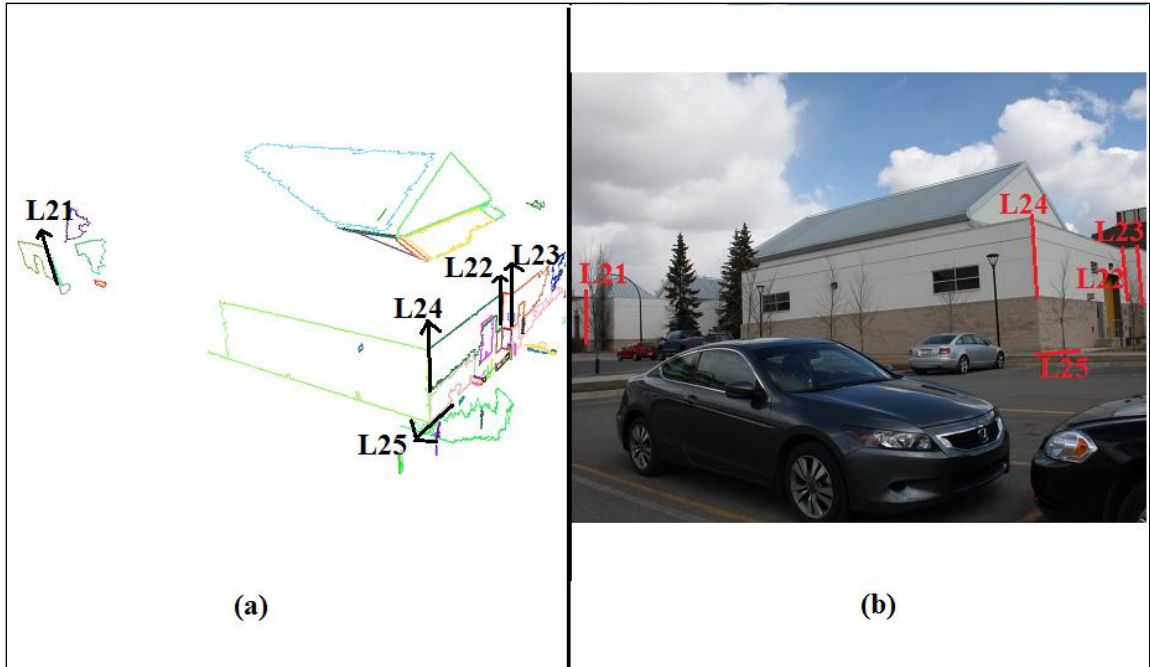


Figure 4.17. Linear features in TLS scan3 (a) and photogrammetric data (b)

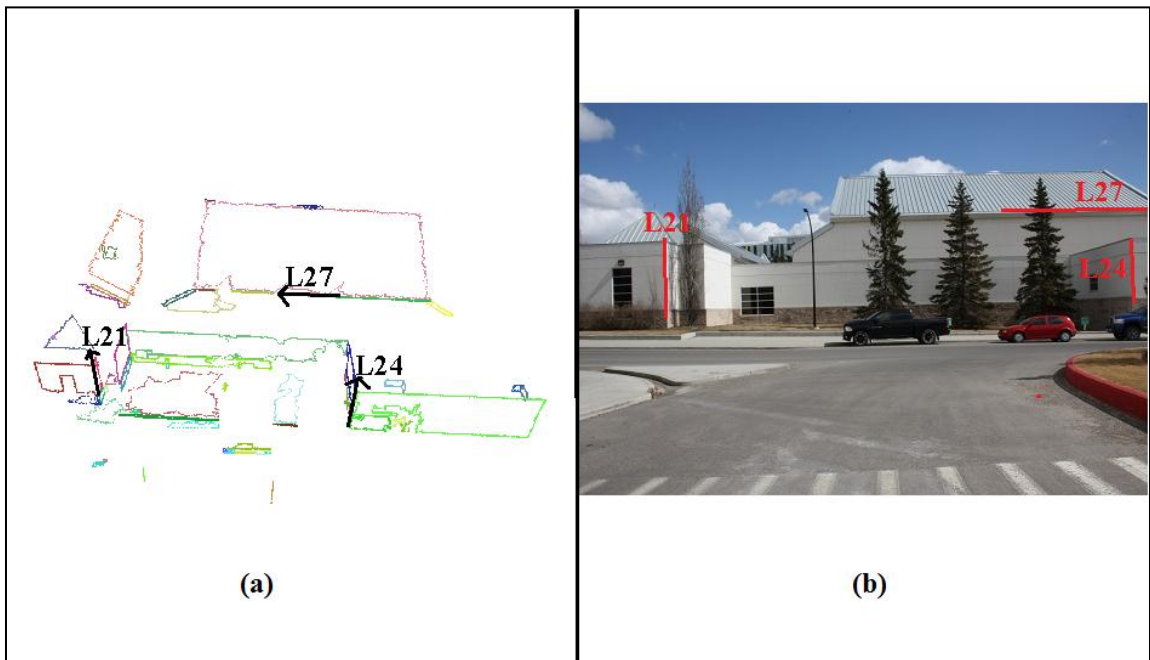


Figure 4.18. Linear features in TLS scan4 (a) and photogrammetric data (b)

The number of linear features in the TLS scans is summarized in Table 4.7. Two non-coplanar linear features were the absolute minimum number to estimate the registration parameters between two scans. As can be seen in Table 4.6, more than the absolute minimum number of linear features was available to estimate registration parameters.

Table 4.7. The number of linear features in the four TLS scans of Rozsa Center

	Vertical	Horizontal	Slope	Total
TLS scan1	4	2	1	7
TLS scan2	4	2	-	6
TLS scan3	4	1	-	5
TLS scan4	3	1	-	3

The registration parameters, estimated with the 3D similarity function, are shown in Table 4.8. TLS scan1 was chosen as a reference frame for the linear feature-based registration as was done for the planar feature-based registration of the Rozsa Center. The standard deviations of the estimated parameters indicate that the translation parameters in the X and Y (XT and YT) axes and some of the rotation angles are reliable. However, the Z translation (ZT) and some of the rotation parameters (values highlighted in yellow) have large standard deviation values.

Table 4.8. The result of the linear feature-based registration procedure for Rozsa Center

	XT (m)	YT (m)	ZT (m)	Scale	Ω (°)	Φ (°)	κ (°)
TLS scan1	0	0	0	1	0	0	0
TLS scan2	-23.217 (± 0.0685)	-14.792 (± 0.0341)	-0.667 (± 0.1226)	1	0.869 (± 0.2571)	1.073 (± 0.5158)	8.421 (± 0.1569)
TLS scan3	69.639 (± 0.0661)	92.565 (± 0.0646)	1.284 (± 0.7231)	1	0.681 (± 0.4161)	0.824 (± 0.5422)	121.411 (± 0.1071)
TLS scan4	-41.787 (± 0.0983)	91.305 (± 0.0724)	-0.751 (± 0.3747)	1	-0.803 (± 0.4175)	0.009 (± 0.2541)	-145.441 (± 0.1263)
PRD	5.461 (± 0.0722)	1.635 (± 0.0393)	37.384 (± 0.0336)	0.998 (± 0.0006)	31.338 (± 0.8272)	-74.372 (± 0.1408)	91.914 (± 0.7643)

The standard deviation values highlighted in yellow in Table 4.8 for the ZT , Ω , and Φ parameters indicate a problem with the registration results when the linear features were used as the primitives. The linear feature-based registration parameters' standard deviations show errors of up to 0.72 meters in translation and 0.54 degrees in rotation. In contrast, in Table 4.3, which shows the planar feature-based registration results, the standard deviation overall was below 0.10 meters and 0.22 degrees for the translation and the rotation parameters, respectively. More specifically, a one by one comparison for each parameters' standard deviation of the TLS scans and the PRD, calculated by the planar and linear feature-based registration shows that the planar feature-based registration always produced better results than the linear feature-based registration.

In summary, according to the standard deviation of the estimated registration parameters, the linear feature-based registration results were worse than the planar feature-based registration. To investigate the causes of the mis-registration error with the linear features, quality control was necessary, which is evaluated in the following subsections.

4.2.3.3 Quality Control of the Linear Feature-Based Registration Results

Following is an evaluation of the quality of the linear feature-based registration results qualitatively and then quantitatively.

a) Qualitative Quality Control

The standard deviation of the ZT translation and Ω and Φ rotation parameters indicated that the TLS scans were incorrectly registered (Table 4.8). The problem was also obviously seen while plotting the registered TLS scans. Figures 4.19 and 4.20 illustrate

the problem in height (Z axis). More specifically, in Figure 4.19, the top part of the lightning rod in the different TLS scans has different heights. Figure 4.20 also illustrates the problem of the mis-registration in the Z axis.

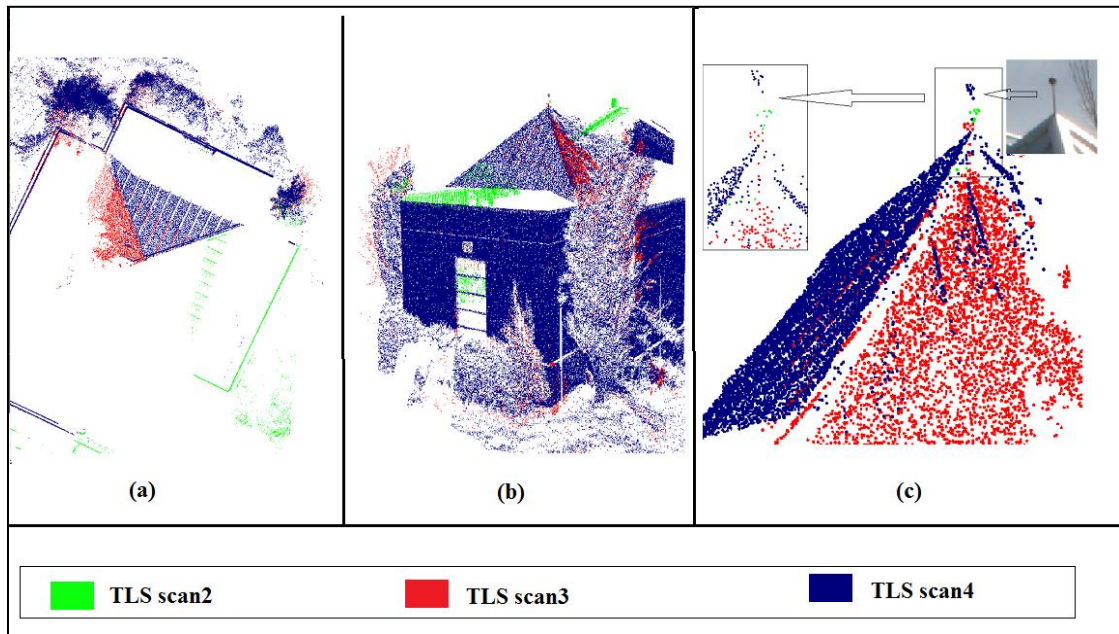


Figure 4.19. Rozsa Center registered TLS scan 2, 3, and 4: top view (a), 3D view (b), and lightning rod (c)

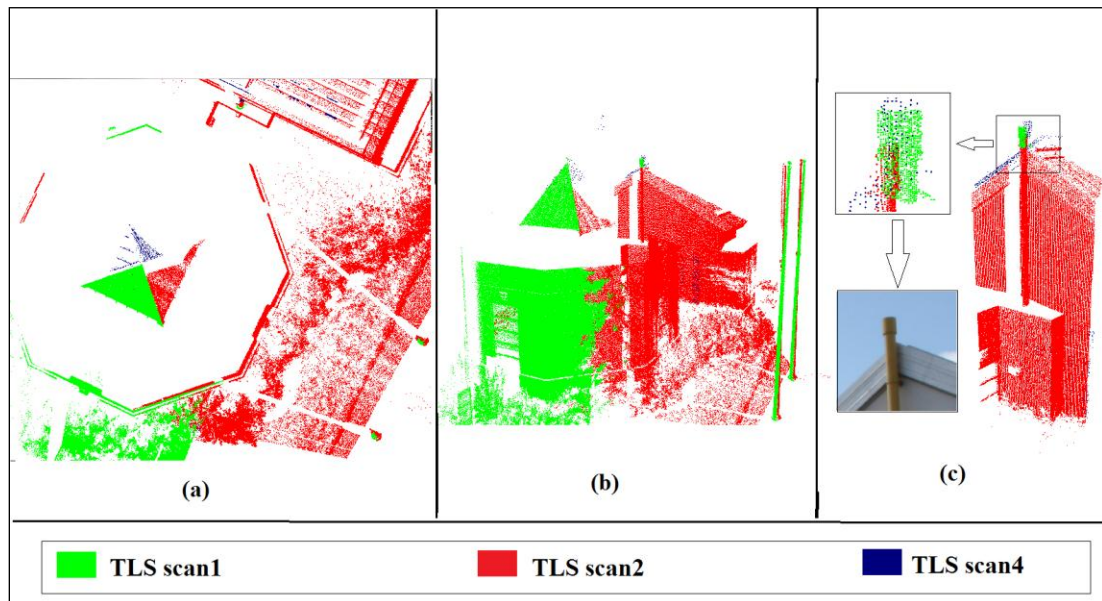


Figure 4.20. Rozsa Center registered TLS scan 1, 2, and 3: top view (a), 3D view (b), and pipe (c)

b) Quantitative Quality Control

The quantitative quality control of the linear feature-based registration method results was evaluated as it was performed for the planar feature-based registration results by analyzing the point-to-plane normal distances between the PRD and the TLS scans' planes as well some of the planes between the TLS scans. The linear feature-based registration did not have PRD planes. However, as previously explained, the PRD planes were defined by selecting three or four reconstructed points on the plane from the PRD, and these points were also used as tie points during the estimation of the linear features in the bundle adjustment procedure. Therefore, the same PRD planes' points, which were used for the planar feature-based registration, were also estimated with the linear features during the bundle adjustment procedure. These plane points were then used for quality control analysis by calculating the normal distance between the two data sets' planes

First, all the plane points of the segmented TLS scans were used to calculate the normal distance between the two data sets. The results for each plane are listed in Table 4.9. Then, only the TLS scans' segmented plane points, which were within the planar polygon defined by the PRD, were used for the normal distance calculation (Table 4.10). The planes together with their IDs are presented in Figures 4.4, 4.5, 4.6, 4.7, and 4.12. As highlighted in Table 4.9 and Figure 4.22, planes 20 and 26 have large normal distance values. Plane 26 is a sloping plane and plane 20 is an XY plane. These planes were used to estimate the shift in the Z axis as well as the Ω and Φ rotation angles. Similarly, as can be seen in Table 4.8, the ZT translation and Ω and the Φ rotation angles had large standard values.

Moreover, the comparison between the planar and linear feature-based registration quality control by normal distance calculation shows that the normal distances between the PRD and the TLS scans' planes are smaller when the planar features were the registration primitives. For instance, in Table 4.10 (normal distances calculated using linear feature-based registration results), the RMSE of plane 20 in TLS scan2 is 0.231 meters, while it is only 0.049 meters in Table 4.5 (normal distances calculated using planar feature-based registration results).

Table 4.9. The mean, standard deviation, and RMSE of the calculated normal distances results of linear feature-based registration method for planes between PRD and TLS scans of Rozsa Center using all points of segmented planes from the scans

TLS scan1 vs. PRD	Plane ID	Plane 1	Plane 2	Plane 3	Plane 4	Plane 5	Plane 8	Plane 9	Plane 12	Plane 13
	Plane Orientation	XZ-plane	YZ-plane	XZ-plane	XY-plane	XZ-plane	Slope plane	XZ-plane	XY-plane	YZ-plane
	\overline{nd} (m)	-0.001	0.017	-0.010	-0.013	0.005	0.030	-0.073	-0.002	-0.003
	σ (m)	0.013	0.086	0.009	0.016	0.008	0.034	0.019	0.007	0.004
	RMSE (m)	0.013	0.019	0.014	0.020	0.010	0.046	0.076	0.007	0.005
TLS scan2 vs. PRD	Plane ID	Plane 14	Plane 16	Plane 17	Plane 20	Plane 21				
	Plane Orientation	YZ-plane	XZ-plane	YZ-plane	XY-plane	YZ-plane				
	\overline{nd} (m)	0.044	-0.116	-0.011	0.229	-0.014				
	σ (m)	0.099	0.053	0.033	0.019	0.018				
	RMSE (m)	0.108	0.128	0.035	0.231	0.023				
TLS scan3 vs. PRD	Plane ID	Plane 22	Plane 23	Plane 24	Plane 26	Plane 27	Plane 28	Plane 29	Plane 30	
	Plane Orientation	XZ-plane	YZ-plane	XZ-plane	Slope plane	YZ-plane	Slope plane	YZ-plane	YZ-plane	
	\overline{nd} (m)	0.006	0.002	-0.021	-0.021	-0.051	-0.095	0.011	-0.008	
	σ (m)	0.004	0.007	0.010	0.024	0.045	0.018	0.008	0.004	
	RMSE (m)	0.008	0.007	0.023	0.032	0.069	0.009	0.014	0.009	
TLS scan4 vs. PRD	Plane ID	Plane 22	Plane 23	Plane 24	Plane 26	Plane 35	Plane 36			
	Plane Orientation	XZ-plane	YZ-plane	XZ-plane	Slope plane	XZ-plane	YZ-plane			
	\overline{nd} (m)	-0.002	0.016	-0.023	-0.262	-0.029	-0.021			
	σ (m)	0.007	0.007	0.010	0.030	0.023	0.003			
	RMSE (m)	0.007	0.017	0.026	0.264	0.037	0.022			

Table 4.10. The mean, standard deviation and RMSE of the calculated normal distances results of linear feature-based registration method for the planes between the PRD and the TLS scans of Rozsa Center using only points of segmented planes which are within planar polygon defined by the PRD

TLS scan1 vs. PRD	Plane ID	Plane 1	Plane 2	Plane 3	Plane 4	Plane 5	Plane 8	Plane 9	Plane 12	Plane 13
	Plane Orientation	XZ-plane	YZ-plane	XZ-plane	XY-plane	XZ-plane	Slope plane	XZ-plane	XY-plane	YZ-plane
	\overline{nd} (m)	-0.030	0.032	-0.001	-0.113	0.010	0.030	-0.097	-0.002	-0.003
	σ (m)	0.044	0.036	0.039	0.068	0.016	0.034	0.038	0.007	0.007
	RMSE (m)	0.054	0.049	0.040	0.133	0.019	0.046	0.105	0.007	0.007
TLS scan2 vs. PRD	Plane ID	Plane 14	Plane 16	Plane 17	Plane 20	Plane 21				
	Plane Orientation	YZ-plane	XZ-plane	YZ-plane	XY-plane	YZ-plane				
	\overline{nd} (m)	0.035	-0.068	0.013	0.229	-0.013				
	σ (m)	0.102	0.078	0.036	0.019	0.018				
	RMSE (m)	0.108	0.104	0.038	0.231	0.022				
TLS scan3 vs. PRD	Plane ID	Plane 22	Plane 23	Plane 24	Plane 26	Plane 27	Plane 28	Plane 29	Plane 30	
	Plane Orientation	XZ-plane	YZ-plane	XZ-plane	Slope plane	YZ-plane	Slope plane	YZ-plane	YZ-plane	
	\overline{nd} (m)	0.004	0.021	0.041	0.026	0.002	0.017	0.013	-0.061	
	σ (m)	0.009	0.006	0.046	0.036	0.053	0.021	0.011	0.067	
	RMSE (m)	0.011	0.022	0.062	0.045	0.054	0.028	0.018	0.091	
TLS scan4 vs. PRD	Plane ID	Plane 22	Plane 23	Plane 24	Plane 26	Plane 35	Plane 36			
	Plane Ori.	XZ-plane	YZ-plane	XZ-plane	Slope	XZ-plane	YZ-plane			
	\overline{nd} (m)	-0.009	0.014	0.037	-0.194	-0.105	-0.008			
	σ (m)	0.010	0.006	0.025	0.025	0.119	0.036			
	RMSE (m)	0.014	0.015	0.045	0.195	0.159	0.037			

Final quantitative quality control for the linear feature-based registration results was conducted by calculating the normal distances of the planes in the different TLS scans, which are also listed in Table 4.11. Since the TLS scans in this experiment did not have large overlap areas, only a few normal distances of planes between TLS scans were calculated. The comparison of Tables 4.11 and 4.6 shows that the calculated normal distances are smaller in Table 4.6., which lists the normal distances of the same planes that are registered by the planar feature-based registration method.

Table 4.11. The mean, standard deviation, and RMSE of the calculated normal distances of linear-feature based registration method for planes between different TLS scans

TLS scan1 vs. TLS scan2	Plane ID	Plane 40			
	Plane Orientation	Vertical-plane			
	\overline{nd} (m)	0.061			
	σ (m)	0.012			
	RMSE (m)	0.054			
TLS scan3 vs. TLS scan4	Plane ID	Plane 22	Plane 23	Plane 26	Plane 24
	Plane Orientation	XZ-plane	YZ-plane	Slope plane	XZ-plane
	\overline{nd} (m)	0.016	0.023	0.011	0.012
	σ (m)	0.048	0.015	0.009	0.004
	RMSE (m)	0.017	0.027	0.014	0.013

Finally, the registered TLS scans were plotted and colored based on the calculated normal distances for the planes between the PRD and the TLS scans. Figure 4.21 illustrates the normal distance when only the points of the segmented planes that are within the polygon defined by the PRD planes were used. On the other hand, Figure 4.22 shows the normal distance when all of the points of the segmented planes from the TLS scans were used. The same problem with ZT translation can be seen again at the roof portion (Figures 4.21 and 4.22). In the next subsection, the reasons that might cause the mis-registration results will be investigated.

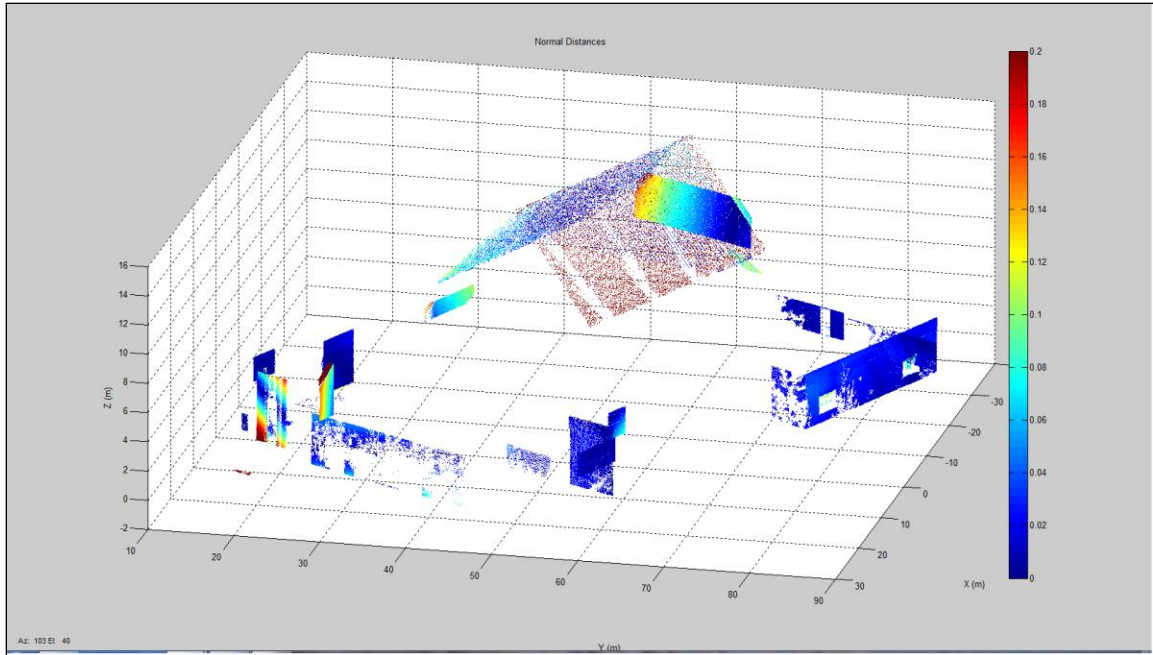


Figure 4.21. 3D view of the registered TLS scans of Rozsa Center by linear feature-based registration method (color based on normal distances derived by using only the points of the segmented plane from the TLS scans within the area of PRD planes)

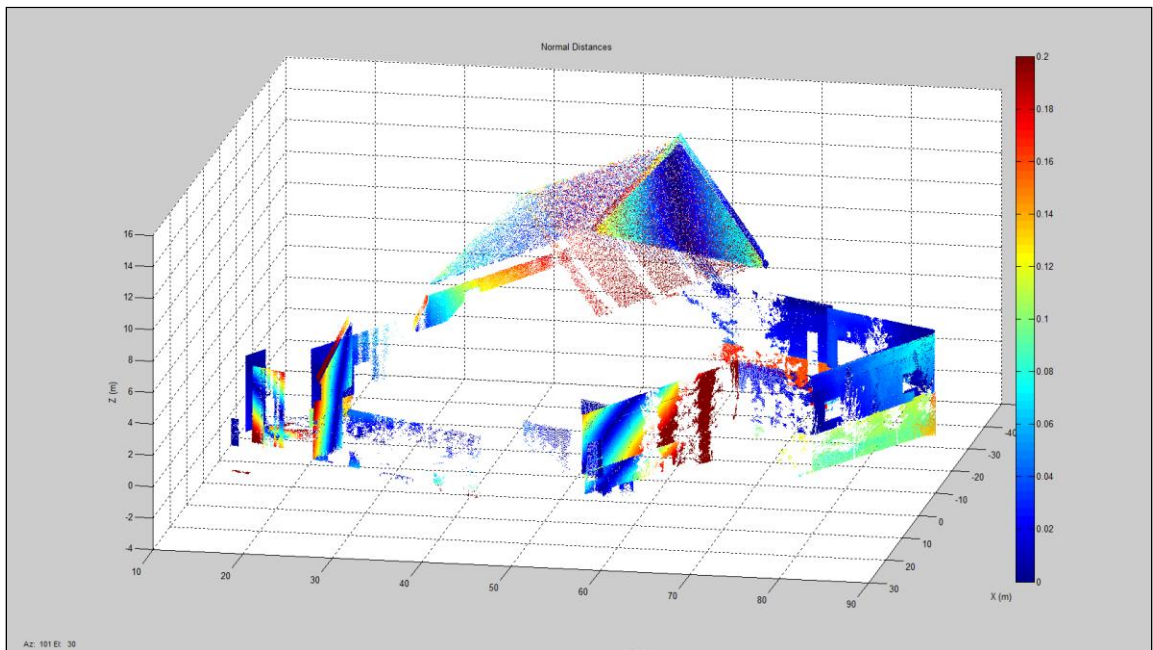


Figure 4.22. 3D view of the registered TLS scans of Rozsa Center by linear feature-based registration method (color based on normal distances which were calculated by using all points of the segmented plane from TLS scans)

c) Mis-registration in Z axis

Both the qualitative and quantitative quality controls indicated a problem with the estimated ZT , Ω , and Φ parameters using linear features as registration primitives. The problem occurred because of the sloping/horizontal linear features that were used to estimate these parameters. These derived linear features from the neighboring plane intersections in the TLS scans did not correspond to the physical linear features that could be identified in the imagery. Figure 4.23 illustrates an example of two neighboring planes and the derived linear features between the planes from a TLS scan. However, the linear feature in the TLS scan does not correspond to any physical line in the photogrammetric data (imagery). This type of problem generally occurs in the roof portion of a building, which commonly has the sloping/horizontal linear features. The non-corresponding sloping/horizontal linear features from the PRD and the TLS scans are the main causes of incorrect estimation of the ZT , Ω , and Φ parameters.

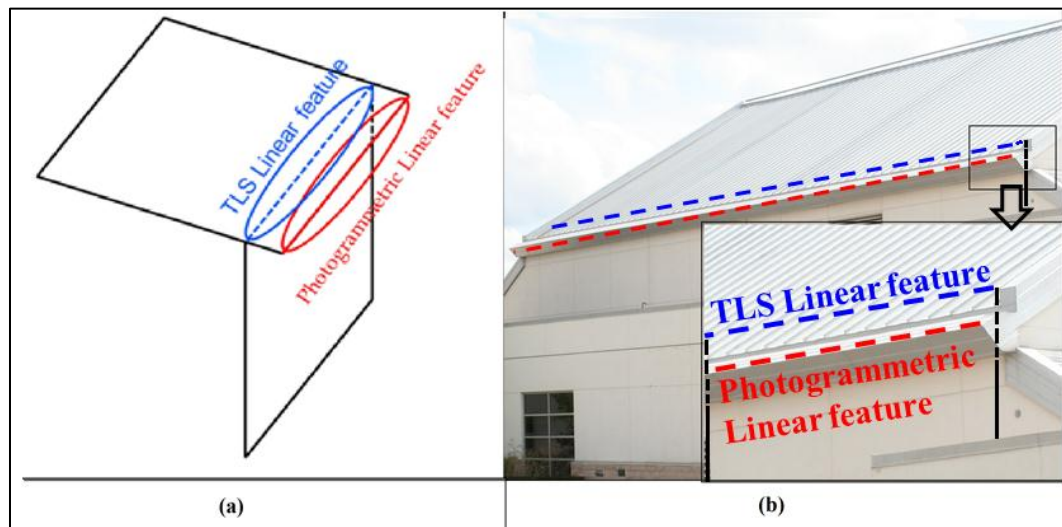


Figure 4.23. An example of the intersection of two planes and the linear features that could be derived from the TLS scans and photogrammetric data: schematic (a) and image (b)

4.2.4 Comparisons of the Results of the Proposed Feature-Based Registration and ICPP Method for Rozsa Center

Finally, the proposed registration with the planar and linear primitives and the ICPP method results are compared. Table 4.12 compares the different registration results.

Table 4.12. Comparison of the different registration results of Rozsa Center TLS scans

TLS scans	Parameters	the ICPP method	Planar based registration	Linear based registration	the ICPP vs. Planar Based	the ICPP vs. Linear Based	linear vs. planar Based
TLS scan2	XT (m)	-23.258	-23.186	-23.217	-0.072	-0.041	0.031
	YT (m)	-14.733	-14.801	-14.792	0.067	0.058	-0.009
	ZT (m)	-0.605	-0.687	-0.667	0.082	0.062	-0.020
	Scale	1	1	1	0	0	0
	$\Omega(^{\circ})$	0.177	0.234	0.869	-0.056	-0.691	-0.635
	$\phi(^{\circ})$	-0.189	-0.429	1.073	0.239	-1.262	-1.502
	$\kappa(^{\circ})$	8.168	8.373	8.421	-0.204	-0.252	-0.048
TLS scan3	XT (m)	69.613	69.677	69.639	-0.063	-0.025	0.038
	YT (m)	92.579	92.511	92.565	0.068	0.014	-0.054
	ZT (m)	1.375	1.335	1.284	0.040	0.091	0.051
	Scale	1	1	1	0	0	0
	$\Omega(^{\circ})$	0.095	0.243	0.681	-0.147	-0.585	-0.438
	$\phi(^{\circ})$	0.194	0.313	0.824	-0.118	-0.629	-0.511
TLS scan4	$\kappa(^{\circ})$	121.388	121.373	121.411	0.015	-0.022	-0.038
	XT (m)	-41.751	-41.693	-41.787	-0.057	0.036	0.094
	YT (m)	91.313	91.37	91.305	-0.056	0.008	0.065
	ZT (m)	-0.259	-0.251	-0.751	-0.008	0.491	0.500
	Scale	1	1	1	0	0	0
	$\Omega(^{\circ})$	-0.204	-0.291	-0.803	0.086	0.598	0.512
	$\phi(^{\circ})$	0.002	0.165	0.009	-0.162	-0.006	0.156
	$\kappa(^{\circ})$	-145.53	-145.531	-145.441	-0.007	-0.097	-0.09
PRD	XT (m)	-	5.372	5.461	-	-	-0.089
	YT (m)	-	1.611	1.635	-	-	-0.025
	ZT (m)	-	37.383	37.384	-	-	-0.001
	Scale	-	0.998	0.998	-	-	0
	$\Omega(^{\circ})$	-	30.584	31.338	-	-	-0.754
	$\phi(^{\circ})$	-	-74.546	-74.372	-	-	-0.174
	$\kappa(^{\circ})$	-	91.168	91.914	-	-	-0.746

It should be noted that a minimum of four overlapping TLS scans were used for the proposed feature-based registration method, while two additional TLS scans and an airborne laser scan were added to estimate the registration parameters with the ICPP method. The differences are highlighted in yellow if they are larger than 10 cm for translation and 0.5 degrees for rotation angles. The results of ICPP and the planar feature-based registration method are very close to each other. On the other hand, the linear feature-based registration results are different from those of the planar feature-based registration and the ICPP method. The differences are observed in the ZT translation and the Ω and ϕ rotations parameters. As explained before, horizontal and sloping lines contribute to the computation of the ZT, (Ω), and (Φ) parameters. The parameters have errors because the horizontal and sloping lines from the TLS scans have no physical correspondences in the images.

4.3 Experiment II

Yamnuska Hall, which is a residence building at the University of Calgary, was chosen for the second experiment. The previous experiment proved that the usage of planar features as registration primitives produces better registration results than linear features primitives. Therefore, only the planar features were used as primitives to register the TLS scans in this experiment.

4.3.1 Data Description

Twenty three images were collected by the same camera used in the previous experiment (Canon EOS Rebel XS) to cover Yamnuska Hall with good intersection geometry and large overlap areas between images. However, it was difficult to find identifiable land

marks to measure points on the ground. Therefore, some targets were placed on the ground and fifteen more images were collected and added to the bundle adjustment procedure. In total, thirty eight images were used.

Seven TLS scans with very small overlap areas were used for the Yamnuska Hall experiment. The TLS scans were collected by Leica TCR 803 TLS with 1 inch of display resolution. In contrast to the proposed registration method, the ICPP method used 14 large overlapping TLS scans. Figure 4.24 shows a top view of the overlap areas of the seven TLS scans and the locations of the TLS for each scan. The lines with different colors represent the covered areas of Yamnuska Hall by the TLS scans. The black line is the top view of Yamnuska Hall. The symbol “V” shows the approximate location of the TLS for each scan. As in the first experiment, the percentages of the overlap areas between the TLS scans were evaluated roughly by calculating the ratio between the number of points in the overlap area and the total points of the scan. The percentages of the overlap areas are listed in Table 4.13

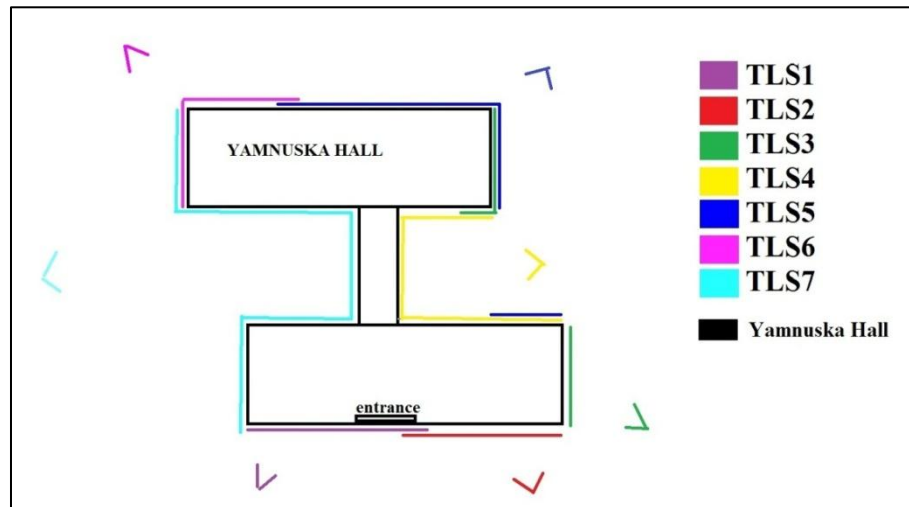


Figure 4.24. Top view of Yamnuska Hall with the covered area by the different TLS scans and the position of TLS for each scan

Table 4.13. The percentages of overlap area of the seven TLS scans of Yamnuska Hall

	TLS scan1	TLS scan2	TLS scan3	TLS scan4	TLS scan5	TLS scan6	TLS scan7
TLS scan1		23	0	0	0	0	0
TLS scan2	21		10	0	0	0	0
TLS scan3	0	12		21	20	0	0
TLS scan4	0	0	10		28	0	0
TLS scan5	0	0	20	10		3.5	0
TLS scan6	0	0	0	0	9		27
TLS scan7	0	0	0	0	0	22	

As can be seen in Table 4.13, the overlap areas between the TLS scans were very small and under 30%.

4.3.2 Bundle Adjustment Results

The overlap areas among the thirty eight images covering Yamnuska Hall are illustrated in Figure 4.25. Figure 4.26 shows the position of the camera for each image. The black line is the top view of the Yamnuska Hall, and the other colors designate different images, whose IDs are on the right side of the figures. The lines with different colors show the covered areas of Yamnuska Hall by the different images. 28 planar features were measured for Yamnuska Hall. MSAT software was used for bundle adjustment procedure to reconstruct 3D coordinates of planar features of Yamnuska Hall. The square root of the a-posteriori variance factor of the bundle adjustment was 0.00536, which was less than the pixel size of the implemented camera. The average standard deviation of the reconstructed tie points was 0.0904 m, which indicated that the results are reliable.

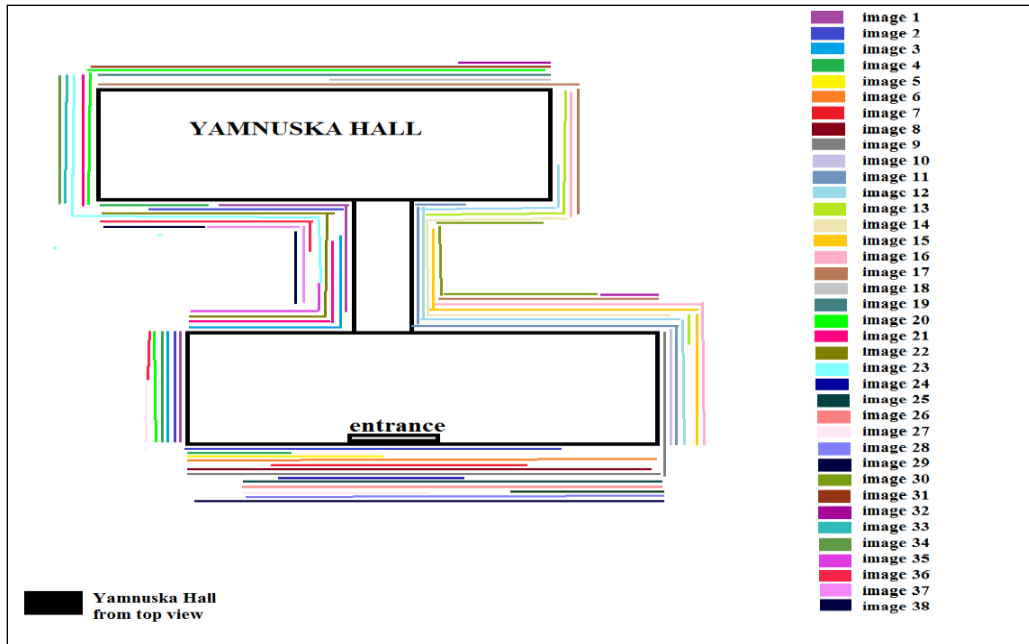


Figure 4.25. Top view of the Yamnuska Hall with the covered area by the different images

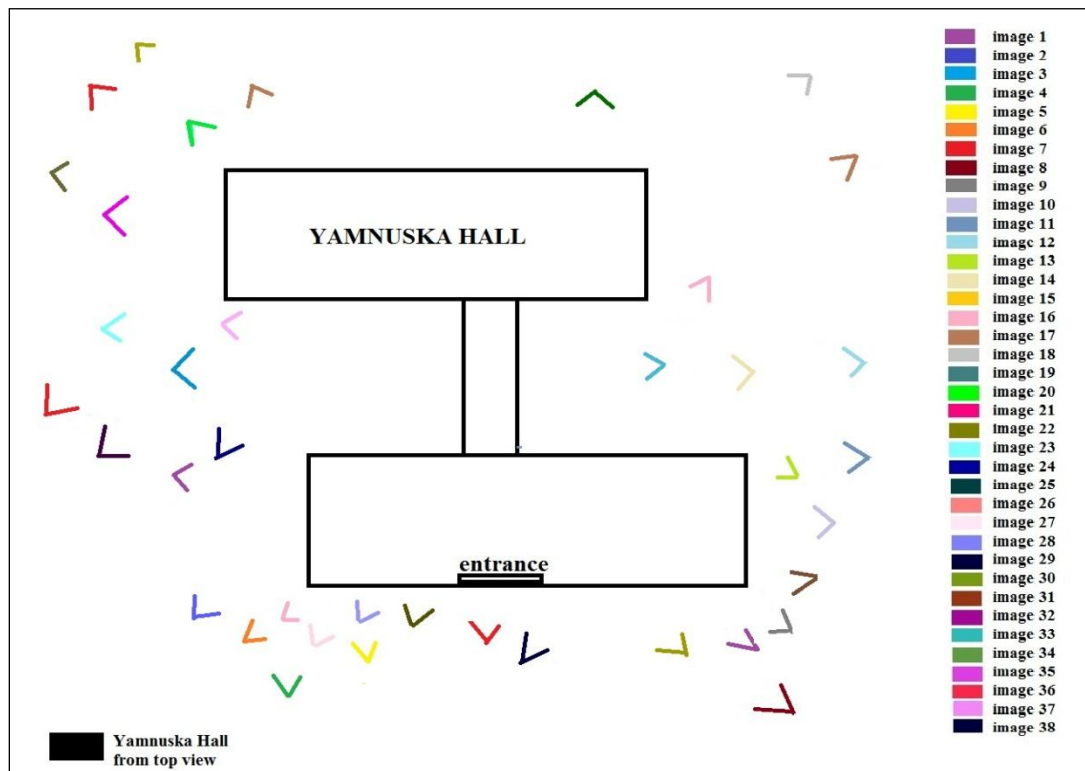


Figure 4.26. Top view of the Yamnuska Hall building with the position of the different images

4.3.3 Results of the Planar Feature-Based Registration Method

As previously mentioned, only the planar feature-based registration method was performed for the second experiment because the linear feature-based registration did not successfully register the scans in the first experiment. Moreover, in the second experiment there were not enough linear features to register the TLS scans.

Figures 4.27, 4.28, 4.29, 4.30, 4.31, 4.32, and 4.33 are illustrations of the planar features, which were used to register the TLS scans in this experiment, for photogrammetric data and TLS scan1, scan2, scan3, scan4, scan5, scan6, and scan7, respectively.

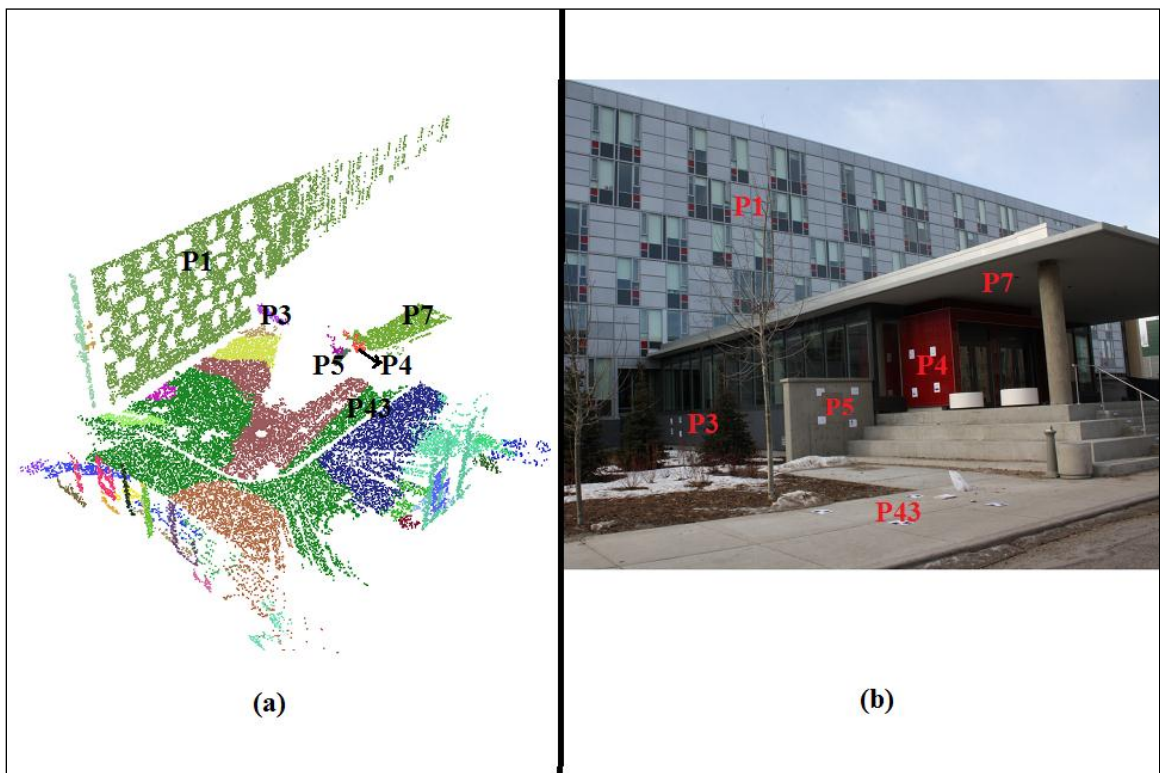


Figure 4.27. Planar features in TLS scan1 (a) and photogrammetric data (b) for the experiment II

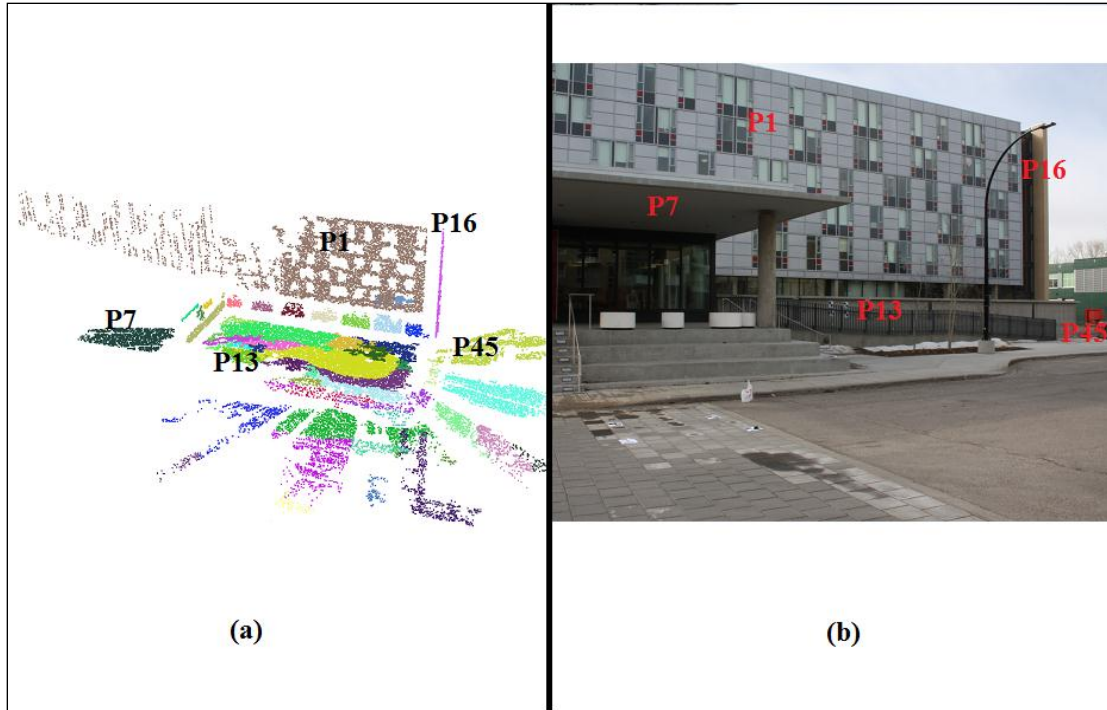


Figure 4.28. Planar features in TLS scan2 (a) and photogrammetric data (b) for the experiment II

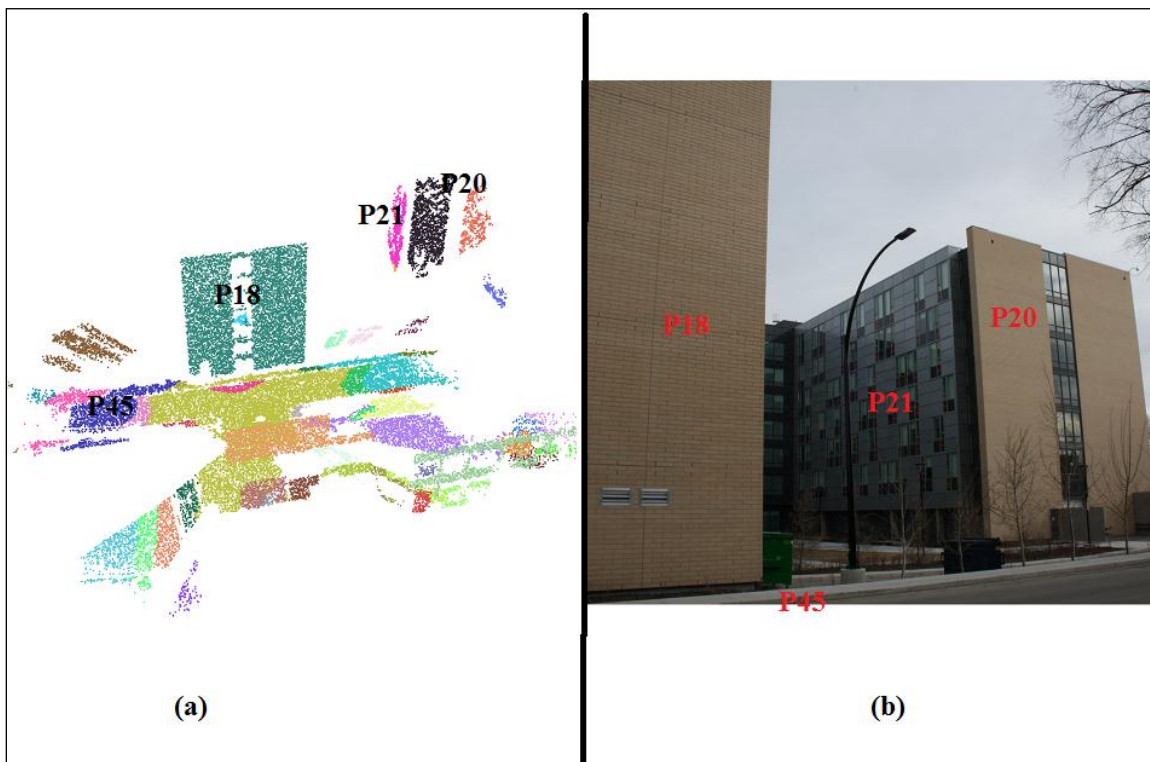


Figure 4.29. Planar features in TLS scan3 (a) and photogrammetric data (b) for the experiment II

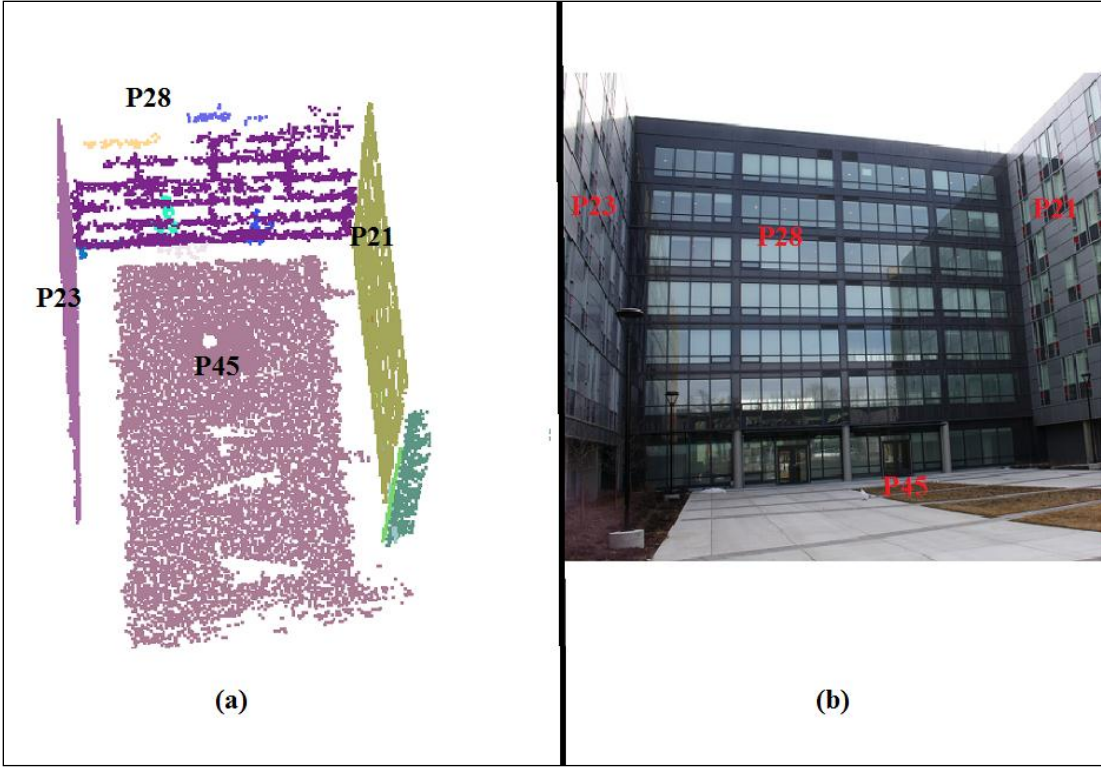


Figure 4.30. Planar features in TLS scan4 (a) and photogrammetric data (b) for the experiment II

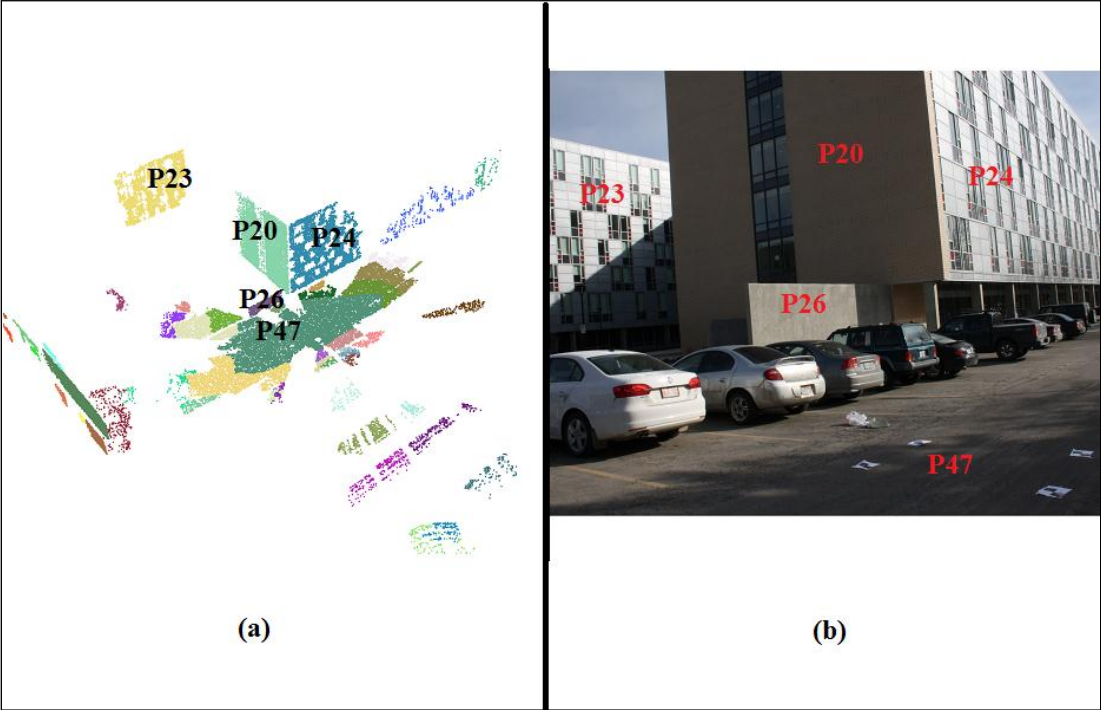


Figure 4.31. Planar features in TLS scan5 (a) and photogrammetric data (b) for the experiment II

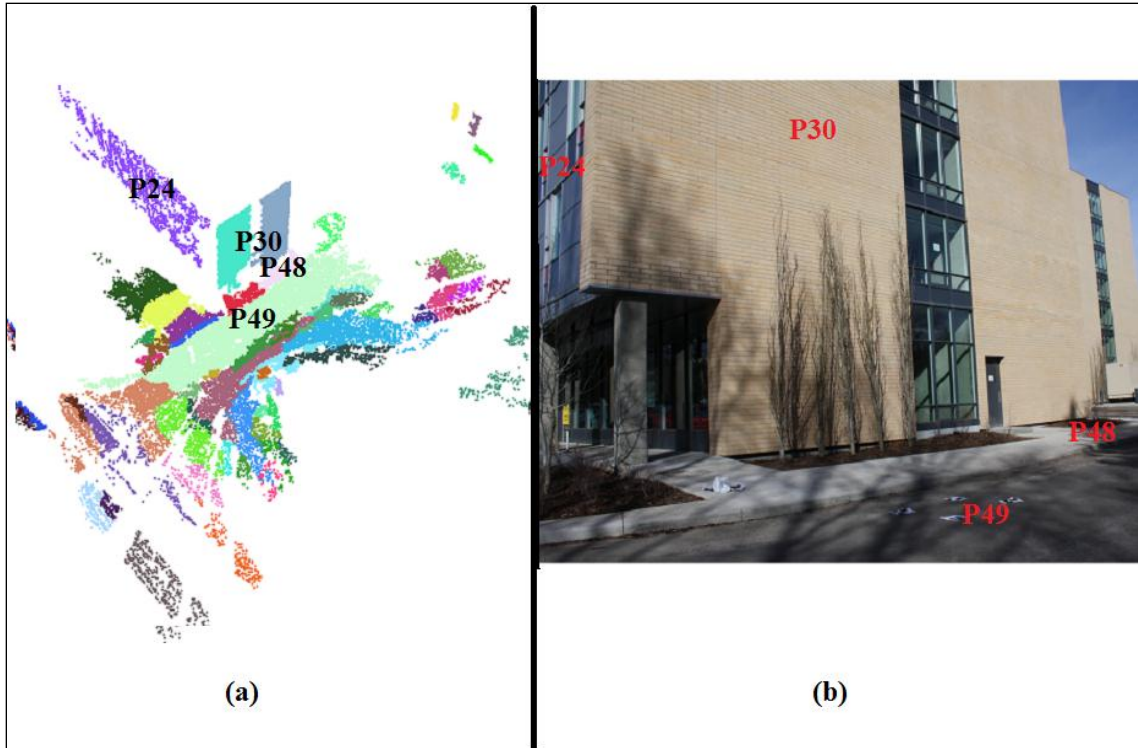


Figure 4.32. Planar features in TLS scan6 (a) and photogrammetric data (b) for the experiment II

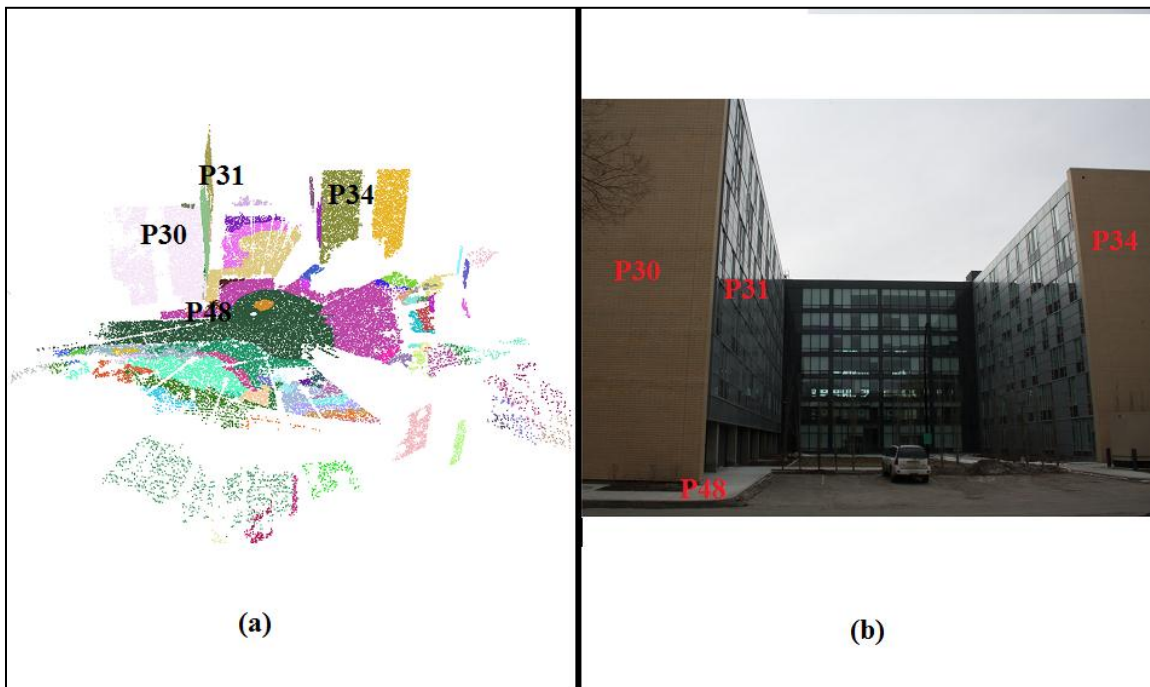


Figure 4.33. Planar features in TLS scan7 (a) and photogrammetric data (b) for the experiment II

Table 4.14 is a summary of the number of the planar features that were used in this experiment. Figure 4.34 illustrates the orientation of the planes in Yamnuska Hall: XY, XZ, and YZ-planes.

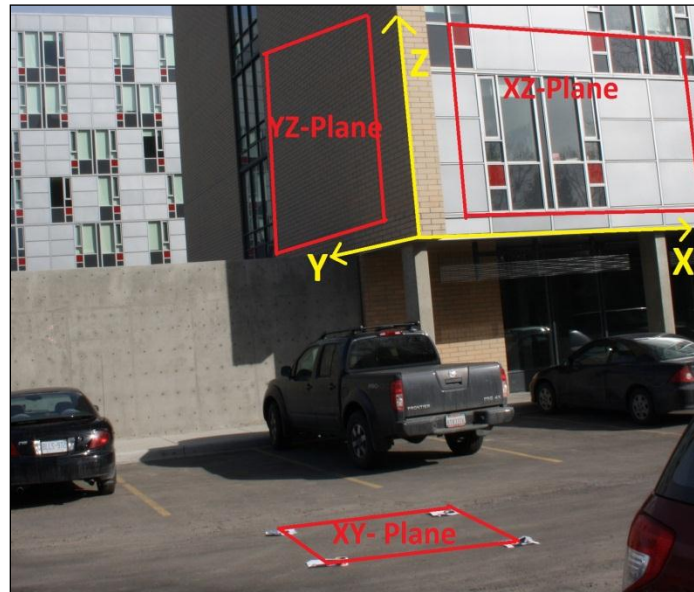


Figure 4.34. Examples of planar features with different orientation of Yamnuska Hall

Table 4.14. The number of planar features in the seven TLS scans of Yamnuska Hall

	YZ-plane	XZ-plane	XY-plane	Slope	Total
TLS scan1	1	3	2	-	6
TLS scan2	2	1	2		5
TLS scan3	1	2	1	-	4
TLS scan4	2	1	1	-	4
TLS scan5	3	1	1	-	5
TLS scan6	1	1	2	-	4
TLS scan7	1	2	1	-	4

The registration parameters, which were estimated using the planar feature-based technique, are shown in Table 4.15. TLS scan1 coordinate system is the reference frame in this experiment. The small values of the standard deviations, which are shown in

parentheses, indicate that the results are reliable. More specifically, almost all of the standard deviation values are below 10 cm for the translation parameters and 0.5 degree for the rotation parameters.

Table 4.15. The results of Yamnuska Hall from the planar feature-based registration procedure

	XT (m)	YT (m)	ZT (m)	Scale	Ω (°)	Φ (°)	κ (°)
TLS scan1	0	0	0	1	0	0	0
TLS scan2	63.612 (±0.0305)	-0.757 (±0.0239)	0.602 (±0.0480)	1	-0.384 (±0.0887)	0.229 (±0.0963)	97.254 (±0.0287)
TLS scan3	60.686 (±0.0471)	-64.455 (±0.0493)	0.623 (±0.1469)	1	0.170 (±0.1447)	0.012 (±0.1254)	42.504 (±0.0654)
TLS scan4	42.114 (±0.0465)	41.013 (±0.0488)	1.408 (±0.1181)	1	0.214 (±0.1141)	0.362 (±0.1509)	96.861 (±0.0539)
TLS scan5	19.671 (±0.0386)	-105.223 (±0.0390)	1.765 (±0.1725)	1	-0.043 (±0.1285)	-0.351 (±0.1443)	-29.752 (±0.0316)
TLS scan6	79.545 (±0.0497)	-40.263 (±0.0270)	2.152 (±0.1012)	1	-0.027 (±0.1130)	-0.443 (±0.1254)	-34.034 (±0.0346)
TLS scan7	58.652 (±0.0379)	-11.173 (±0.0309)	1.735 (±0.1157)	1	0.184 (±0.1155)	-0.207 (±0.1240)	-23.851 (±0.0365)
PRD	-16.927 (±0.0444)	79.309 (±0.0195)	51.039 (±0.0146)	0.998 (±0.0004)	88.065 (±0.4558)	282.435 (±0.0732)	-162.245 (±0.4450)

4.3.4 Quality Control of the Planar Feature-Based Registration Results

The quality of the results was analyzed as was performed in the first experiment. First, the estimated registration results were evaluated qualitatively by plotting the registered TLS scans. Then, quantitative quality control of the results was conducted by calculating the point-to-plane normal distance.

a) Qualitative Quality Control

The seven registered TLS scans of Yamnuska Hall were plotted together and were evaluated by closer investigation of the overlap areas. Figure 4.35 illustrates the general

view of the seven registered TLS scans, which were colored according to the height of the points.

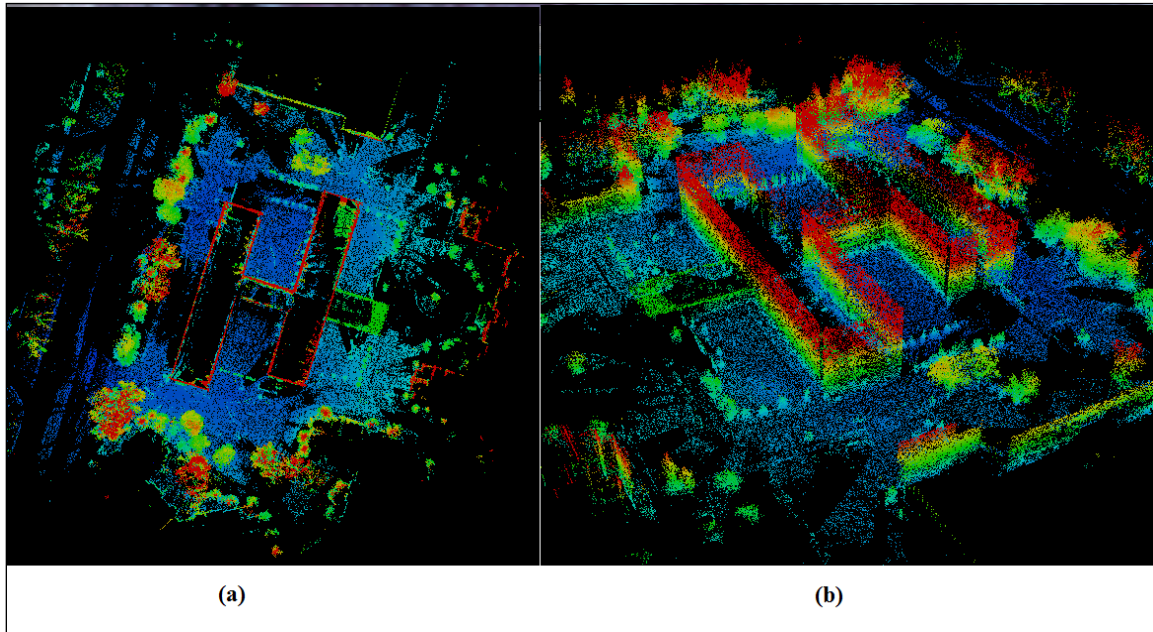


Figure 4.35. General view of the seven registered TLS scans of Yamnuska Hall: top view (a) and 3D view (b)

Figures 4.36 and 4.37 are examples of reliably registered TLS scans. TLS scan3, TLS scan4, and TLS scan5 registered very well and can be seen in the overlap area of the TLS scans (Figure 4.36). TLS scans6 and TLS scans7 also had overlap areas, which helped to analyze the quality of the registration results. Parts of windows from different TLS scans registered very well in the overlap area of the TLS scans, which proves that the registration was reliable and can be seen in the overlap areas in Figure 4.37.

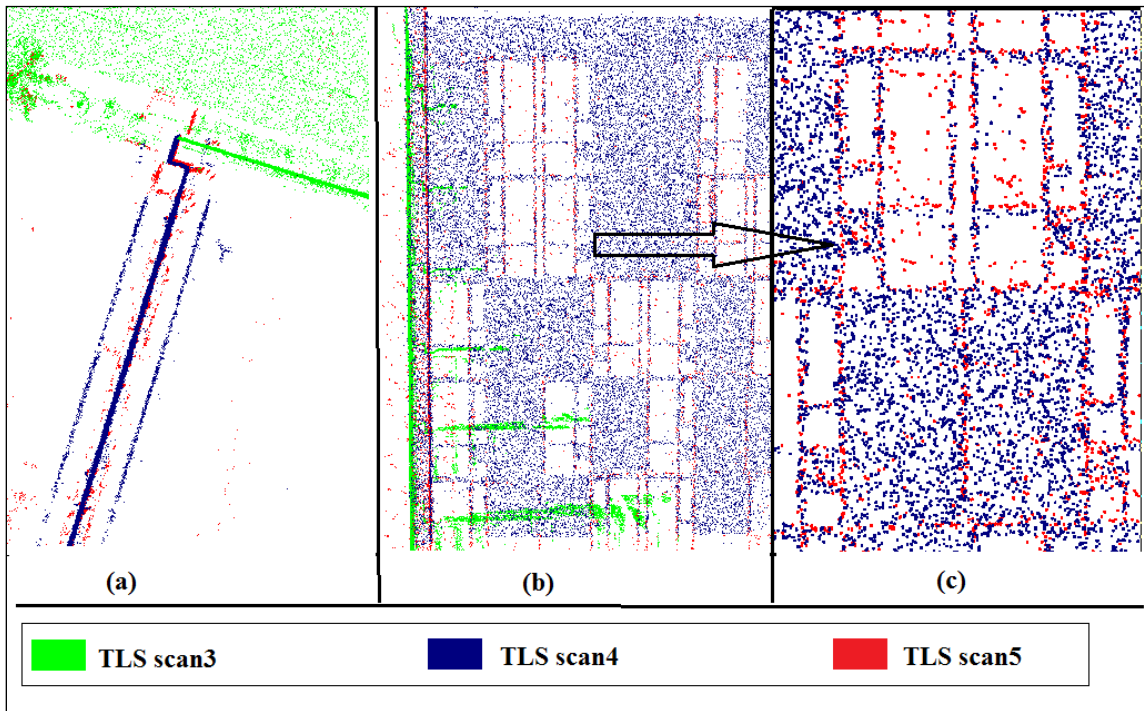


Figure 4.36. Registered TLS scan3, scan4, and scan5: top view (a), 3D view (b), and close-up of windows (c)

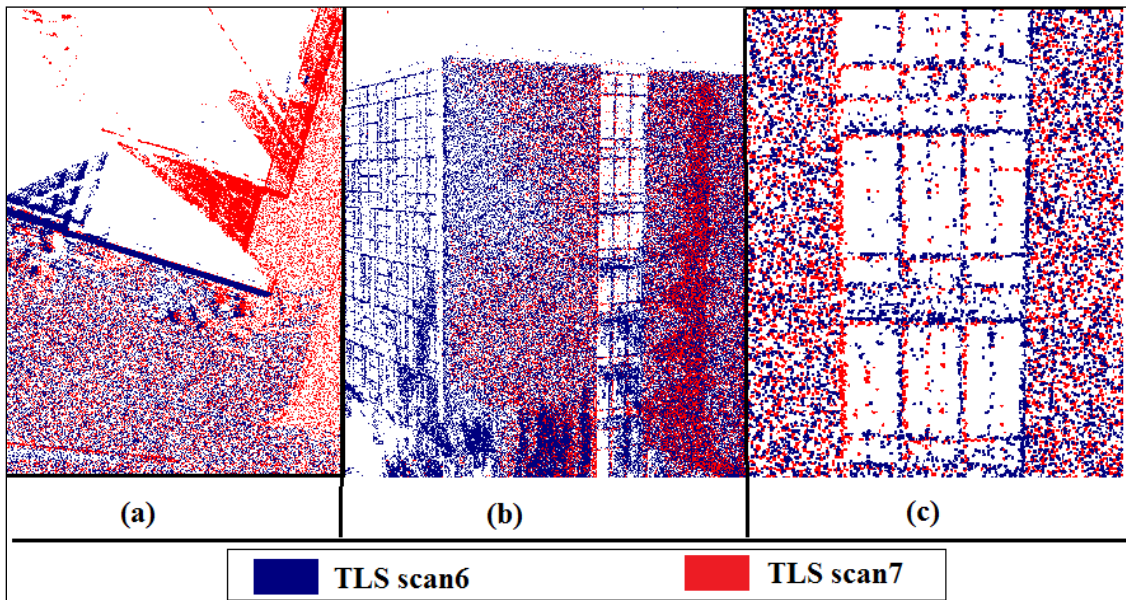


Figure 4.37. Registered TLS scan6 and scan7: top view (a), 3D view (b), and close-up of windows (c)

b) Quantitative Quality Control

The point-to-plane normal distances between the registered TLS scans and the PRD planes were calculated. As in the previous experiment, all of the points of the segmented planes were first used for the normal distance calculations. The mean, standard deviation, and RMSE of the normal distances for each plane are listed in Table 4.16. Then, only the points of the segmented planes, which are inside the PRD plane points, were used for normal distance calculation (Table 4.17).

Generally, the normal distances were larger when all of the segmented plane points were used from the TLS scans. For instance, in Table 4.17, RMSE of the calculated normal distance for the plane 45 is 0.017 meters, while the same plane has 0.136 meters RMSE value in Table 4.16.

If there were any available planes in the overlap area of the TLS scans, the normal distance calculations for the planes between different TLS scans were also done and are listed in Table 4.18. The mean, standard deviation, and RMSE of the normal distances of Yamnuska Hall in Tables 4.16, 4.17, and 4.18 are below 10 cm, and they demonstrate that the registration results are reliable. The planes, together with their IDs, can be seen in Figures 4.27, 4.28, 4.29, 4.30, 4.31, 4.32, and 4.33.

Table 4.16. The mean, standard deviation, and RMSE of the calculated normal distances results for planes between the PRD and the TLS scans of Yamnuska Hall using all points of the segmented planes

TLS scan1 vs. PRD	Plane ID	Plane 1	Plane 3	Plane 4	Plane 5	Plane 7	Plane 43
	Plane Ori.	XZ-plane	YZ-plane	YZ-plane	XZ-plane	XY-plane	XY-plane
	\overline{nd} (m)	-0.039	0.016	0.004	0.018	-0.035	0.130
	σ (m)	0.027	0.045	0.015	0.013	0.019	0.044
	RMSE (m)	0.047	0.046	0.015	0.018	0.039	0.134
TLS scan2 vs. PRD	Plane ID	Plane 1	Plane 16	Plane 7	Plane13	Plane 45	
	Plane Ori.	XZ-plane	YZ-plane	XY-plane	XZ-plane	XY-plane	
	\overline{nd} (m)	0.013	-0.042	-0.036	0.073	-0.010	
	σ (m)	0.037	0.103	0.016	0.048	0.035	
	RMSE (m)	0.039	0.111	0.040	0.088	0.037	
TLS scan3 vs. PRD	Plane ID	Plane 18	Plane 20	Plane 21	Plane 45		
	Plane Ori.	YZ-plane	YZ-plane	XZ-plane	XY-plane		
	\overline{nd} (m)	0.001	-0.022	0.019	0.035		
	σ (m)	0.026	0.018	0.031	0.082		
	RMSE (m)	0.026	0.028	0.037	0.090		
TLS scan4 vs. PRD	Plane ID	Plane 21	Plane 23	Plane 28	Plane 46		
	Plane Ori.	XZ-plane	XZ-plane	YZ-plane	XY-plane		
	\overline{nd} (m)	-0.040	0.029	0.047	0.076		
	σ (m)	0.032	0.018	0.077	0.113		
	RMSE (m)	0.052	0.034	0.090	0.136		
TLS scan5 vs. PRD	Plane ID	Plane 20	Plane 23	Plane 24	Plane 26	Plane 47	
	Plane Ori.	YZ-plane	XZ-plane	XZ-plane	XZ-plane	XY-plane	
	\overline{nd} (m)	0	0.005	0.045	-0.084	0.017	
	σ (m)	0.014	0.022	0.018	0.007	0.053	
	RMSE (m)	0.014	0.023	0.049	0.085	0.056	
TLS scan6 vs. PRD	Plane ID	Plane 24	Plane 30	Plane 48	Plane 49		
	Plane Ori.	XZ-plane	YZ-plane	XY-plane	XY-plane		
	\overline{nd} (m)	0.032	0.016	0.127	0.109		
	σ (m)	0.029	0.016	0.115	0.084		
	RMSE (m)	0.032	0.019	0.127	0.109		
TLS scan7 vs. PRD	Plane ID	Plane 30	Plane 31	Plane 33	Plane 34	Plane 48	
	Plane Ori.	YZ-plane	YZ-plane	YZ-plane	YZ-plane	XY-plane	
	\overline{nd} (m)	0.012	0.005	0.084	-0.012	-0.036	
	σ (m)	0.017	0.017	0.031	0.012	0.025	
	RMSE (m)	0.021	0.018	0.090	0.017	0.044	

Table 4.17. The mean, standard deviation, and RMSE of the calculated normal distances for planes between PRD and TLS scans of Yamnuska Hall using only points of segmented planes that are inside the PRD planes borders

TLS scan1 vs. PRD	Plane ID	Plane 1	Plane 3	Plane 4	Plane 5	Plane 7	Plane 43
	Plane Ori.	XZ-plane	YZ-plane	YZ-plane	XZ-plane	XY-plane	XY-plane
	$\bar{n}d$ (m)	-0.042	0.016	0.008	0.015	-0.035	0.097
	σ (m)	0.025	0.045	0.002	0.001	0.019	0.032
	RMSE (m)	0.049	0.047	0.009	0.015	0.040	0.103
TLS scan2 vs. PRD	Plane ID	Plane 1	Plane 16	Plane 7	Plane13	Plane 45	
	Plane Ori.	XZ-plane	YZ-plane	XY-plane	XZ-plane	XY-plane	
	$\bar{n}d$ (m)	-0.015	-0.038	-0.036	0.039	-0.010	
	σ (m)	0.042	0.020	0.029	0.038	0.016	
	RMSE (m)	0.045	0.045	0.040	0.049	0.037	
TLS scan3 vs. PRD	Plane ID	Plane 18	Plane 20	Plane 21	Plane 45		
	Plane Ori.	YZ-plane	YZ-plane	XZ-plane	XY-plane		
	$\bar{n}d$ (m)	0.002	-0.023	0.010	-0.018		
	σ (m)	0.024	0.017	0.030	0.025		
	RMSE (m)	0.024	0.029	0.032	0.032		
TLS scan4 vs. PRD	Plane ID	Plane 21	Plane 23	Plane 28	Plane 46		
	Plane Ori.	XZ-plane	XZ-plane	YZ-plane	XY-plane		
	$\bar{n}d$ (m)	-0.026	0.027	0.034	0.005		
	σ (m)	0.026	0.019	0.059	0.016		
	RMSE (m)	0.037	0.033	0.068	0.017		
TLS scan5 vs. PRD	Plane ID	Plane 20	Plane 23	Plane 24	Plane 26	Plane 47	
	Plane Ori.	YZ-plane	XZ-plane	XZ-plane	XZ-plane	XY-plane	
	$\bar{n}d$ (m)	-0.001	0.007	0.045	-0.084	0.008	
	σ (m)	0.014	0.021	0.007	0.007	0.036	
	RMSE (m)	0.014	0.022	0.048	0.085	0.037	
TLS scan6 vs. PRD	Plane ID	Plane 24	Plane 30	Plane 48	Plane 49		
	Plane Ori.	XZ-plane	YZ-plane	XY-plane	XY-plane		
	$\bar{n}d$ (m)	0.011	0.006	0.012	-0.005		
	σ (m)	0.029	0.016	0.008	0.007		
	RMSE (m)	0.032	0.018	0.015	0.009		
TLS scan7 vs. PRD	Plane ID	Plane 30	Plane 31	Plane 33	Plane 34	Plane 48	
	Plane Ori.	YZ-plane	YZ-plane	YZ-plane	YZ-plane	XY-plane	
	$\bar{n}d$ (m)	0.012	0.006	0.084	-0.011	-0.017	
	σ (m)	0.017	0.017	0.031	0.011	0.011	
	RMSE (m)	0.021	0.018	0.090	0.016	0.020	

Table 4.18. The mean, standard deviation, and RMSE of the calculated normal distances between different TLS scans of Yamnuska Hall

TLS scan1 vs. TLS scan2	Plane ID	Plane 1	Plane 7	TLS scan4 vs. TLS scan5	Plane ID	Plane 23			
	Plane Ori.	XZ-plane	XY-plane		Plane Ori.	XZ-plane			
	\overline{nd} (m)	0.041	-0.004		\overline{nd} (m)	0.006			
	σ (m)	0.037	0.013		σ (m)	0.016			
	RMSE (m)	0.055	0.014		RMSE (m)	0.018			
TLS scan3 vs. TLS scan4	Plane ID	Plane 45			TLS scan5 vs. TLS scan6	Plane ID	Plane 24		
	Plane Ori.	XY-plane				Plane Ori.	XZ-plane		
	\overline{nd} (m)	-0.011				\overline{nd} (m)	-0.009		
	σ (m)	0.016				σ (m)	0.025		
	RMSE (m)	0.023				RMSE (m)	0.027		
TLS scan3 vs. TLS scan5	Plane ID	Plane 20			TLS scan6 vs. TLS scan7	Plane ID	Plane 30	Plane 48	
	Plane Ori.	YZ-plane				Plane Ori.	YZ-plane	XY-plane	
	\overline{nd} (m)	0.008				\overline{nd} (m)	0.015	0.008	
	σ (m)	0.016				σ (m)	0.075	0.019	
	RMSE (m)	0.018				RMSE (m)	0.076	0.021	

Finally, the registered TLS scans were plotted for visual representation of the calculated normal distance for each point-to-plane (Figure 4.38 and 4.39). The normal distances in Figure 4.39 were calculated by using all the segmented plane points from the TLS scans. Therefore, in the case of under-segmentation, the normal distances between the PRD and the TLS scans planes are large. Moreover, as previously explained, the TLS segmented plane points were generally not in the area of the PRD plane points. For these reasons, there were large normal distances, which are visible in Figure 4.39.

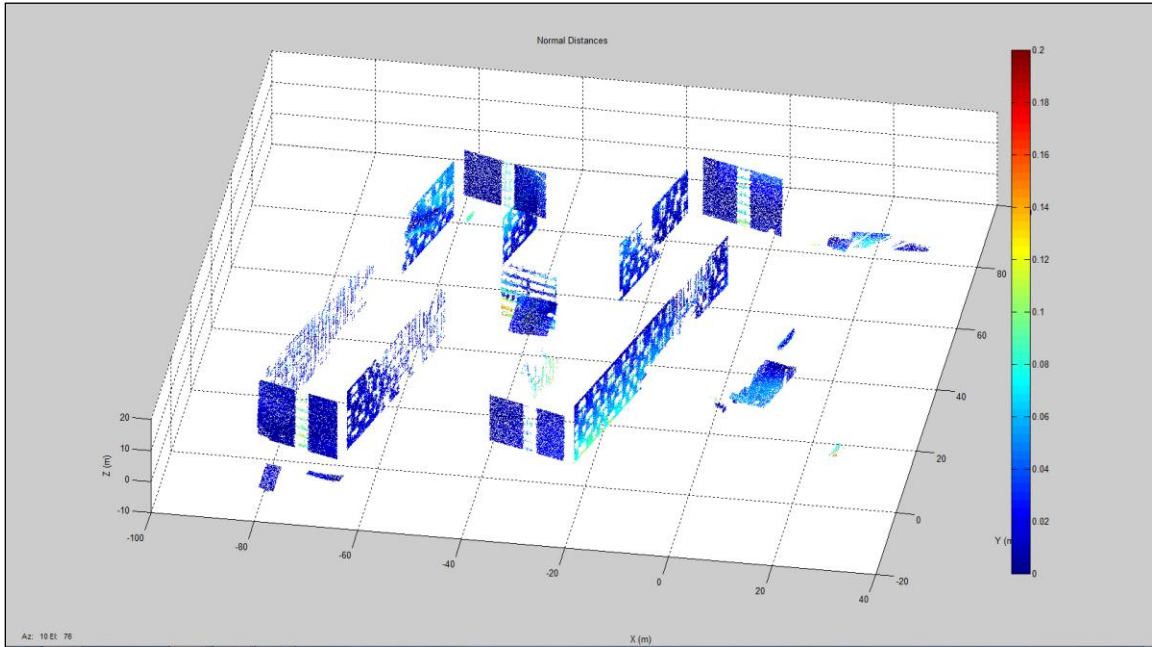


Figure 4.38. 3D view of the registered TLS scans of Yamnuska Hall (color based on normal distances calculated using only points of the segmented planes from TLS scans which are inside the polygon of PRD planes points)

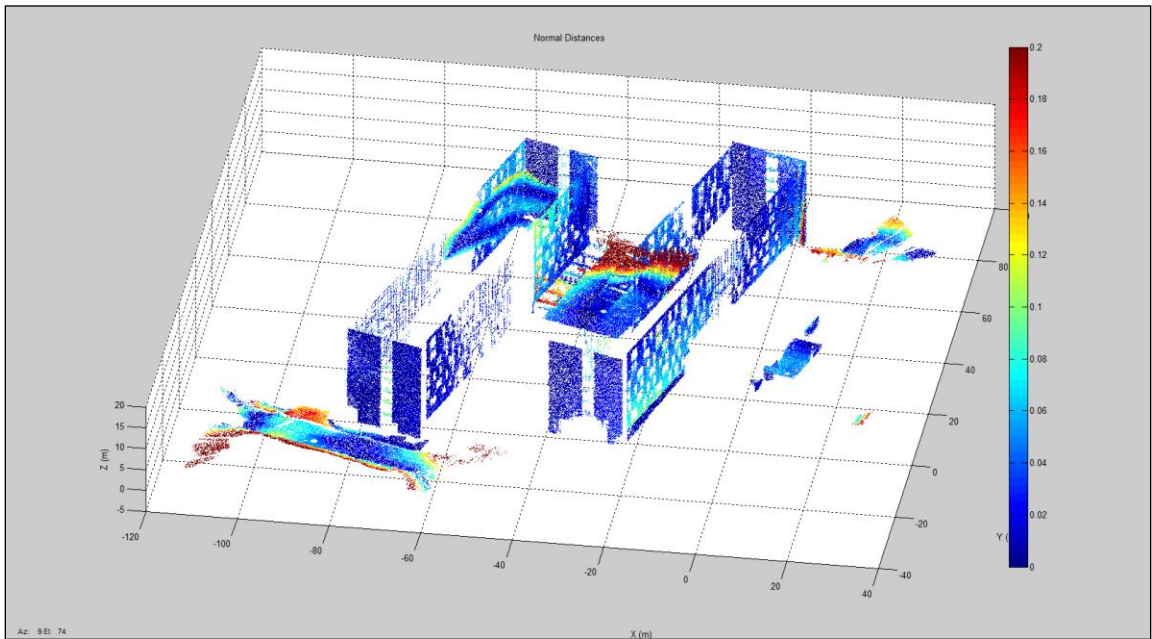


Figure 4.39. 3D view of the registered TLS scans of Yamnuska Hall (color based on normal distances calculated using all points of the segmented planes from TLS scans)

The differences of the calculated point-to-plane normal distances between the Tables 4.16 and 4.17 are also obvious in Figures 4.38 and 4.39. Especially for the planes that are on the ground.

4.3.5 Comparison of the Results of the Planar Feature-Based Registration and ICPP Method for Yamnuska Hall

A final evaluation of the registration results for this experiment was conducted by comparing the proposed registration method results with those from the ICPP method. It is worth mentioning again that 14 large overlapping TLS scans were used for the ICPP method, while only seven minimum overlapping TLS scans were used for the proposed registration method. There are some differences between the two registration methods of up to 20 cm, which are highlighted in Table 4.19.

Table 4.19. Comparison of the proposed planar feature-based and ICPP method results for Yamnuska Hall

		XT (m)	YT (m)	ZT (m)	Scale	Ω (°)	Φ (°)	K (°)
TLS scan2	Planar-Based	63.612	-0.757	0.602	1	-0.384	0.229	97.254
	the ICPP	63.507	-0.733	0.605	1	0.128	0.025	97.171
	Difference	0.104	-0.024	-0.002	0	-0.512	0.204	0.083
TLS scan3	Planar-Based	60.686	-64.455	0.623	1	0.170	0.012	42.504
	the ICPP	60.537	-64.495	0.618	1	0.031	0.060	42.437
	Difference	0.149	0.040	0.004	0	0.138	-0.048	0.066
TLS scan4	Planar-Based	42.114	41.013	1.408	1	0.214	0.362	96.861
	the ICPP	42.028	40.810	1.362	1	0.164	0.071	96.764
	Difference	0.086	0.202	0.046	0	0.049	0.291	0.097
TLS scan5	Planar-Based	19.671	-105.223	1.765	1	-0.043	-0.351	-29.752
	the ICPP	19.597	-105.052	1.573	1	0.008	-0.004	-29.789
	Difference	0.073	-0.170	0.192	0	-0.051	-0.347	0.0369
TLS scan6	Planar-Based	79.545	-40.263	2.152	1	-0.027	-0.443	-34.034
	the ICPP	79.363	-40.140	1.864	1	0.0765	-0.024	-34.006
	Difference	0.181	-0.122	0.287	0	-0.104	-0.419	-0.027
TLS scan7	Planar-Based	58.652	-11.173	1.735	1	0.184	-0.207	-23.850
	the ICPP	58.569	-10.968	1.796	1	0.059	-0.063	-23.697
	Difference	0.083	-0.205	-0.060	0	0.125	-0.143	-0.153

To understand which method produces better results, it will be more helpful to plot the registered TLS scans together and examine the overlap areas more closely. A 19 cm difference in ZT for TLS scan5 between the proposed planar feature-based registration and ICPP method can be seen in Table 4.19. However, the ZT parameter of the TLS scan4 has the same results for both registration methods. Moreover, TLS scan4 and TLS scan5 are overlapping in some parts. Therefore, registered TLS scan4 and TLS scan5, by using the estimated parameters of both methods, were plotted to investigate which method had the 19 cm problem. Figure 4.40a illustrates how the proposed method registers the two TLS scans successfully. On the other hand, the 19 cm difference for ZT in the circled area is observed for the registered TLS scans using the ICPP method (Figures 4.39b and 4.39c), and it can be seen that the 19 cm difference occurred in TLS scan5 because of the incorrect registration results of the ICPP method.

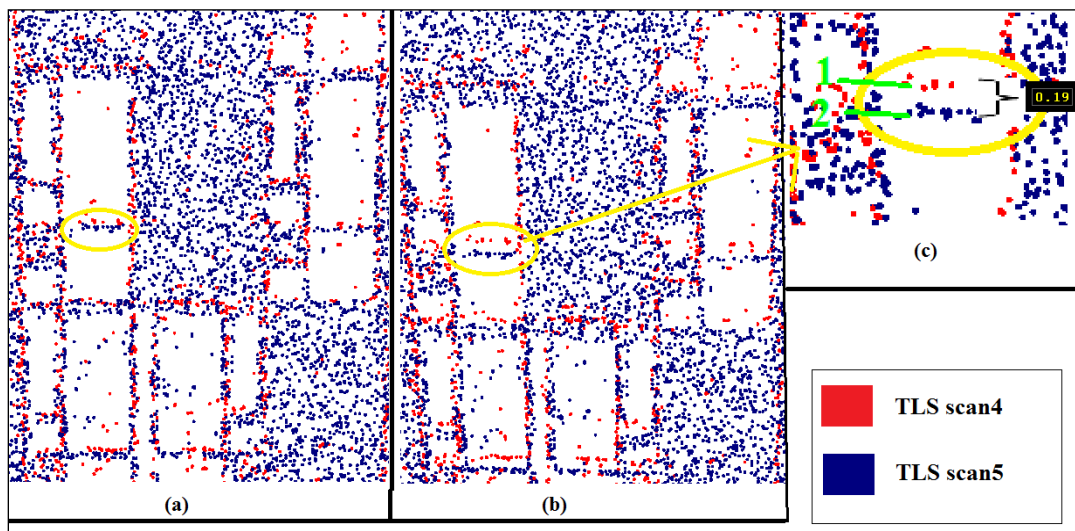


Figure 4.40. The proposed planar feature-based registration method (a) versus ICPP registration results (b) & (c)

Another comparison of the proposed planar feature-based registration and ICPP method is illustrated in Figure 4.41. As highlighted in Table 4.19, there was a 20 cm difference in the YT translation parameter between the two registration methods for TLS scan7. To investigate which method had more reliable results, TLS scan7 and TLS scan1 were registered together using the estimated results of the proposed registration and the ICPP methods, separately (Figure 4.41). It should be noted that the TLS scan1 was chosen as the reference frame. The green points belong to TLS scan1. The registered TLS scan7 using the ICPP method is shown in red, while the registered TLS scan7 by the proposed planar feature-based registration method is shown in dark blue. The three walls of the building from the top and side view are illustrated in Figure 4.41c. As can be seen in Figure 4.41b, TLS scan7 and TLS scan1 were registered well with the proposed planar feature-based registration. On the other hand, TLS scan7, which was registered by the ICPP method and shown in red color, has 16 cm. In summary, as we can see in Figure 4.41, the proposed planar feature-based method registered TLS scan7 slightly better than the ICPP method.

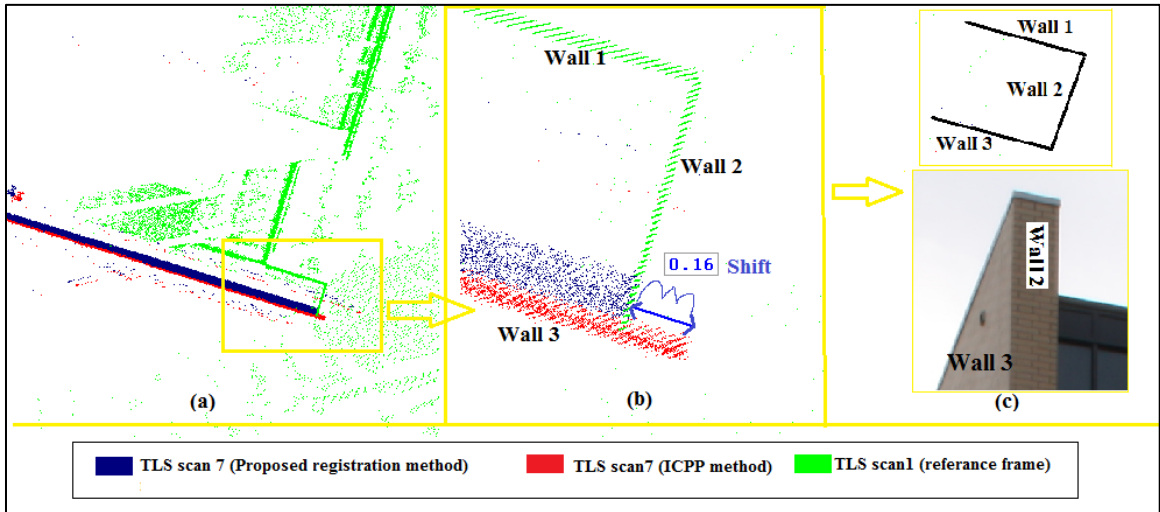


Figure 4.41. The proposed registration versus the ICPP registration results for TLS scan7 and scan1 (reference frame)

CHAPTER 5

CONCLUSIONS and RECOMMENDATIONS FOR FUTURE WORK

5.1 Conclusions

In this research, a registration method for registering TLS scans with minimum overlap areas is proposed, which is contrary to many registration methods that require large overlap areas among TLS scans. The overlap areas among the TLS scans are less than %20 and %30 for the first and second experiments, respectively. While commonly used registration methods, such as the ICP and its variants, fail to register the TLS scans with minimum overlap area, the proposed registration method has succeeded in registering the scans with minimum overlapping using photogrammetric data.

Since the proposed registration method depends on the photogrammetric model to register TLS scans with minimum overlap, the accuracy of the object space reconstruction from photogrammetric data, which is highly dependent on the operator, is crucial for a reliable result with the proposed registration method. Therefore, the operator should be very careful during the bundle adjustment procedure for object space reconstruction from photogrammetric data.

The proposed registration method uses linear or planar features instead of all of the available points from the scans. Therefore, in terms of the run time for relating the registration primitives and estimating the registration parameters, the proposed registration method is faster than many other registration methods (i.e. the ICP and

ICPP), which use all of the available points to register TLS scans. The most time consuming part of the proposed registration method is the creation of a photogrammetric model and extracting the planar and linear features from the photogrammetric data.

The proposed registration method with planar feature primitives (the planar feature-based registration) requires at least four planes which do not intersect with each other in one point in order to estimate the seven registration parameters (three translations, three rotations, and the scale). On the other hand, the proposed registration method with linear features (the linear feature-based registration) requires only two non-coplanar lines for estimating the seven registration parameters. It might not always be possible, however, to have four planes in one TLS scan for the surveyed structure. Therefore, in terms of the number of required features to estimate the registration parameters, the proposed linear feature-based registration method is more flexible than the proposed planar feature-based registration method.

A quantitative quality control is proposed in this research to evaluate the results of the proposed registration. For this purpose, point-to-plane normal distances between the registered surfaces were calculated.

According to the quality control analysis, the proposed planar feature-based registration method gives more reliable results than those of the proposed linear feature-based registration. The TLS scans' extracted linear features, which are the intersection of the segmented neighboring planar features, sometimes do not have a physical correspondence in photogrammetric data. This problem generally occurs on the roof

portion of the experimental data set 1, which consists of complex and many small planar features. The vertical/sloping linear features are used to estimate the shift in height (ZT , translation in Z axis) and the associated rotation angles. Therefore, the linear feature-based registration method has errors in the parameters corresponding to the Z axis translation (ZT) and the Ω and Φ rotation angles. However, the other registration parameters were estimated reliably by the linear feature-based registration method. The point-to-plane normal distances between the registered TLS scans and the photogrammetric model using the estimated registration parameters are less than 10 cm except for the planes which are perpendicular to the Z axis. A comparison was done between the proposed registration and the ICPP methods. It should be noted again that additional TLS scans were added to the scans with minimum overlap for estimating the registration parameters with the ICPP method. Less than 10 cm accuracy was observed for the X and Y translation parameters between the results of the proposed registration and the ICPP methods.

The planar feature-based registration method estimated all of the registration parameters reliably. The estimated registration parameters exhibited a difference of less than 10 cm in the point-to-plane normal distances for the planes between the registered TLS scans and the photogrammetric model using the estimated registration parameters. The planar feature-based registration results are also very close to the ICPP method results. Less than a 10 cm and 0.3 degree difference were observed for the translation and rotation parameters respectively, between the results of the planar feature-based registration and the ICPP method.

The photogrammetrically-reconstructed points for the two experimental data sets using a bundle adjustment procedure attained an accuracy of around 10 cm, and the same accuracy was observed by calculating the point-to-plane normal distances between the registered TLS scans and the photogrammetric model using the estimated registration parameters. This again confirmed the significance of the object space reconstruction to achieving the accuracy of the proposed registration method.

In conclusion, the planar feature-based method registered the TLS scans with minimum overlaps reliably, while the linear feature-based registration experienced problems with some of the registration parameters. Mis-registration occurred with the proposed linear feature-based registration method because of the extracted linear features from the scans, which do not have a physical correspondence in photogrammetric data.

5.2 Recommendations for Future Work

As highlighted in the previous subsection, the accuracy of the proposed registration method depends on the reconstructed model from the photogrammetric data. The object space reconstruction accuracy depends on the operator. The image measurements, which are performed manually, might contain errors. Therefore, an automatic object space reconstruction method from photogrammetric data can be investigated and studied (i.e., dense matching; e.g. Hullo et al., 2009.).

Planar and linear features are used separately as primitives for the proposed registration method. In this research, there is enough number of planar and linear features were available to estimate registration parameters for both experiments I and II. Since it might

not always be possible to have the minimum required number of planes or lines in each TLS scan to estimate the registration parameter, it might be useful to combine and use these two features together for the proposed registration method.

Some of the current laser scanners provide color information of the surveyed objects/structures. However, in the cases that the laser scanner does not provide any color information, the photogrammetric data can be used for texturing the TLS scans.

REFERENCES

- Al-Durgham M., 2007. Alternative Methodologies for the Quality Control of LiDAR Systems. *M.Sc. Thesis*. Department of Geomatics Engineering, University of Calgary, Canada, pp. 66-68.
- Al-Durgham M., I. Datchev, and A. Habib, 2011. Analysis of Two Triangle-Based Multi-Surface Registration Algorithms of Irregular Point Clouds. *ISPRS Workshop Laser Scanning 2011*. Volume XXXVIII-5/W12. Calgary, Canada. 29-31 August, 2011.
- Al-Manasir K., and C. S. Fraser, 2006. Automatic Registration of Terrestrial Laser Scanner Data via Imagery. *The International Archives of the Photogrammetry Remote Sensing and Spatial Information Sciences (IAPRS)*, Dresden 25-27 September, Vol. 35 No.5 pp. 26-31.
- Al-Ruzouq R., 2004. Semi-Automatic Registration of Multi-Source Satellite Imagery with Varying Geometric Resolutions. *Ph.D. Dissertation*. Department of Geomatics Engineering, University of Calgary, Canada, pp. 10-24.
- Bae K. and D. Lichti, 2008. A method for automated registration of unorganized point clouds. *ISPRS Journal of Photogrammetry and Remote Sensing*, 63(1), pp. 36-54.
- Besl P. J., and N. D. McKay, 1992. A method for registration of 3-D shapes. *IEEE Transactions on Pattern Analysis and Machine Intelligence*, 14(2):pp. 239–256.
- Bogue R., 2010. Three-dimensional measurements: a review of technologies and applications. *Sensor Review*, Vol. 30 Iss: 2 pp. 102 – 106.
- Chen Y. and G. Medioni, 1991. Object Modeling by Registration of Multiple Range Images. *International Conference on Robotics and Automatim*, Sacramento, California - April 1991.

Cooper M.A.R. and S. Robson, 2001. Theory of Close Range Photogrammetry. In: Atkinson K. B. ed. *Close Range Photogrammetry and Machine Vision*. Caithness, Scotland, UK. pp.9-52.

Detchev I. D., 2010. Implementation of a Close Range Photogrammetric. System for 3D Reconstruction of a Scoliotic Torso. M.Sc. Thesis. Department of Geomatics Engineering, University of Calgary, Canada, pp. 10-27.

Dold C. and C. Brenner, 2006. Registration of Terrestrial Laser Scanning Data Using Planar Patches and Image Data. *IAPRS Volume XXXVI, Part 5*, Dresden 25-27 September 2006.

Guan Y. and H. Zhang , 2011. Initial Registration for Point Clouds Based on Linear Features. *Fourth International Symposium on Knowledge Acquisition and Modeling*, 2011. pp.474-477, 2011

Habib A., M. S Ghanma., and M. Tait, 2004. Integration of LIDAR and Photogrammetry for Close Range Applications. *XXth ISPRS Congress: Proceedings of Commission V*, 12/07/2004, Istanbul, Turkey, 2004.

Habib A., 2007. ENGO 531 - Advanced Photogrammetric and Ranging Techniques [Online] // <http://dprg.geomatics.ucalgary.ca>.

Habib A., A. P. Kersting, Z. Ruifanga, M. Al-Durgham, C. Kim, and D. C. Lee, 2008. Lidar Strip Adjustment Using Conjugate Linear Features in Overlapping Strips. *The International Archives of the Photogrammetry, Remote Sensing and Spatial Information Sciences*. Vol. XXXVII. Part B1. Beijing 2008 . pp. 386-390.

Habib A., I. Detchev, and K. Bang, 2010. A Comparative Analysis of Two approaches for Multiple-Surface Registration of Irregular Point Clouds. *International Archives of the Photogrammetry, Remote Sensing and Spatial Information*, XXXVIII(Part1).

- Habib A., E. Kwak, M. Al-Durgham, 2011. Model-Based Automatic 3D Building Model Generation by Integrating LiDAR and Aerial Images. *Archives of Photogrammetry, Cartography and Remote Sensing*, Vol. 22, 2011, pp. 187-200 ISSN 2083-2214.
- Hullo J. F., P. Grussenmeyer, S. Fares, 2009. Photogrammetry and Dense Stereo Matching Approach Applied to the Documentation of the Cultural Heritage of Kilwa(Saudi Arabia). *22nd CIPA Symposium*, October 11-15, 2009, Kyoto, Japan.
- Jaw J. J. and T. Y. Chaung, 2008. Feature-Based Registration of Terrestrial LiDAR Point Clouds. *The International Archives of the Photogrammetry, Remote Sensing and Spatial Information Sciences*. Vol. XXXVII. Part B3b. Beijing 2008 . pp.303-308.
- Kraus K.,1993. Photogrammetry part 1: Fundamentals and standard processes, Ferd. Dümler Verlag, Bonn,1993.
- Kersting A. P. B., 2012. ‘Quality Assurance of Multi-Sensor Systems’ *Ph.D. Dissertation*. Department of Geomatics Engineering, University of Calgary, Canada, pp. 15-160.
- Koch K. R., 1988. Parameter estimation and hypothesis testing in linear models, *Springer-Verlag New York, Inc. New York, NY, USA*, 378.
- Lari Z., A. Habib, and E. Kwak ,2011. An Adaptive Approach for Segmentation of 3D Laser Point Cloud. *ISPRS Workshop Laser Scanning 2011 Calgary, Canada 29 – 31 August 2011*
- Lari Z. and A. Habib,2012. A new approach for segmentation of multi-resolution and multi-platform LiDAR data. *Proceedings of Global Geospatial Conference* , Québec City, Canada, 14-17 May 2012.
- Lichti D. and J. Skaloud, 2010. Registration and Calibration. In: Vosselman, G. and H. Maas ed. *Airborne and Terrestrial Laser Scanning*. Dunbeath:Scotland, UK, pp. 111-122.

Luhmann T., S Robson, S. Kyle, and I. Harley, 2006. *Close Range Photogrammetry*. Caithness, Scotland, UK. pp 13-14.

Petrie G. and C.K. Toth, 2009. Introduction to Laser Ranging, Profiling, and Scanning. In: J. Shan and C.K. Toth (Editors), *Topographic Laser Ranging and Scanning: Principles and Processing*. CRC Press, Taylor & Francis Group, Boca Raton, Florida, pp. 4-18.

Rabbani T., S. F. Dijkman, van del Heuvel, and G. Vosselman, 2007. An Integrated Approach for Modeling and Global Registration of Point Clouds. *ISPRS Journal of Photogrammetry and Remote Sensing*, 61(6),pp 355-370.

Renaudin E., A. Habib, and A. P. Kersting, 2011. Featured-Based Registration of Terrestrial Laser Scans with Minimum Overlap Using Photogrammetric Data. *ETRI Journal*, Volume 33 Number 4, August 2011. pp. 517-527.

Rusinkiewicz S. and M. Levoy, 2001. Efficient Variants of the ICP Algorithm. *International Conference on 3-D Digital Imaging and Modeling*.

Shin S. W., A. Habib, M. Ghanma, K. Changjae, and E-M Kim., 2007. Algorithms for Multi-sensor and Multi-primitive Photogrammetric Triangulation. *ETRI Journal*, Volume 29, Number 4, August 2007. pp. 411-420.

Talaya J., R. Alamus, E. Bosch, A. Serra, W. Kornus, and A. Baron, 2004. Integration of a terrestrial Laser Scanner with GPS/IMU orientation Sensors. *International Archives of Photogrammetry and Remote Sensing*, Vol. commission 5, ThS 17, Istanbul, Turkey.

APPENDIX A

2.1. Model

$$\vec{y} = A\vec{x} + d\vec{X} + \vec{e} \quad \vec{e} \sim (0, \Sigma') \quad \text{where } \Sigma' = \sigma_o^2 P'^+ \quad \text{and} \quad P' d\vec{X} = 0 \quad \text{A.1}$$

2. Solution vector (\vec{x}) of the model (A.1)

A.2 shows the LSA target function.

$$\vec{e}^T P' \vec{e} = (\vec{y} - A\vec{x} - d\vec{X})^T P' (\vec{y} - A\vec{x} - d\vec{X}) = \min_{|\vec{x}, d\vec{X}} \quad \text{A.2}$$

$P' d\vec{X} = 0$, therefore we can get the following form of the A.2.

$$\vec{e}^T P' \vec{e} = (\vec{y} - A\vec{x})^T P' (\vec{y} - A\vec{x}) = \min_{|\vec{x}} \quad \text{A.3}$$

The extended form of A.3 is:

$$\phi(\vec{x}) = \vec{y}^T P' \vec{y} - \vec{y}^T P' A\vec{x} - \vec{x}^T A^T P' \vec{y} + \vec{x}^T A^T P' A\vec{x} = \min_{|\vec{x}} \quad \text{A.4}$$

The simplified for of A.4 is:

$$\phi(\vec{x}) = \vec{y}^T P' \vec{y} + \vec{x}^T A^T P' A\vec{x} - 2\vec{x}^T A^T P' \vec{y} = \min_{|\vec{x}} \quad \text{A.5}$$

Finally the solution vector (A.7) can be derived by differentiating A.5 w.r.t. \vec{x} and equating it to zero (A.6).

$$\frac{\partial \phi}{\partial \vec{x}} = 2A^T P' A\vec{x} - 2A^T P' \vec{y} = 0 \quad \text{A.6}$$

$$\vec{\hat{x}} = (A^T P' A)^{-1} A^T P' \vec{y} = N^{-1} A^T P' \vec{y} \quad \text{where; } N = A^T P' A \quad \text{A.7}$$

² The Appendix A was cited from Kersting, 2011. PhD Thesis.
http://www.ucalgary.ca/engo_webdocs/AH/11.20346_AnaKersting.pdf

2. A-posteriori variance factor (σ_o^2)

The expected value of the sum of squares of the weighted predicted residuals is used to derive the a- posteriori variance factor (A.8)

$$E(\tilde{\mathbf{e}}^T P' \tilde{\mathbf{e}}) = E \left\{ (\hat{\mathbf{y}} - A\hat{\mathbf{x}} - d\vec{X})^T P' (\hat{\mathbf{y}} - A\hat{\mathbf{x}} - d\vec{X}) \right\} \quad \text{A.8}$$

Since $P' d\vec{X} = 0$, A.8 is modified as:

$$E(\tilde{\mathbf{e}}^T P' \tilde{\mathbf{e}}) = E \left\{ (\hat{\mathbf{y}} - A\hat{\mathbf{x}})^T P' (\hat{\mathbf{y}} - A\hat{\mathbf{x}}) \right\} \quad \text{A.9}$$

The expanded form of the Equation A.9 using the derived solution for $\hat{\mathbf{x}}$ in Equation A.7 is (A.10):

$$E(\tilde{\mathbf{e}}^T P' \tilde{\mathbf{e}}) = E \left\{ \hat{\mathbf{y}}^T P' \hat{\mathbf{y}} - \hat{\mathbf{y}}^T P' A \hat{\mathbf{x}} - A^T \hat{\mathbf{x}}^T P' \hat{\mathbf{y}} + A^T \hat{\mathbf{x}}^T P' A \hat{\mathbf{x}} \right\}$$

$$E(\tilde{\mathbf{e}}^T P' \tilde{\mathbf{e}}) = E \left\{ \hat{\mathbf{y}}^T P' \hat{\mathbf{y}} - \hat{\mathbf{y}}^T P' A N^{-1} A^T P' \hat{\mathbf{y}} \right\} \quad \text{where, } \hat{\mathbf{x}} = N^{-1} A^T P' \hat{\mathbf{y}} \quad \text{A.10}$$

The trace of a scalar equals to the scalar. (i.e. $tr(A)=A$) and the trace operation is commutative. (i.e. $tr(AB)=tr(BA)$). Thus, A.10 is modified as follows:

$$E(\tilde{\mathbf{e}}^T P' \tilde{\mathbf{e}}) = E \left\{ tr(P' \hat{\mathbf{y}} \hat{\mathbf{y}}^T) - tr(P' A N^{-1} A^T P' \hat{\mathbf{y}} \hat{\mathbf{y}}^T) \right\} \quad \text{A.11}$$

Since $tr(a)+tr(B)=tr(A+B)$ and $E\{tr(A)\}=trE(A)$:

$$E(\tilde{\mathbf{e}}^T P' \tilde{\mathbf{e}}) = tr P' [E(\hat{\mathbf{y}} \hat{\mathbf{y}}^T) - A N^{-1} A^T P' E(\hat{\mathbf{y}} \hat{\mathbf{y}}^T)] = tr P' (I_n - A N^{-1} A^T P') E(\hat{\mathbf{y}} \hat{\mathbf{y}}^T) \quad \text{A.12}$$

where: I_n is an $n \times n$ identity matrix.

The term $E(\hat{\mathbf{y}} \hat{\mathbf{y}}^T)$ can be derived from the variance-covariance matrix of the observations vector $\Sigma\{\hat{\mathbf{y}}\}$ as follows:

$$\Sigma\{\vec{y}\} = \sigma_o^2 P'^+ = E \left\{ (\vec{y} - A\vec{x} - d\vec{X})(\vec{y} - A\vec{x} - d\vec{X})^T \right\} \quad \text{A.13}$$

The expanded form of A.13 as follows:

$$\begin{aligned} E(\vec{y}\vec{y}^T) &= \sigma_o^2 P'^+ + (A\vec{x} + d\vec{X})(A\vec{x} + d\vec{X})^T \\ &= \sigma_o^2 P'^+ + A\vec{x}\vec{x}^T A^T + A\vec{x}d\vec{X}^T + d\vec{X}\vec{x}^T A^T + d\vec{X}d\vec{X}^T \end{aligned} \quad \text{A.14}$$

The substituting Equation A.14 and A.12:

$$E(\vec{e}^T P \vec{e}) = \text{tr} P' (I_n - AN^{-1}A^T P') [\sigma_o^2 P'^+ + A\vec{x}\vec{x}^T A^T + A\vec{x}d\vec{X}^T + d\vec{X}\vec{x}^T A^T + d\vec{X}d\vec{X}^T] \quad \text{A.15}$$

Since $P' d\vec{X} = 0$, The simplified form of A.15 is:

$$E(\vec{e}^T P \vec{e}) = \sigma_o^2 \text{tr} P' (I_n - AN^{-1}A^T P') P'^+ = \sigma_o^2 \text{tr} P' P'^+ - \sigma_o^2 \text{tr} N^{-1} A^T P' P'^+ P' A \quad \text{A.16}$$

Since $\text{tr}(AB) = \text{rank}(AB)$ and $\text{rank}(AB) \leq (\text{rank}A, \text{rank}B)$, the following Equation can be specified:

$$\text{tr}(P' P'^+) = \text{rank}(P' P'^+) = \min(\text{rank}P', \text{rank}P'^+) = \text{rank}P' = q \quad \text{A.17}$$

According to Equation A.17: Equation A.16 gets the form to:

$$E(\vec{e}^T P \vec{e}) = \sigma_o^2 q - \sigma_o^2 \text{tr} N^{-1} N = \sigma_o^2 q - \sigma_o^2 \text{tr} I_m = \sigma_o^2 q - \sigma_o^2 m \quad \text{A.18}$$

where, m is the number of unknown parameters.

Finally, the estimated a-posteriori variance factor (σ_o^2) can be established as follows:

$$\sigma_o^2 = (\vec{y} - A\vec{x})^T P' (\vec{y} - A\vec{x}) / (q - m) \quad \text{A.19}$$